AN ABSTRACT OF THE THESIS OF

N. Donald Morrison (Name) for the Doctor of Philosophy (Degree)

in Zoology (Major) presented on December 11, 1973 (Date)

Title: SPHAEROMYXA MAIYAI SP. N. (PROTOZOA:MYXOSPORIDEA): A LIGHT MICROSCOPIC AND ULTRASTRUCTURAL ANALYSIS EMPLOYING THE SCANNING AND TRANSMISSION ELECTRON MICROSCOPES

Abstract approved: Redacted for Privacy

Dr. Stuart E. Knapp

Dr. Ivan Pratt, deceased

Sphaeromyxa maiyai sp. n. (Myxosporidea:Myxiidae) is described from the gall bladder of the Pacific tomcod, Microgadus proximus Girard, from Newport, Oregon. The plasmodial (=trophic, trophozoite) stage is discoid averaging between 1 and 2 cm. The spore averages 27.6 x 5.6 μm with pyriform polar capsules averaging 9.3 x 3.7 μm. Sphaeromyxa maiyai was found to be nonpathogenic and produced no appreciable alterations in bile color or viscosity.

In cross section the plasmodial stage consists of three distinct regions: a homogenous outer ectoplasm, a dense syncytial organelle containing endoplasm and a central organelle containing endoplasm and a central alveolar region. The ectoplasm and the mucous layer surrounding the exterior of the plasmodium are rich in acid mucopolysaccharides.

The thick mucoid layer impeded observation of the ectoplasmic surface by scanning electron microscopy; however, ethylenediaminetetraacetic acid treatment removed the mucous and allowed partial visualization of the surface microvilli. Scanning electron microscopy of the spore revealed the presence of longitudinal striations and extruded polar filaments. The evagination of the polar filament is shown.

By ultrastructural analysis the ectoplasm was shown to consist of a simplified homogenous zone composed of glycogen aggregates, scattered microtubules, pinocytotic vesicles and electron dense cylindrical bodies. The endoplasm constitutes the major organelle zone of the plasmodium. It was shown to be composed of vegetative and sporoblast nuclei, mitochondria, myeloid figures, smooth and rough endoplasmic reticulum, and scattered microtubules.

Developing spores were found to consist of five distinct cells: two capsulogenic cells forming the polar capsules and polar filament, two shell valve cells forming the spore valves, and a single sporoplasm cell. The shell valves are joined at the sutural line by separate desmosomes.

The polar filament was longitudinally folded within the polar capsule and contained four filament folds. The first coil differed from the remaining coils by being wider and thinner and having a wrinkled lumen. The filament matrix is composed of a homogenous electron dense material. The sporoplasm was centrally located within the

spore and contained loboform extensions extending from the sporoplasm between the shell valve cells and the capsulogenic cells.

Ultrastructural studies showing the complex polycellularity of the fully differentiated spore and the complex syncytial plasmodium containing polycellular aggregates of developing sporoblasts indicate the nonprotozoan character of the Myxosporidea.

Sphaeromyxa maiyai sp. n. (Protozoa:Myxosporidea): a Light Microscopic and Ultrastructural Analysis Employing the Scanning and Transmission Electron Microscopes

by

N. Donald Morrison

A THESIS

submitted to

Oregon State University

in partial fulfillment of
the requirements for the
degree of

Doctor of Philosophy

June 1974

APPROVED:

Redacted for Privacy

Professor of Veterinary Parasitology
in charge of major

Redacted for Privacy

Chairman of Department of Zoology

Redacted for Privacy

Dean of Graduate School

Date thesis is presented December 11, 1973

Typed by Cheryl E. Curb for N. Donald Morrison

. . . . . and so there ain't nothing more to write about, and I am rotten glad of it, because if I'd a knowed what a trouble it was to make a book I wouldn't a tackled it and I ain't agoing to no more.

Mark Twain

ACKNOWLEDGMENTS

Grateful acknowledgment is made to the late Dr. Ivan Pratt of the Department of Zoology for his helpful guidance and constructive criticisms throughout this investigation. I also acknowledge the assistance of the following individuals: Dr. S. E. Knapp, Dr. A. Owczarzak, Dr. C. Bayne, Dr. S. Pilcher, Dr. W. Noonan and Mr. K. Fernald, Oregon State University, for their suggestions and criticisms. I wish particularly to thank Mr. A. Soeldner of the Department of Botany, Oregon State University, without whose essential advice and electron microscope facilities this project could not have been completed.

Special thanks must be extended to my wife Maiya and daughter Maiya II for special consideration during the entirety of this project and for enduring many rainy days fishing on the Oregon coast.

TABLE OF CONTENTS

TABLE OF CONTENTS (Cont.)

LIST OF TABLES

SPHAEROMYXA MAIYAI SP. N. (PROTOZOA:MYXOSPORIDEA): A LIGHT MICROSCOPIC AND ULTRASTRUCTURAL ANALYSIS EMPLOYING THE SCANNING AND TRANSMISSION ELECTRON MICROSCOPES

INTRODUCTION

Sphaeromyxa maiyai (Morrison and Pratt, 1973) (Figures 1, 2, 4, 21 and 24) represents a coelozoic myxosporidian parasite of the Pacific tomcod Microgadus proximus Girard. Sphaeromyxa maiyai like the majority of coelozoic myxosporidians is characterized by low pathogenicity. Pathogenicity is usually restricted to bile discoloration and increased bile viscosity. Coelozoic forms are generally non-invasive. The Genus Sphaeromyxa is characterized by fusiform spores with truncated ends, short ribbon-like polar filaments, and large discoidal plasmodial or trophic stages (Kudo, 1966). Sphaeromyxa maiyai possesses the largest plasmodium yet described from a myxosporidian measuring up to 2.0 cm in diameter.

Shulman (1966) stated that Jurine in 1825 was the first to mention the occurrence of myxosporidian infections in fish. He found cysts containing caseous material in the musculature of the white fish Coregonus fera from Lake Geneva, Switzerland. Jurine described neither the spore nor the trophic stage. Mayer (1864) quoted himself as finding myxosporidian spores in the retina of the Crucian carp Carassius carassius and sperm-like tailed spores of the Henneguya-type in the gills of perch in 1838 and 1840, respectively.

Müller (1841 a, b, c and 1843) briefly described the morphology of Henneguya-like spores but did not report finding trophic stages. He called these organisms, which were found as inclusion bodies in the skin and internal organs, "Psorospermien" as they closely resembled spermatozoa in having an ovoid body and long caudate processes. Creplin (1842) noted that the spore was formed within a cyst. He also noted similarities and possible phylogenetic relationships between fish "Psorospermien" and the "Pseudonavicillen" or Actinomyxida found in oligochaete testes and coelomic fluids.

Dŭjardin (1845) described psorosperms in the gill tissues of Leuciscus erythrophthalmus where they occurred as branched plasmodial masses. Because of the nonencysted nature of Dujardin's plasmodial masses, Robin (1853) suggested that the psorosperms might be related to slime-molds.

Lieberkühn (1854) observed the splitting of the myxosporidian spore and the subsequent release of the minute amoeboid sporoplasm. Balbiani (1863) expanded on Lieberkühn's description by designating the psorosperms as spores. He also described the polar capsule, which contained the spiral filament and its extrusion under selected stimuli.

Bütschli (1881) first recognized the similarity of the myxosporidian polar capsule and the coelenterate nematocyst. He described the cellular nature of the polar capsule and established

the Subclass Myxosporidia to include all sporozoa whose spores consisted of bivalve cases and contained polar capsules. Bütschli (1887) separated the sporozoa into two groups: 1. the Gregarinida, Coccidia and Haemosporidia and, 2. the Myxosporidia and Sarcosporidia.

Thélohan (1892) first attempted to establish a classification of the Subclass Myxosporidia. He pointed out that only the spore furnished characteristics adequate to serve as a basis for classification. Additionally, Thélohan described the pansporoblast, contained in the trophic stage, as a transparent plasma sphere formed by the condensation of plasma around one of the endoplasmic nuclei. According to Thélohan all spores containing polar capsules were to be classified as myxosporidians.

Gurley (1893) revised the classification proposed by Thelohan and separated the Myxosporidia into two groups: 1. the Cryptocystes, having small spores with a single polar capsule and pansporoblast producing many spores, and 2. the true Myxosporidia having relatively large spores, two or more capsules and pansporoblast producing few spores. Gurley (1894) published the first English monograph on myxosporidians dealing principally with taxonomy and epidemics.

Labbé (1894) suggested that the sporozoa be divided into two groups: the intracellular species as Cytosporidia consisting of the Gregarinidia, Coccidia, and the Haemosporidia, and the intercellular

species as Histosporidia consisting of the Myxosporidia, Microsporidia and Sarcosporidia. Delage and Hérouard (1896) subsequently revised Labbé's classification. They divided the sporozoa into two subclasses namely the Rhabdogeniae having elongate to falciform sporozoites and the Amoebogeniae having an amoeboid sporozoite. The Amoebogeniae contained a single suborder, the Myxosporidia, combining both the true myxosporidians and the microsporidians.

Thélohan (1895) in his monograph "Recherches sur les Myxosporidies" first described the binucleate condition of the sporoblast. He also described the nuclei of the capsulogenous cells as small deeply staining bodies adherent to the polar capsules. Thélohan listed all the known species of myxosporidians and devised the currently employed terminology of spore structure.

Dolflein (1898) distinguished between multiplicative and propagative reproduction. The former indicated autoinfection or the increase in number of organisms within the host while the latter indicated the formation of resistant spores involved in the passage of the parasite from one host to another.

Schaudinn (1900) classified the sporozoa into two subclasses based on morphological and developmental attributes. In the subclass Telopsoridia, sporulation occurred at the terminus of the life cycle and produced simple spores without polar capsules and polar filaments. In the subclass Neosporidia, sporulation occurred throughout the life

cycle and produced complex spores with polar capsules and spiral filaments.

Dolfein (1901) established the order Cnidosporidia which contained the Myxosporidia, Microsporidia and the Sarcosporidia.

Laveran and Mesnil (1902) described endogenous multiplication in the Myxosporidia which occurred by means of equal and unequal plasmotomy of young plasmodial stages. They denied that budding as described by Cohn (1896) occurred. They reasoned that the small plasmodia formed by plasmotomy often adhere temporarily to larger plasmodia. They felt the adherence of plasmodia was erroneously interpreted by Cohn as budding.

Caullery and Mesnil (1905) noted a cellular origin of the spore valves in Sphaeractinomyxon stolci (Cnidosporidia, Actinomyxida). The cellular origin of the myxosporidian spore valve was reported simultaneously by Leger (1906) in Chloromysum truttae and by Mercier (1906 a, b) in Myxobolus pfeifferi. Cellularity was later substantiated by Leger and Hesse (1906) in Myxidium, Henneguya and Myxobolus and by Schröder (1907) in Sphaeromyxa sabrazesi.

Schröder (1907) studied plasmodial and spore development in the polysporous myxosporidian Sphaeromyxa sabrazesi. He found that there existed a fusion of the two sporoplasm nuclei in the fully differentiated spore. Additionally, he described the mechanism by which the two shell valve cells overlap and form a protective covering around

the maturing amoeboid sporoplasm. At the incipience of sporogenesis, Schröder described plasmogamy which results in the pansporoblast formation. He stated that in Sphaeromyxa sabrazesi the pansporoblast, a single cell containing four nuclei (two large nuclei and two small nuclei), after a series of mitotic divisions, produced 14 nuclei. The plasma then divided to form two ellipsoidal sporoblasts. At the termination of spore formation the pansporoblast contained two mature spores and two "restherne" or residual nuclei. Schröder also found the anlagen of the polar capsule-filament complex in the pansporoblast as a small faintly staining spindle enclosed by a vacuole.

Emery (1909) suggested that the myxosporidians were metazoans or at least related to the Mesozoa, particularly Dicyema. He based this assumption on the functional complexity of the myxosporidian reproductive and nonreproductive subordinate protective cells and their similarity to similar elements in the Mesozoa rather than morphological relationships.

Auerbach (1910) published "Die Cnidosporidien" constituting the first major review of the Myxosporidia, Actinomyxida, and Microsporidia. Auerbach's monograph was principally a taxonomic review; however, sections were devoted to life cycle studies and phylogeny.

Georgévitch (1914, 1916, 1917, 1919, 1929, 1935 and 1936) studied nuclear behavior, sexuality and life cycles in the genus Ceratomyxa. He found that the karyosome is involved in the

formation of centrioles and that a centrodesmose forms between the two halves of the developing karyosome. The karyosome may be formed from chromosomal material. According to Georgévitch (1935, 1936) the trophic stage is diploid and contains four chromosomes. Reduction division occurs at the completion of sporogenesis just prior to the fusion of the sporoplasm nuclei. He reaffirmed Schröder's observations on the formation of the generative cell via cytoplasmic condensation around vegetative nuclei. He also described complex methods of autoinfection by spores within the host and by plasmotomy of the multinucleate trophozoite.

Davis (1916) described the occurrence of both disporous and polysporous plasmodia in Sphaerospora dimorpha and reported finding no evidence of sexual reproduction. Mavor (1916) working with Ceratomyxa acadiense observed amitotic nuclear division in the plasmodial stage. He also suggested that each sporoblast originates from a single propagative cell. He further concluded that the polar capsules are formed in their own cells and that the polar filament developed from "metamorphosed cytoplasm."

Erdmann (1917) reviewed the literature related to sexual reproduction in the Myxosporidia. She concluded that neither the place nor time of meiosis had been established. Erdmann suggested that no synkaryon is formed and that plasmogamy occurs between two cells. According to her, the so-called reduction nuclei of Schröder (1907),

Mercier (1906a), and Awerinzew (1911) inside the spore are chromatic or glycogenous bodies involved in spore membrane formation.

Kudo (1919) listed 409 species of myxosporidians in his classic Monographic "Studies on Myxosporidia, A synopsis of genera and species of Myxosporidia."

Kudo (1922) studied the life history of the histozoic myxosporidian Leptotheca ohlmacheri from the kidneys of frogs. He concluded that both endogenous and exogenous budding occur during the trophic stages and that prior to spore formation at the beginning of sporogony a trinucleate stage is developed. He also described the formation of the polar capsule-filament complex. The capsule formed from a deeply staining club-shaped mass contained within a vacuole. The capsulogenous cell became bulb shaped at one end, then the fine distal extremity coiled around the bulbous mass.

Dunkerly (1925) described the life cycle of Agarella gracilis placing special emphasis on the origin and relationships of spore forming nuclei. He further elaborated on the Mesozoan ancestry hypothesis of Emery (1909). Dunkerly suggested that the myxosporidian spore was multicellular and physiologically analogous to the infusiform embryo of Dicyema. Multicellularity in the myxosporidians according to Dunkerly evolved as a protective mechanism for the germ cells.

Naville (1930) reviewed the life cycle of Sphaeromyxa sabrazesi, S. balbianii, and Myxidium incurvatum. He suggested that in the myxosporidians there were two fertilizations and two zygotes in the life cycle. The diploid zygote released from the spore formed numerous diploid schizonts some of which underwent a reduction division resulting in the formation of microgametes and macrogametes. The micro and macrogametes fused to form the diploid zygote or pansporoblast. After fusion, a reduction division occurred resulting in the formation of haploid nuclei which divided several times to form the haploid spores containing two nuclei in the dihaploid phase which fused to restart the cycle. Naville's observations are not generally accepted according to Noble (1944).

Myxosporidian life cycles were reviewed extensively by Noble (1944). He concluded that true schizogony did not occur and that asexual multiplication occurred by plasmotomy or budding rather than multiple fission in the monosporous and disporous species. In the large polysporous genera such as Myxidium and Sphaeromyxa multiplication was by nucleogony occurring within the original zygote membrane. Noble felt that meiosis occurred at the last nuclear division in sporogony. Three methods of pansporoblast formation were listed:

1. Synkaryon formation by fusion of two nuclei.
2. By plasmogamy or cytoplasmic union.

3. By differentiation and growth of a single cell without the previous union of nuclei or of cytoplasm.

Noble suggested that the "differentiation without union" method most closely described the nuclear cycle as it did not require double fertilization or plasmogamy.

Grassé (1960) first studied the ultrastructure of myxosporidians employing the plasmodial stage of Sphaeromyxa sabrazesi. In cross section the so-called brush-edge seen by light microscopy was found to be composed of densely packed irregular villosities or micro-villosities. These were frequently anastomotic and delimited by a thin poorly differentiated cell membrane. The endoplasmic zone of light microscopy was shown to contain numerous large mitochondria containing short thick tubuli, osmiophilic lipid inclusions, trophic nuclei, and generative cells. The latter were observed to possess an electron opaque membrane three to four times thicker than the ecto-plasmic membrane and a more electron dense cytoplasm than the plasmodial ground substance. Pseudopodial surface extensions and a two layered nuclear membrane devoid of ribosomes were observed. He reported that neither dictyosomes nor ergastroplasm were detected in the sampled material. Grassé (1960) concluded that there was a separation between germinal elements and the syncytial somatic elements. He suggested that the myxosporidians were definitely advanced beyond the protozoan unicellular level and that they probably

represented an autonomous phylum showing the beginning of cellular differentiation. However, they were not metazoan as they lacked sperm and ova.

Cheissin, Schulman and Vinnitchenko (1961) compared the structure of the polar capsule and polar filament of Myxobolus uniporus and M. carassi as seen with the light and electron microscope. They ascertained that the spore wall consisted of two osmiophilic layers approximately 20 nm thick separated by two additional layers approximately 30 nm thick. The two shell valves were demonstrated to be separated by a cement-like substance.

Cheissin et al. (1961) described the cnidaria (= polar filament) as consisting of 9-10 lateral coils with the distal end being free while the proximal end was attached to the capsular wall. The polar filament was erroneously interpreted to consist of two parts coiled around each other, one flat and the other crescent shaped. Cheissin et al. provided little information related to sporoplasm structure except that a Golgi apparatus-like structure consisting of 3-5 pairs of slightly bent membranes was situated anterior to the nucleus.

Lom and Vávra (1964) briefly described the formation of the polar capsule-filament complex and compared its development to the morphogenesis of the cnidarian nematocyst. They showed that the capsular primordium consisted of a long tubular formation coiled within the capsulogenous cell. Development consisted of tubular

enlargement followed by the aggregation of granular elements within the capsulogenous cell forming the first threads of the polar capsule.

Lom and Vávra (1965) further elaborated on the morphogenesis of myxosporidian polar filaments in Henneguya psorospermica. They reported that the polar capsule-filament complex first appeared within the capsulogenous cells as a spherical body which appeared to be equivalent to the capsulogenous vacuoles of the light microscope. The spherical bodies increased in size almost filling the capsulogenous cell. The filament proper first appeared in a tubular structure then invaginated together with the tubular structure into the precapsular body. Lom and Vávra clarified Cheissin et al. (1961) misinterpretation regarding the shape of the polar filament. They proved that the polar filament, in actuality, consisted of a single folded tubular structure that, because of its folding, was mistakenly interpreted by Cheissin et al. as consisting of two separate filaments.

Lom and Vávra (1964, 1965) concluded that a definite homology between myxosporidian polar filament and Coelenterate nematocyst morphogenesis was questionable. The latter differentiated in association with the Golgi complex while no evidence was shown for Golgi involvement in the case of myxosporidian polar filament morphogenesis. They pointed out, however, that certain homologies existed. Slender microtubules were observed in association with nematocysts and the capsulogenic tube. In some types of coelenterate

nematocysts, according to Chapman and Tilney (1959 a and b), and in myxosporidian polar capsules, the filamentous elements originated from the intracapsular matrix.

Lom and de Puytorac (1965 a) studied the plasmodial ultrastructure and polar capsule development in Chloromyxum cristatum, Henneguya psorospermica, Myxidium lieberkühni, Myxobolus sp., and Zschokkella nova. They found that the plasmodial ectoplasm differed between species by the presence or absence of microvillosities and adherent mucous coats. The endoplasm was morphologically similar in all species examined. They reported that sporogenesis commenced with the envelopment of the germinal cell by another larger cell. Pansporoblast formation was initiated by mitotic division of the enveloped cell subsequently forming the valvogenic cells, capsulogenic cells, and the germinal sporoplasm.

Schubert (1967) examined sporogenesis in Henneguya pinnae. He described the ultrastructure of the host-parasite epitheloid, the plasmodium, and the stages involved in sporogenesis. Host epithelial tissue surrounds the plasmodium, interdigitating with the parasite surface membrane thus affording an increased area for nutrient transfer. An electron transparent parasitophorous vacuole some 75-100 nm in breadth separates the host-derived epitheloid layer from the plasmodium. Beneath the plasma membrane, the ectoplasm contained pinocytotic vesicles and a network of smooth endoplasmic

reticulum. The ectoplasm was devoid of ribosomes. Schubert concurred with Lom and de Puytorac (1965a and b) regarding polar capsule development. He could not identify the organelle from which the capsule developed; however, he suggested that the granular endoplasmic reticulum may be involved as its concentration greatly increased immediately prior to polar capsule formation. He concluded that the amoeboid sporoplasm developed its binucleate condition by means of nuclear partition or amitosis without subsequent cytoplasmic partition.

Lom and Corliss (1967) focused attention on the physiological and morphological differences between the Myxosporidians and the Microsporidians. They concluded that no close affinity exists between these groups phylogenetically or taxonomically. Structurally and functionally the extrusible organelles are unrelated and represent evolutionary convergence having evolved independently within each group. The only linking factor is the presence of an amoeboid sporoplasm serving as the infectious stage. Lom and Corliss suggested that the Myxosporidia should be removed completely from the Phylum Protozoa as Grell (1956), Gottschalk (1958) and Grassé (1960) originally proposed and established as a new Phylum.

Lom (1969a) further clarified Grassé's observations on the ultrastructure of the plasmodium and sporogenic stages in the Genus Sphaeromyxa. He found an extensive system of tubular elements measuring 0.5 μ x 500 $\mathring{A}$ which existed solely in the ectoplasm. These

tubuli, forming compact aggregates, morphologically resembled viral inclusion bodies. At the endoplasmic-ectoplasmic junction a dense zone of fine irregular fibrils was shown which according to Lom were not microtubular in structure. The ectoplasm contained numerous unattached ribosomes approximately 270 Å in diameter. Lom was able to trace and described in detail the spore development from a single nucleated generative cell through the mature spore stage. He noted that the mitochondria of the developing sporogenic cells possessed remarkably high concentrations of DNA in addition to electron dense bodies of unknown function. Lom concluded by reviewing the arguments of homology between the myxosporidian polar capsule and the coelenterate nematocysts. He suggested that on the basis of nematocyst homology, cytological development and the usual polycellularity of the spore, that the myxosporidians should be taxonomically separated from the true protozoa.

Gould (1970) studied the ultrastructure of the spore of Ceratomyxa shasta. The spore valves were shown to be trilaminate, consisting of an inner and outer electron dense layer between which was situated a less electron dense granular matrix. Spore valves were separated by a sutural space of approximately 400 Å containing septate desmosomes approximately 80 Å apart which connect the two valves within the sutural line. Poor fixation and resin infiltration restricted a detailed description of the sporoplasm organelles.

Gould reported finding granular endoplasmic reticulum, Golgi-like bodies, mitochondria and spiral structures resembling vesicular endoplasmic reticulum or myeloid figures in the sporoplasm. The sporoplasmic nucleus was of the vesicular type having a double membrane and large nuclear pores. The wall of the polar capsule was found to be approximately 50-125 mμ thick.

Using the scanning electron microscope, Lom and Hoffman (1971) described the spore surface morphology of Myxosoma cerebralis and M. cartilaginis. They describe in M. cerebralis a deep ridge running parallel to the sutural border and on the anterior side of the sutural line. Two small orifices believed by the authors to represent the polar filament discharge canal were reported posterior to the anterior furrow. Shrinkage was quite evident in all spores. Spores of M. cerebralis were covered by irregular mucous strands while M. cartilaginis was observed to be free of adherent mucous.

Because of the uniquely large size of the plasmodium of Sphaeromyxa maiyai and the high infectivity rate (approximately 30% in the tomcod), studies were undertaken to ellucidate several aspects of the biology of this myxosporodian parasite. The studies consisted of:

1. The identification and taxonomic description of a new species of myxosporidian parasite herein named Sphaeromyxa maiyai (Morrison and Pratt, 1973).

2. The light microscopy of the plasmodial stage and of the spores with particular attention to the structure of the extruded polar filament and its method of extrusion.
3. The scanning electron microscopy of the plasmodial surface, the spore surface, and the extruded polar filaments.
4. An ultrastructural analysis of the plasmodial ectoplasmic layer, endoplasmic layer, and the near mature spore within the endoplasm.

MATERIALS AND METHODS

General Methods

Infected Pacific tomcod, Microgadus proximus, were collected by otter trawl off Newport, Oregon, between 10 and 40 fathoms during the spring and summers of 1969-1972. Live specimens were subsequently transported to the Oregon State University Marine Science Center for examination and initial histological preparation. It was usually impossible to keep living fish in aquarium tanks for any length of time probably due to depressurization effects. When the physoclistous swim bladder was punctured and aspirated with a fine gauge hypodermic needle, the fish usually survived for several weeks.

The gall bladder was removed and examined for the presence of spores and trophozoites. Infected gall bladders were usually dissected in order to obtain whole specimens of both spores and trophozoites, for either examination of live material or examination by transmission electron microscopy (TEM) or scanning electron microscopy (SEM). Other infected gall bladders were fixed in toto for routine histological and cytochemical examination.

Specific Methods

Light Microscopy

Infected gall bladders were dissected from the host and fixed in toto in either Bouin's or Zenker's fixatives, washed, then treated with iodine alcohol, if necessary, dehydrated in a graded series of ethyl alcohol, cleared in either xylene or toluene and embedded in Paraplast (m.p. 56-57°C.). Sections were cut at 5 μm, 10 μm and 15 μm and subsequently stained with Harris' hematoxylin and eosin or Heidenhain's iron-hematoxylin or aqueous Periodic Acid-Schiff's Reagent and counterstained with 0.05% fast green or Feulgen's nuclear Reagent (Humason, 1967). Plasmodial stages were stained for acid mucopolysaccharids by the Alcian blue 8GX method (Pearse, 1968).

Spore smears were prepared on coverslips or glass slides, fixed with either warm Schaudinns' or air dried and then fixed with absolute methanol. The Schaudinns' fixed material was stained with Giemsa's fluid, PAS, or Feulgen's reagent while air dried material was stained with Giemsa's fluid.

Fresh spores were prepared for microscopic examination by embedment in 0.8% ionagar using a No. 0 coverslip (Lom, 1969b). Measurements of spores were made either with an ocular micrometer under phase contrast microscope at 1000x or from photographic enlargements of photomicrographs taken with a Nikon AFM automatic

camera attached to a Zeiss RA microscope equipped with neoflor phase contrast optics. At least 50 spores were measured for each biometric entry.

Transmission Electron Microscopy

Trophozoite. Trophozoites were excised from the gall bladder then washed briefly in marine teleost physiological saline (Hale, 1965). Whole trophozoites were subsequently fixed in:

a. 3% Gluteraldehyde in 0.1 M Na cacodylate buffer pH 7.2 at 4°C. for 2-4 hours (Hayat, 1970).

b. 3% Gluteraldehyde in 0.2 M Sorensen's phosphate buffer pH 7.2 at 4°C. for 2-4 hours (Hayat, 1970).

The samples were washed overnight in several changes of their respective buffer at 4°C. Trophozoites were then minced into small pieces approximately 1.0 mm x 1.0 mm x 0.1-0.3 mm. All samples were postfixed in 1.0% osmium tetroxide buffered with either 0.1 M Na cacodylate pH 7.2 or 0.2 M Sorensen's phosphate buffer pH 7.2 at 4°C. for 1-4 hours in the dark. The organisms were then dehydrated through a graded series of ethyl alcohol or acetone. After the latter dehydrant the specimens were stained for 8-12 hours in a solution of 70% acetone saturated with uranyl acetate.

Samples were infiltrated and flat embedded in aluminum weighting dishes in:

a. Bojax mixture

b. Spurr's Low Viscosity Media

c. Araldite 506

The Bojax and Spurr's media (Spurr, 1969) were cured overnight at 70°C. Araldite 506 samples were polymerized at 35°C. overnight, 45°C. the next day, and 60°C. overnight.

Thin sections were cut with either glass or diamond knives on a Sorvall MT-2 Porter-Blum Ultramicrotome, and mounted on formvar coated grids (150, 200, or 300 mesh). The alcohol dehydrated specimens were stained with a saturated aqueous solution of uranyl acetate followed by lead citrate staining (Reynolds, 1963). The acetone dehydrated uranyl acetate stained specimens were also stained with lead citrate.

Spores. Prior to fixation the spores were washed by alternating gentle centrifugation with several changes of marine teleost physiological saline. Spores were fixed in 3.0% gluteraldehyde in 0.2 M Sorensen's phosphate buffer pH 7.2 at 4°C. for 12-24 hours. Samples were then centrifuged into a pellet, embedded in 6.0% ionagar and sectioned at 25-50 μm on a Sorvall TL-2 tissue sectioner.

Other spore aliquots were treated with 5.0% KOH or saturated urea (Lom, 1964; Hoffman et al., 1965) to extrude the filament. Upon extrusion of the filaments, the spores were fixed in 3.0% gluteraldehyde in 0.2 M Sorensen's phosphate buffer pH 7.4 at 4°C. for 12-24

hours. The spore samples were gently centrifuged to form a pellet, embedded in 4.0% ionagar, and diced into 1.0 sq. mm pieces.

Agar embedded spores were then washed in several changes of phosphate buffer and post-fixed in 1.0% osmium tetroxide in 0.2 M Sorensen's phosphate buffer pH 7.4 at 4°C. for three hours. Subsequent processing was the same as that of the acetone dehydrated araldite 506 embedded trophozoites.

Electron micrographs were taken with a Philips EM 300 operated at 40 or 60 Kv. Initial magnifications ranged from 1000x to 116,700x. The micrographs were subsequently photographically enlarged 2.6x.

Scanning Electron Microscopy

Air Dried Samples. For scanning microscopy (SEM) the trophozoites were removed from the gall bladder, washed in several changes of Sorensen's phosphate buffer then fixed immediately in 4% gluteraldehyde in 0.2 M Sorensen's phosphate buffer pH 7.4 at 4°C. for 6-24 hours. The trophozoites were subsequently washed in several changes of cold buffer and stored at 4°C. until examination. The specimens were mounted on SEM stubs by floating the trophozoite on a large drop of buffer then allowing the buffer to evaporate. A 200 nm thick gold coating was deposited over the trophozoite surface using a Varian-Mikros Model VE-10 vacuum evaporator. During evaporation the specimen stub was rotated in both the horizontal and vertical axes with

respect to the gold wire source. The samples were stored in vacuum over silica gel until examined.

Spores were cleaned by alternately washing in Sorensen's buffer and gentle centrifugation. A clean concentrated suspension of spores was placed on formvar coated slotted transmission electron microscope grids by means of micropipettes. After most of the buffer had evaporated the spores were fixed on slides in Petri dishes with 1.0% osmium tetroxide in 0.2 M Sorensen's phosphate buffer at pH 7.2 for 6 to 12 hours. The grids were then washed with several changes of distilled water, air dried, and mounted on SEM stubs using conductive paste. Samples were subsequently coated with a thin layer of carbon, 0.5 μm thick, followed by a gold layer, 2.0 μm thick. The coated specimen stubs were stored in vacuum over silica gel until examination.

Critical Point Drying of Trophozoites and Spores. Trophozoites were thoroughly washed in several changes of Sorensen's phosphate buffer prior to fixation. Several samples were then treated with 0.005% EDTA for 2-4 minutes with constant agitation to remove the adherent mucous coating (Miller and Danagan, 1971). Subsequently the plasmodia were fixed in 3.0% gluteraldehyde in 0.1 M Na cacodylate buffer pH 7.2 for 12 hours at 4°C. Other samples were fixed by immersion in Párducz fixative (Párducz, 1967) for ten minutes after which they were washed with several changes of double glass distilled water. The specimens were then dehydrated in a graded series of

acetone-water 10%, 20%, 30%----100%, for seven minutes per change followed by a graded series of acetone Freon FT 10%, 20%, 30%---- 90% plus two changes of 100% Freon FT for seven minutes each. The specimens were then transferred to the SPC-900's precooled chamber and processed through critical point. After drying, the specimens were affixed to SEM stubs and coated with a thin film of gold (about 20 nm thick).

Spores were processed in one of three manners: 1. as whole spores without extrusion of polar filaments, 2. as spores with polar filaments extruded, and 3. as spores that have been ruptured with saturated urea and their filaments extruded. The spores were subsequently fixed in centrifuge tubes with Pârducz fixative, thoroughly washed in several changes of distilled water, then affixed to carbon coated electron microscopy grids. The grids were then dehydrated in an ascending series of acetone and transferred to an ascending series of Freon TF-acetone solutions. Complete removal of acetone was accomplished by two washings in 100% Freon TF. The specimen stubs containing the grids were transferred to the critical point drier and dried through the critical point transitional liquid/gas phase using Freon 13.

After drying, the specimens were coated with a thin layer of carbon 0.5 μm thick followed by a thicker layer of gold 2.0 nm thick. The samples were examined with a Cambridge Stereoscan Mark II-A

at 20 Kv accelerating potential and 150 microamps beam current. Micrographs were made on Polaroid type 55 P/N film.

RESULTS

Light Microscopy

Plasmodial (Trophic) Stage

The observed trophic stages of Sphaeromyxa maiyai ranged in size between approximately 1.0 mm and 2.0 cm. Small plasmodial stages were of a flattened disc shape. Peripherally the plasmodium was surrounded by a narrow transparent homogenous ectoplasm internal to which was the more optically dense endoplasm. Large plasmodia, 5.0 mm and above, had a convex dorsal surface and a slit-like aperture opening into a large internal atrium on the concave ventral surface (Figure 1). The large trophic stages greatly exceed the gall bladder in length and breadth and were consequently folded within the gall bladder (Figures 2 and 3). The larger plasmodial stages were clearly visible in situ through the gall bladder membrane. Small plasmodia were somewhat transparent while larger plasmodia were grayish white to yellow green. Plasmodial stages were not attached to the gall bladder epithelium but were free floating in the bile. One to several plasmodia may be present in a single gall bladder. When multiple plasmodia occurred, the plasmodia were frequently layered one inside the other (Figure 3). The bile from infected fishes was not markedly different from the normal deep green

bile of uninfected fishes and showed only a slight increase in viscosity. The gall bladder was frequently enlarged especially when several large plasmodia were involved in multiple infections.

The trophic stages were non-motile and showed no apparent evidence of active pseudopodial formation common in other genera of coelozoic myxosporidians.

In cross section the concave inner ectoplasmic surface differed microtopographically from that of the outer convex ectoplasmic surface. The outer surface was generally smoother, being either smooth or showing only moderate rugosity (Figures 4 and 6) while the inner surface was seldom smooth and usually consisted of a moderate (Figures 4 and 6) to extreme rugosity especially at flexure points (Figure 5).

The ectoplasmic surface was covered by a thin layer of mucoid substance (Figures 8, 9, 10 and 14). The mucoid layer stained a clear blue-green when subjected to the alcian blue method thus indicating that the external coat was composed of an acid mucopolysaccharide or mucin. Extending into the mucoid layer was the so-called brush border zone of the ectoplasm which consisted of a fine layer of densely staining microvilli approximately 0.9 μm thick (Figures 8, 9, 10, 13 and 14). The ectoplasmic zone appeared as a structurally homogeneous pseudosyncytial layer of varying thickness and surface microtopography. The surface contained occasional deep

furrows extending almost into the outer endoplasmic zone (Figures 7 and 11).

The ectoplasmic-endoplasmic junction was of two distinct types. In the first type there was a sharp structural demarcation between the ectoplasm and the endoplasm (Figures 9, 10, 11, 12, 13 and 14). In the second type the junction was indistinct with endoplasmic nuclear elements diffusing into the ectoplasm (Figures 4, 5, 6 and 8).

The endoplasm contained free vegetative and generative nuclei and developing sporonts surrounded by dense cytoplasm (Figures 10, 11 and 12). Early sporonts contained one to several nuclei (Figures 11 and 14) while older sporonts contained from 14 to 16 nuclei (Figures 10 and 12). Mature sporonts containing fully differentiated spores were disporoblastic or pansporoblastic and contained within remnants of the sporonts (Figure 13). Spores at the periphery of the endoplasm were usually parallel to each other and situated perpendicular to the ectoplasmic membrane (Figures 9 and 13), in the alveolar portion of the endoplasm the spores were generally without this orientation. The outer endoplasm contained numerous small vacuoles of two types:

1. Optically transparent vacuoles representing areas of lipid extraction (Figure 11).
2. Optically opaque vacuoles containing a dense homogeneous material (Figure 11).

A highly vacuolar central zone was located internal to the organelle-containing outer endoplasmic zone. The vacuoles varied greatly in size (1.8 μm-40 μm) and usually contained a flocculent amorphous material of unknown composition (Figures 9 through 15). Contained within the vacuolar zone and situated between the limiting membranes are found sporonts and mature spores (Figure 15). Spores and differentiating sporoblasts were less numerous in the alveolar endoplasm than in the outer endoplasm.

Histochemistry of the Plasmodial Stage

The alcian blue 8GX method for acid mucopolysaccharides showed an intense blue green reaction product in the ectoplasmic zone and on the mucoid strands extending from the ectoplasmic surface. The endoplasmic-vacuolar zone was only lightly stained. The presence of intense acid mucopolysaccharide staining in the ectoplasm indicated that the mucoid layer or glycocalyx (Figures 8, 9, 47 and 52) was synthesized within the ectoplasm and subsequently released to the exterior of the trophozoite surface.

Both the ectoplasm and endoplasm showed a PAS(+) reaction. The ectoplasm stained intensely while the endoplasm showed a moderate reaction. Diastase digestion reduced the intensity of the PAS reaction especially in the ectoplasm.

The ectoplasm and endoplasm of the trophozoite both showed a positive Feulgen reaction. The reaction was most intense in the endoplasm immediately interior to the ectoplasm. This region contained the majority of nuclei, both vegetative and sporoblastic.

Spore

Filaments not Extruded. The spores of S. maiyai were elongated, arcuate in frontal view (Figures 16, 18, 20 and 22) and sinuous in sutural view (Figures 17, 19 and 21). The capsular ends were bluntly rounded to truncate. Dimensions of fresh and of fixed and stained spores are presented in Table 1.

Table 1. Dimensions of fresh Sphaeromyxa maiyai spores and of spores air dried-methanol fixed and stained in Giemsa solution. Dimensions in micrometers (μm).

	Fresh		Fixed and Stained	
Character	Mean	Range	Mean	Range
Spore				
Length	27.6	23.0-30.0	23.9	22.4-26.6
Breadth	5.6	5.0- 7.2	4.3	2.9- 5.3
Polar capsule (filament not extruded)				
Length	9.3	8.0-10.0	8.9	8.2-10.6
Breadth	3.7	4.0- 4.2	3.6	2.9- 4.4
Polar capsule (filament fired)				
Length	7.4	6.0- 8.4	---	---
Breadth	3.2	2.8- 3.6	---	---

Air dried methanol-fixed material underwent moderate shrinkage which according to Kudo (1921) is normal for myxosporidian spores. The polar capsules underwent less shrinkage than other spore elements.

Unlike other myxosporidian polar filaments which are spirally wound within the polar capsules, the polar filament of Sphaeromyxa is longitudinally folded (Figures 17, 18 and 20). The ovate polar capsules show the remnants of the capsulogenous cell and nuclei (Figures 16, 17, 20, 22 and 24) at the proximal end of the capsule. The sporoplasm more or less fills the space between the two polar capsules. One or two nuclei are visible within the sporoplasm depending on the degree of maturation of the spore (Figures 19, 22 and 24). The sutural line bisects the spore longitudinally forming an "S" shaped line. Parallel to the longitudinal axis of the spores and bisecting the sutural line are a series of faint longitudinal grooves (Figures 21 and 23).

Feulgen staining revealed the presence of two pycnotic valvular nuclei mid peripherally, one pycnotic nucleus attached to the proximal aspect of each polar capsule, and one or two sporoblastic nuclei.

Filaments Extruded. The extent of polar filament extrusion was dependent on the agent used to cause the extrusion. Saturated urea generally caused complete extrusion (about 100-150 μm) (Figure 24) and partial to complete lysis of the spore (Figures 25, 27 and 28)

along the sutural line. Five percent KOH caused a great percentage of incompletely extruded filaments and no lysis at the sutural plane. Observed by phase microscopy, incomplete extrusion of the polar filament revealed the mechanism of outfolding from the capsule. In the intact filament (Figures 20 and 26) a plug-like dense area can be seen at the distal terminus of the spore. This area is thicker than the remainder of the filament. Upon partial extrusion (Figures 26 and 27) the thinner optically dense medial portion of the polar filament can be seen extruding itself into the thicker proximal aspect of the polar filament as a dark line. Within the polar capsules undischarged elements of the filament were visible. Additionally the outer spore valvular membrane appeared to cover the polar capsule prior to extrusion; however, after extrusion had commenced, the valvular membrane was forced open to form a funnel-shaped orifice. After complete filament discharge the polar capsule became structurally homogeneous and decreased in optical density.

An isolated undischarged filament (Figure 28) showed a cap-like protuberance which can also be seen in fully extruded polar filaments (Figures 24 and 25). The cap, in fully extruded filaments, appeared to be connected to the conical depression of the valvulogenic cells. This connection is probably not very strong as the polar capsules were easily released from the valvular cells when the sutural line split.

Scanning Electron Microscopy

Plasmodial Stage

The plasmodial membrane of the trophic stage of Sphaeromyxa maiyai is obscured by a dense mucoid layer. Low magnification scanning electron micrographs revealed the presence of several morphologically distinct types of surface patterns (Figures 29, 30, 32, 35 and 36). Typically the surface consisted of rugose patterns (Figures 29, 30, 31 and 33) which corresponded to the features seen with higher magnifications of the dissecting microscope and sectioned material observed by light microscopy (Figures 4 and 6). Other areas showed a much smoother surface (Figures 29, 31 and 32) which corresponded to the smooth surfaces seen in sectioned material (Figures 4 and 6). High magnification micrographs of the surface (Figures 35 and 36) show the surface to be covered by a smooth structureless layer of mucus.

Trophic stages treated with 0.005% EDTA to remove the mucous layer showed the presence of fine sinuous bifurcating filaments (Figure 34) probably representing the microvilli described by Grasse (1960). The filaments varied in thickness between 0.1 and 0.4 μm to form a woven mat-like effect.

In one non-treated sample a surface canal penetrated into the microvillar area showing a cross section of the mucous coat (Figure 37).

Spore

Filaments not Extruded. Scanning electron micrographs revealed the presence of numerous parallel longitudinal grooves on the spore surface (Figures 38, 39 and 40). The grooves extended almost the entire length of the spore arising and terminating near the truncated spore terminus. The sutural line appeared as a deep groove at an oblique angle to the longitudinal striations and consequently bisected the spore (Figures 38 and 40). The discharge canal of the polar filament in S. maiyai was plugged or at least not a patent opening. Located in the center of the truncated terminus was a small depression or infolding of the undischarged polar filament (Figure 39).

The shell valves of air dried spores showed evidence of collapse especially in the central area under which is located the sporoplasm (Figures 38, 39 and 40). The polar capsules at the distal ends of the spore seemed to lend rigidity to the spore. Critical point drying caused less shrinkage and it was possible to find a few spores that showed minimal shrinkage (Figures 41 and 42).

Filaments Extruded. Fully extruded polar filaments (Figure 41) of S. maiyai (elongated spore) and a Myxobolus sp. from the mottled

sanddab Citharichthys sordidus (circular in shape) indicated that the polar filaments both possessed two different zones of structural rigidity. In both species the proximal 3-5 micrometers were structurally rigid, being able to support themselves while the remainder of the filament is very pliable showing considerable bending and a tendency to stick to other objects (Figure 42).

The polar filament upon extrusion formed a bulb-like protuberance at the spore terminus measuring approximately 1.0 μm (Figure 43). The filament had a central groove extending for at least 4.0 μ m and probably the entire length of the filament. A junction line was visible between the polar filament and the polar capsule in Figures 43 and 44. The polar filament in Figure 44 showed evidence of compression and wrinkling thus indicating that the proximal filament is larger than the discharge canal.

Some polar filaments (Figure 45) showed blebs (0.55-0.62 μm x 0.28-0.35 μm); however, it was not possible, due to the limited sample size, to determine if these represent artifact or structural entities.

Figure 46 shows a partially extruded filament in the process of eversion. Proximally the filament is thickened containing the outfolding filament. The distal tip shows the actual process of filament eversion which occurred like turning a glove inside out.

Transmission Electron Microscopy (TEM)

The fine structure of the plasmodial stage of Sphaeromyxa maiyai was quite similar to that of the other sphaeromyxan species which have been examined with the electron microscope. The body of the plasmodium consists of two distinct structural zones, an outer structurally simplified ectoplasmic zone and a structurally complex inner endoplasmic zone (Figures 47, 48 and 49). The endoplasmic zone consists of two subzones: the outer made up of a layer approximately 10 μm in thickness of cell organelles, lipid inclusions and developing sporonts; the inner layer consisting of an alveolar zone of vacuoles of varying size. Between the vacuoles and enclosed within the membranes limiting the vacuoles are developing sporoblasts, ripe spores, occasional cell organelles and scattered glycogen granules.

Ectoplasm

Transmission electron micrographs of cross sections of the plasmodial surface showed that the plasmalemma was covered by a single or multilayered reticulate external coating of filamentous mucin-like material. The mucoid layers or glycocalyx consisted either of a single layer varying in thickness between 0.5 and 1.2 μm which usually did not extend appreciably beyond the microvillar apices (Figure 50) or of a bilaminate system in which a more electron dense

layer occurred external to the inner layer (Figure 51). The external layer was approximately 1.6 μm thick. In sections where both layers occurred, the external coat was diffuse between the microvilli and within the invaginations formed by the microvilli while the glycocalar density was maximal in the region around the microvillar apices (Figure 52). The filamentous strands appeared to be firmly attached to the microvillar plasmalemma (Figure 53). The delicate reticulate filaments were anastomotic and not of uniform diameter while thicker filaments were approximately 12-15 nm. The filaments were thickest at or near their sites of bifurcation (Figure 54). Bifurcation sites were more electron dense than the fine filaments and measured approximately 27 nm.

The outer layer of the glycocalyx consisted of much larger filamentous strands approximately 0.025 μm in diameter and the filament bifurcation sites measured approximately 0.12 μm (Figure 54).

The plasmodium was limited by a single simple unit membrane (= plasmalemma) approximately 7.5 nm thick which was made up of two osmiophilic layers separated by an electron transparent layer (Figure 54). The plasmalemma was not observed dividing the ectoplasm or endoplasm into cellular compartments in either electron micrographs or light micrographs. Consequently, the cytoplasm of Sphaeromyxa maiyai appears to be a syncytium composed of ectoplasm and endoplasmic vegetative nuclei exclusive of sporoblasts. The

plasmalemma was not supported by any observed organelles and appeared to form a simple limit to the ectoplasmic matrix.

The ectoplasm proper consisted of the following elements: aggregations of electron dense glycogen particles, aggregations of less electron dense particles resembling unattached ribosomes, pinocytotic vesicles and phagocytotic vacuoles, cylindrical rod-shaped particles, agranular endoplasmic reticulum, and microtubules.

Low power electron micrographs (Figures 47, 48 and 56) showed that the glycogen particles were mostly present in vacuole-like electron transparent deposits dispersed in the ectoplasm. Smaller aggregates of glycogen were present in the dense ectoplasmic matrix. Individual glycogen particles or particles in the beta configuration measured 30-38 nm and the aggregates measured up to approximately 0.2 μm.

Small pinocytotic vesicles were seen invaginating from the plasmalemma (Figures 52 and 57). The pinocytotic vesicles were limited by a single unit membrane and had an internal density slightly greater than the ectoplasmic matrix. The vesicles were dispersed throughout the ectoplasm (Figures 53 and 58).

Large nonsymmetrical vacuoles were frequently evident in communication with the plasmalemma (Figure 59) immediately below the plasmalemmar surface (Figures 50 and 60). The large vacuoles were frequently observed to contain small spherical bodies (Figures 59 and 60).

Cross sections of the plasmodium showed that the so-called brush border of light microscopy was made up of an irregular layer of microvilli approximately 1.0 μm thick. The microvillar layer was uniformly present over the entire plasmodial surface. The microvilli were circular to slightly ovate in cross section (Figure 61) measuring approximately 0.1 μm in diameter. Individual microvilli appeared to be sinuous and were probably several micrometers in length (Figures 34, 48, 53 and 62). Microvilli emanated either individually from the ectoplasm (Figures 68 and 60) or in groups from ectoplasmic crests (Figures 52, 53 and 57). The microvillar core was composed of material of the same density as the ectoplasmic matrix and lacked the formed ectoplasmic elements and glycogen granules. Fine filaments extended from the microvillar core into the outer regions of the ectoplasm (Figures 53 and 63).

Electron dense rod-shaped particles or dense inclusions were dispersed throughout the ectoplasm in some plasmodial samples (Figures 47, 48, 51, 58 and 63). These particles appeared to be more concentrated in some ectoplasmic regions than in others. The particles occurred either singularly or in small clusters; however, they did not show evidence of crystal or aggregate structure characteristic of many viruses as suggested by Lom (1969a). The particle core was electron dense and half a striated appearance. The particles appeared to be limited by a unit membrane (Figure 63). The particles

were approximately 40 nm thick and up to 0.5 μm in length. These particles were always limited to the ectoplasm.

The ectoplasmic layer contained numerous tubules which closely resembled the agranular endoplasmic reticulum (Figures 51, 52, 53, 60 and 65). The agranular tubuli were limited by a simple unit membrane and were approximately 0.045 μm in diameter. No cisternae were observed.

Microtubules were present in the ectoplasm of the occasional sections of the Sphaeromyxa maiyai (Figures 51, 55 and 65). The microtubules were generally not very distinctive nor very abundant.

The occurrence of the microtubules in only occasional sections may represent a regional distribution as the ectoplasm was more sharply delimited from the endoplasm in areas where microtubuli were observed.

In an unusual instance where a developing sporoblast was present within the ectoplasm proper (Figure 65), microtubules were dispersed throughout the ectoplasm. Aside from the presence of the developing sporoblast within the ectoplasm, the ectoplasmic-endoplasmic junction was of the sharp Type 1 (see p. 21) which was commonly associated with the presence of ectoplasmic microtubules.

The ectoplasm contained numerous unattached ribosome-like particles measuring approximately 27 nm in diameter (Figures 53 and 60). The ribosome-like particles were approximately the same size

as the beta glycogen particles. Ribosomal particles were more electron transparent than either the alpha or beta glycogen particles.

The Ectoplasmic-Endoplasmic Junction

The transition between ectoplasm and endoplasm as seen with the electron microscope, was of two basically distinct types.

Type 1. Microtubular-mitochondrial junction. In this type of junction a sharp and distinct separation between ectoplasmic and endoplasmic organelles occurred. A zone of ectoplasmic microtubules formed a boundary between the two layers (Figures 48, 51 and 55). Immediately below the ectoplasmic microtubuli, the endoplasm contained a dense zone of mitochondria, vacuoles, and sporonts in different developmental stages. The mitochondria were orientated parallel to the ectoplasmic microtubuli. The sharply defined Type 1 junction was not common and was observed only in a few sections.

Type II. The Indistinct Junction. The indistinct type of junction was most prevalent (Figures 49, 62, 65 and 66). In this type the endoplasmic mitochondria, vacuoles and to a lesser extent developing sporonts spread into the ectoplasm for varying distances. However, with one exception (Figure 65), in approximately 100 cross sections neither mitochondria nor sporonts were observed near the ectoplasmic surface. Deposits of ectoplasmic glycogen extended into the endoplasm.

The Endoplasm

The endoplasmic region constitutes the major organelle-containing zone of the myxosporidian plasmodium. The endoplasm, unlike the ectoplasm, formed a true syncytium containing the cellular organelles. Embedded in the endoplasmic syncytium were vegetative and generative nuclei. The vegetative nuclei were free floating (Figure 62) within the endoplasmic syncytium. The generative nuclei were enclosed by cell membranes and are destined to become either the enveloping or enveloped cell of the developing sporoblasts (Lom, 1969).

Mitochondria. Typically the mitochondria within the endoplasm were elongated cylinders situated close to the ectoplasmic-endoplasmic junction. The alveolar region of the endoplasm contained fewer, more widely dispersed mitochondria. The mitochondria of the endoplasmic syncytium measured up to 4.0 μm in length and 0.5 μm in width. The mitochondria were often sinuous. The internal membrane formed sac-like or goblet-shaped cristi (Figures 67, 68 and 69). The mitochondrial matrix was composed of a flocculent structurless material.

Lipid Inclusions. Lipid inclusion bodies were generally present throughout the outer endoplasmic region. The regional distribution of lipid bodies differed throughout the plasmodium. Lipid inclusions were most numerous adjacent to and immediately underneath the microtubular-mitochondrial type of ecto-endoplasmic junction

(Figures 47, 64 and 70). The lipid inclusions were not enveloped by a unit membrane. The alveolar endoplasm contained relatively few lipid inclusion bodies between the vacuolar membranes (Figures 49 and 70). Occasional lipid inclusions occurred in vacuolar spaces surrounding the developing and near mature sporoblasts (Figure 68).

Autophagic Vacuoles and Residual Bodies. The outer endoplasmic region contained a multitude of phagocytic vacuoles (Figures 47, 48, 49, 71 and 72). The vacuoles were limited by a single unit membrane. Vacuoles contained a wide variety of membranous residues varying from simple membrane fragments (Figure 72) and membrane whorls (Figures 47 and 71) to highly structured myeloid figures (Figure 73). Occasionally autophagic vacuoles containing morphologically recognizable cytoplasmic components such as mitochondria microtubules or agranular endoplasmic reticulum were encountered (Figures 67 and 71). Inclusion bodies resembling alpha-glycogen aggregates were frequently seen within the phagocytic vacuoles and additionally within the membrane fragments and whorls within the parent vacuole (Figures 49 and 67). The large vacuoles of the alveolar endoplasmic region contained very few membrane fragments (Figures 48 and 49).

Agranular Endoplasmic Reticulum. Elements of the agranular endoplasmic reticulum occurred in low concentrations throughout the endoplasm. In the cytoplasmic portion of the endoplasm the agranular

endoplasmic reticulum occurred principally as single convoluted tubules (Figures 71 and 72). Within the developing sporoblast, the agranular endoplasmic reticulum most often occurred as isolated tubuli; however, occasional clusters or lamelliform sheets were present.

Microtubules. Microtubules were seldom observed in the outer portion of the endoplasm. The cytoplasmic network separating the alveolar vacuoles of the endoplasm contained a relatively high concentration of microtubules (Figure 74). It was within the developing sporoblasts that the microtubuli became a prominent organelle. They were found to exist either free within the sporoblast cytoplasm (Figure 48) or in linear clusters under the sporoblast membrane (Figure 75). Linear groupings of 8-14 microtubules were aligned immediately under the longitudinal striations and to a lesser extent along the sutural line (Figure 68).

Glycogen Aggregates and Ribosomes. Alpha glycogen particles occurred throughout the cytoplasmic portion of the endoplasm and within the developing sporoblasts (Figures 64 and 76). The region between the alveolar vacuoles contained a lesser concentration of glycogen particles which were also present within some of the endoplasmic autophagic vacuoles (Figures 56 and 67).

Small particles resembling free ribosomes were found throughout the cytoplasmic endoplasm. These particles were slightly smaller

and more electron transparent than the ubiquitous glycogen aggregates (Figures 71 and 72). Rough surface endoplasmic reticulum with its attached ribosomes was found only within the developing sporoblasts.

Golgi Apparatus. Golgi complexes were not encountered with the cytoplasmic portion of the endoplasm in the present study. This finding was in contrast to that of Lom (1969a) who reported finding occasional Golgi complexes in the endoplasm. Golgi complexes first became evident inside the early sporoblasts (Figures 77 and 78) during the process of capsulogenesis and polar formation.

Sporoblasts

The earliest developmental stage of Sphaeromyxa maiyai observed consisted of pairs of cells joined together (Figures 49, 66, 72, 77 and 78). Apparently the outer cell rapidly envelopes the inner sporoblast primordium, forming a covering over this inner enveloped cell. The surface of the outer enveloping cell was covered with bluntly lobulate (Figure 66) to bifurcating filiform pseudopodia. The inner cell was typically rounded, containing a large nucleus with an eccentrically located nucleolus (Figure 66).

The sporoblasts were situated either immediately below the ectoplasm or within the vacuolate endoplasm between the alveolar vacuoles. The sporoblasts immediately adjacent to the ectoplasm formed a distinct boundary with the ectoplasm, and seldom extended

into the ectoplasmic zone. The pseudopodia of the outer enveloping cell extended into the ectoplasmic-endoplasmic junctional area. However, they were not observed to extend appreciably beyond the junction with one exception (Figure 65).

The outer enveloping cell of the developing sporoblast was limited by two unit membranes separated by an uneven space approximately 10-50 nm thick (Figure 69). Cross sections of the pseudopodial extensions also showed the double unit membrane composition of the outer enveloping cell (Figure 69). The cells of the developing sporoblast were limited by single unit membranes.

In accordance with Lom (1969a), it was observed that the cytoplasm of the inner sporoblastic cells were more electron dense and that cisternae of rough endoplasmic reticulum became a prominent cytoplasmic structure.

The inner sporoblastic cell initiated a series of mitotic diversions forming the requisite number of cells to form one or two spores depending on whether the sporoblast under consideration was destined to develop along a monosporoblastic or disporoblastic pattern. In the former, six cells developed in the sporoblast; in the latter, 12 cells developed within the enveloped sporoblast cell. The following cells are derived from the original sporoblast cell: two shell valve cells, two capsulogenous cells, and two sporoplasm cells per spore.

The ontogenetic events from the two-celled state to the juvenile spore in Sphaeromyxa maiyai were essentially identical to those described by Lom (1969a) for S. cf. magna and Sphaeromyxa sp. from Dasycottus sp.

The Differentiated Spore

The nearly mature spore was surrounded by a large vacuole which appeared to have been formed by the degeneration of the outer enveloping cell of the early sporoblastic stage. The vacuole contained degenerating mitochondria, lipid droplets, membrane debris, alpha glycogen particles, and occasional microtubules (Figures 68 and 79). The vacuole was limited externally by two single unit membranes in juxtaposition to each other (Figures 68, 79 and 80). A residual membrane or membranes was closely applied to the external surface of the spore (Figures 79, 81, 83 and 84).

The differentiated mature spore consisted of three distinctly different types of cells: the outer shell valve cells, the polar filament forming capsulogenous cells, and the reproductive sporoblastic cells.

As the spore matured, the external wall, formed by the shell valve cells, became increasingly impervious to the embedding plastics. In the mature spore it was not possible to obtain undamaged specimens even when prolonged infiltration was employed.

Shell Valve Cells. The shell valve cells form the outer or protective covering of the spore. In early sporoblasts the shell valve cells were rich in cell organelles, mitochondria, granular endoplasmic reticulum and microtubules (Figure 68). As the spore matured, cellular organelles disappeared from the shell valve cells (Figures 81 and 85). This was particularly evident in the case of mitochondria and microtubuli. The microtubuli in association with the sutural line degenerated early in the maturation process.

During the process of organelle degeneration the shell valve cells contract and become more electron dense. In the mature spore the shell valve cells were approximately 0.32-0.45 μm in thickness. The shell valve cells consisted of three layers (Figures 86 and 87). The outer surface is limited by a unit membrane which extends inward along the suture line (Figure 87). The inner surface adjacent to and probably adhering to the polar capsule was also limited by a unit membrane (Figure 87). Contiguous with the inner and outer limiting membrane was an electron dense granular band approximately 7.7 nm thick (Figures 86 and 87). The space between the electron dense bands was filled by a granular material of higher electron transparency than the electron dense bands. The lighter middle granular layer varied in thickness, being thickest in the space between longitudinal striations and thinnest under the longitudinal striations (Figure 86).

Externally the shell valve cells were limited by a highly convoluted residual unit membrane.

The longitudinal striations are subtended by groups of longitudinally orientated microtubules (Figure 79). These occurred as a concave linear array of 9-15 tubules under each groove (Figure 88). The microtubules degenerate as the spore matures and are not present in the mature spore (Figures 81 and 86). In the longitudinal groove between the unit membrane and the microtubules a thin sheet-like partition separates the former from the latter. The partition was extremely delicate being somewhat thinner than a unit membrane (Figures 83, 84 and 88).

In less mature spores the shell valve cells were separated from the capsulogenic cells by an irregular space of 25-100 nm containing a flocculent material and occasional alpha glycogen particles (Figure 83).

The shell valve cells were joined together at the sutural line by septate desmosomes. These consisted of parallel arrays of lamellae at right angles to the surface membrane (Figures 79, 81 and 88). The shell valve membranes were separated by a space of 11.7 nm and the parallel lamellae had a periodicity of approximately 30.6 nm.

The Polar Capsule. The polar capsule was surrounded by the capsulogenous cell throughout its entire development (Figures 79, 82, 83 and 89). In the immature spore (Figures 68, 79, 80 and 90) the

capsulogenous cell was rich in cellular organelles, both around the capsular primordium and in the vicinity of the sporoplasm at the basal ends of the polar capsule. Microtubules occurred scattered throughout the distal or capsular region of the capsulogenous cell (Figure 83). As the capsulogenous cell matures the cytoplasm around the polar capsule body condenses and the cellular organelles disappear from this region (Figures 83, 88, 91 and 92). Microtubuli appeared to remain in the capsular region longer than most other organelles. The basal region of the capsulogenous cell retained the cellular organelles throughout capsulogenesis (Figures 17, 89 and 90). A prominent Golgi complex was usually present in the capsulogenous cell in close proximity to the capsular primordium (Figure 90).

The channel for filament discharge, located at the apical ends of the spore, was only partially evident. The polar filament appears to be continuous, in the channel area, with the electron dense granular material which forms the outer layer of the polar capsule (Figures 85 and 91). External to the electron dense layer but still within the capsulogenous cell, an electron transparent striated region separated the discharge canal from the shell valve cell.

Between the striated capsulogenous cap and the external surface of the spore shell valve cell was blocked by an electron dense stopper measuring 0.9 μm x 0.13 μm (Figures 26, 85, 91 and 92).

The polar capsule wall was composed of two layers, an outer thin granular electron dense layer 60-80 nm thick and a much thicker homogenous electron translucent inner layer approximately 150-200 nm thick (Figures 92, 94 and 95).

During capsulogenesis an extremely electron dense material invades the inner capsular wall (Figures 79, 83, 88, 89, 93 and 94). During sectioning the electron dense layer was typically displaced indicating that it had a much higher density than the surrounding tissues (Figures 79 and 93). It appears that this material eventually surrounds the polar capsule (Figure 93). Because of the difficulty in obtaining satisfactory sections of mature spores that showed minimal damage, it was not possible to ascertain the nature of this material in the mature spore.

The Polar Filament. The polar filament was longitudinally folded within the polar capsule (Figure 79). The wide thin filament (fl) attaches to the apical aspect of the polar capsule (Figures 79 and 94). The filament then extends basally, recurves at the basal end and extends apically again (fla) on the opposite wall as the descending filament of the capsule. This coiling process is repeated four times, each filament occurring on the opposite side of the capsule from its mirror image partner.

The wide thin filaments which form the ultimate proximal "stiff" portions of the extruded polar filament were approximately 0.75 μm

by 0.012 μm. Successive filament coils decreased in size: (f2-f2a) 0.56 x 0.019 μm; f3-f3a 0.5 x 0.019 μm; f4-f4a 0.44 μm x 0.019 μm.

The f1-f1a area of the filament differed structurally in several aspects from the remaining filament coils. This portion of the filament was significantly wider and thinner than the other folds. Additionally the filament lumen was irregularly wrinkled (Figure 79). The lumen of the remaining filament was formed by two parallel electron dense lines approximately 2.5 nm thick and separated by a space of about 17.5 nm. The luminal space was of the same density and apparent structure as the filament matrix (Figure 95).

The filament proper was surrounded by several layers of varying electron density (Figures 79, 82, 83 and 95). The outermost layer merges imperceptably with the capsular matrix. Interior to this layer was a less electron dense layer 11.7 nm thick. The filament proper was surrounded by a serrated electron dense zone approximately 12 nm thick, and appeared to be composed of longitudinally orientated fine filaments having a periodicity of approximately 11.1 nm. The filament matrix was composed of a homogenous electron dense material (Figure 95).

The Sporoplasm. The sporoplasm was centrally located within the developing and mature spore (Figures 89, 96, 97, 98 and 99). The sporoplasm was roughly elliptical in longitudinal section and circular in cross section. Longitudinal sections revealed the presence of long

loboform extensions extending from the sporoplasm between the shell valve cells and the capsulogenic cells (Figures 89, 97, 98 and 99). The extensions were filled with a finely granular cytoplasm devoid of cell organelles.

In the sections examined the sporoplasm contained a single centrally located nucleus of the vesicular type with scattered aggregates of condensed chromatin. The nucleus was within the sporoplasm cell.

The cytoplasm of the sporoplasm cell was rich in ribosomes. In the early sporoplasm cell (Figure 79) many irregular masses of rough endoplasmic reticulum were seen. In more developed sporoblasts the rough endoplasmic reticulum appeared as several flat cisternae concentrically arranged around the sporoplasm nucleus (Figures 89, 97, 98 and 99). As the sporoplasm matured the cytoplasm became increasingly electron dense due to the increased density of the ribosomes.

Mitochondria of the developing sporoplasm were delimited by two membranes within which lay many seemingly unattached ovoid-to-spherical vesicles. In occasional sections continuity of such spheres with the inner mitochondrial membrane could be seen (Figure 99). The sporoplasm contained typically from 2-6 mitochondria.

One or two prominent Golgi complexes were observed in the sporoplasm (Figure 97).

DISCUSSION

The present study was concerned with Sphaeromyxa maiyai: its taxonomic description as a new species, the light microscopy of the trophic and spore stages, and the ultrastructure of the trophic and spore stages employing both the scanning and transmission electron microscopes.

Sphaeromyxa maiyai sp. n. (Morrison and Pratt, 1973) belongs to the informal incurvata group of Laird (1953). The incurvata group is characterized by the "arcuate spores having pyriform polar capsules" as opposed to the "straight or slightly curved fusiform or ovoid spores having ovoid polar capsules" of the balbianii group. One species namely S. pultai Tripathi (1953) possesses characteristics intermediate between the two groups. The spore of S. pultai is elongated and straight while the polar capsules are decidedly pyriform.

The trophozoite of S. maiyai sp. n. is larger than any heretofore described sphaeromyxan species. Often it reaches a diameter of 1.0 cm or more. Because trophozoites of many species of Sphaeromyxa remain unknown it is, at present, impossible to make valid speculations on species criteria using trophozoite size as a factor. However, of the known trophozoites only those of the following species approach S. maiyai sp. n. in size: S. incurvata, S. hellandi, S. gasterostei and S. tripterygii. The other sphaeromyxans have considerably smaller trophozoites.

The spores of S. gasterostei and of S. incurvata are larger than those of the present species. S. gasterostei belongs to the balbianii group having decidedly oval polar capsules and is several times larger than S. maiyai sp. n. in all dimensions (Laird, 1953). The spores of S. ovula and S. tripterygii are considerably smaller than S. maiyai sp. n.

The spores of S. hellandi, S. arcuata, and S. sabrazesi closely resemble those of S. maiyai. The spore of S. hellandi is smaller than that of S. maiyai sp. n. (20-26 μm vs. 23-30 μm) while the polar capsule of the former is larger.

S. arcuata in stained preparation closely resembles S. maiyai sp. n. in overall dimensions. The valves of the spore wall are longitudinally striated. The spore length of the two species is similar; however, S. arcuata has a greater maximum spore breadth than S. maiyai sp. n. (6-8 μm vs 2.9-5.3 μm). Also the former species possesses a narrower polar capsule than the latter (1.5-2.0 μm vs 2.9-4.4 μm). Unfortunately in the species description of S. arcuata Fanthan (1930) did not record data for fresh material nor did he record finding trophozoite stages.

S. sabrazesi most closely resembles S. maiyai sp. n. The largest trophozoites recorded for S. sabrazesi Schroder (1907 and 1910) were only one-half the size of those of the Oregon species. The spores differ in that those of S. sabrazesi are slightly narrower

(3-4.3 μm vs. 5.0-7.2 μm) and the polar capsules are narrower in S. sabrazesi than in S. maiyai sp. n. (2-3 μm vs. 3.0-4.2 μm).

It is concluded that Sphaeromyxa maiyai sp. n. of the Pacific tomcod has definite affinities with other members of the incurvata group; however, it differs sufficiently from other members of this group in trophozoite and spore detail to warrant its description as a new species (Morrison and Pratt, 1973).

Fantham and Porter (1912) described the effects of several coelozoic species of myxosporidians namely Myxidium. Ceratomyxa, Chloromyxum and Leptotheca on the gall bladder of host fish. They found that moderately to heavily infected gall bladders were thicker than uninfected gall bladders and that the bile was colored, changing from a normal green or green-yellow to a bright yellow or yellowish brown. Additionally the bile density increased in infected fishes. They attributed these alterations to epithelial irritation caused by the presence of the myxosporidian trophic stages and spores "leading to a catarrhal secretion of mucus and desquamation of epithelium." Sphaeromyxa maiyai caused no apparent changes in the bile or gall bladder mucosa even when several large trophic stages and numerous spores were present. Sphaeromyxan species, unlike many other myxosporidian genera, do not adhere to the gall bladder epithelium and this might account for the lack of changes in the gall bladder epithelium. Sphaeromyxa maiyai did, however, cause a hypertrophy of

the gall bladder apparently due to pressure exerted by the massive trophic stages.

The trophozoite of myxosporidians consists of two recognized zones--an outer limiting amorphous ectoplasmic zone and an inner syncytial endoplasmic zone containing organelles (Schroder, 1907; Mavor, 1916; and Davis, 1916 and 1923). Cohn (1896) described the presence of a third layer "the mesoplasm" in the trophozoite of Myxidium lieberkuhni. This latter, situated in the center of the endoplasm, probably corresponds with the alveolar layer of the sphaeromyxans. In the genus Sphaeromyxa the trophozoite consists of three zones: the outer ectoplasm, the granular endoplasm, and a highly alveolar central zone which Lom (1969a) considers to be an extension of the endoplasm.

Lom and Hoffman (1971) were the first to publish SEM micrographs showing the surface structure of spores of two species of myxosporidians (Myxosoma cerebralis and M. cartilaginis). The present study reports on the SEM of both the previously unstudied trophic stage and the spore stage of a new species of myxosporidian, Sphaeromyxa maiyai.

The dense mucoid layer covering the trophozoite surface limited the usefulness of the SEM. The mucoid layer was partially disintegrated by using 0.005% EDTA (Miller and Danagan, 1971) revealing the presence of delicate microvillus-like projections on the ectoplasmic

surface. This procedure, however, tended to disrupt the trophozoite causing it to fragment and partially disintegrate.

The mechanism by which spores are released from the trophozoite in the genus Sphaeromyxa remains unresolved. The present study failed to find any evidence of pores in the limiting membrane; consequently, it is supposed that spore release is accomplished by one of two methods: the complete disintegration of the trophozoite, or, partial lysis of the limiting membrane. In histozoic myxosporidians spores are liberated by the rupturing of cysts (Davis, 1923; Dunkerly, 1925; Wyatt and Pratt, 1963; and Hoffman et al., 1965) or by the complete degeneration of the host which occurs in species infected by the genus Kudoa (Lom, 1970; Gilchrist, 1924; and Willis, 1949).

In both the Microsporidea and Myxosporidea the polar filament consists of an elongated tube which is released from the polar capsule by a process of evagination (Microsporidea: Morgenthaler, 1922; Ohshima, 1937; West, 1960; Lom and Vávra, 1963; and Lom, 1972. Myxosporidea: Lom, 1964 and 1969a; Lom and Vávra, 1964; and Lom and de Puytorac, 1965a). Functionally the two organelles differ. In the Microsporidea the filament serves as a device to penetrate the host cell and to liberate the sporoplasm (Ohshima, 1937; Lom and Corliss, 1967; and Lom, 1972), while in the Myxosporidea the polar filaments serve as attachment organelles (Lom and Corliss, 1967; and

Lom, 1964).

Scanning electron microscopy showed the polar filament of S. maiyai in the process of evagination (Figure 46). The polar filament was partially evaginated, and the flow of the center of the filament membrane to form the definitive outer surface of the polar filament was evident. The extruded filament as observed in araldite embedded cross sections (Lom, 1964) appeared as a ring with two folds. This configuration was observed in scanning electron microscopy of the present study (Figure 43 as longitudinal groove, Lg).

All fundamental ultrastructural features of S. maiyai agreed with the findings observed in other myxosporidian genera. The ultrastructural organization of the sphaeromyxan trophozoite is quite similar to that of Chloromyxum cristatum, Myxidium lieberkuhni, Henneguya psorospermica, Zschlokkela nova (Lom and de Puytorac, 1965a and b), Henneguya pinnae (Schubert, 1967) and Sphaeromyxa cf. magna (Lom, 1969a).

Ultrastructural studies on mature myxosporidian spores have been beset by technical problems of fixation, resin infiltration and embedment (Cheissin et al., 1961; Gould, 1970; Schubert, 1967; Lom, 1964 and 1969a). Cheissin et al., 1961, recommended fixation for six months in 4.% neutral formalin, postfixation in 1% solution of OsO_4, and embedment in butylmethylacrilate in a ratio of 8:1. Gould (1970) also employed extended formalin fixation (one month in 10%

formalin); however, embedment was in Bojax resin mixture. The micrographs of Cheissin et al. and those of Gould show extensive fracturing of the spore. Fixation seems to be a lesser problem than resin infiltration. In the present study satisfactory results were obtained on spores still within the trophozoite using gluteraldehyde fixation for 12-24 hours followed by extended infiltration with araldite for approximately 1-2 weeks.

Ectoplasmic inclusion bodies (40 nm x 0.5 μm) were found in S. maiyai. Lom (1969a) first reported these tubular inclusion bodies in Sphaeromyxa cf. magna, stating, "their wall consists of unit membrane; the core, more or less electron dense, reveals folded structure. These tubules are often closely packed into irregular bundles and can be found in no other part of the plasmodium but the ectoplasm." According to Lom these inclusion bodies are found only in the genus Sphaeromyxa and resemble certain types of viral inclusions. The inclusions in S. maiyai were structurally identical with those described by Lom differing only in that they were not observed in closely packed bundles.

Lom (1969a) reported finding long, irregular simple fibrils throughout the ectoplasm being most concentrated at the ecto-endoplasmic junction. He emphatically stated that these were not microtubules. Lom's failure to observe microtubules at the endoplasmic-ectoplasmic junction was possibly a result of the fixation techniques

employed. Lom (1964 and 1969a) principally used Palade's fixative (Veronal buffered 1% osmic acid solution). According to Du Praw (1968), and Hayat (1970), microtubules are not well preserved by standard OsO_4 fixation procedures. Observations on S. maiyai are not in agreement with Lom's findings. Numerous microtubules were found in the ectoplasm in addition to the fibrillar meshwork. Microtubules were also present in the septae separating the vacuoles of the alveolar layer, and as supporting elements subtending the longitudinal grooves of the developing spore. The latter microtubules disappear as the spore approaches maturity.

Centrioles have not been reported from either developing sporoblasts within the trophozoite or from mature spores.

Lom and de Puytorac (1965a) first reported observing "myeloid" formations in the trophic stage of Henneguya psorospermica and Myxidium lieberkuhni. Gould (1970) reported finding myelin figures within the spore of Ceratomyxa shasta. Myeloid figures were quite prevalent in Sphaeromyxa maiyai. Functionally the myeloid figures are an enigma. Myeloid figures (multilaminate whorls of smooth membranes) are usually associated with the lysosomal-autophagic vacuolar system. According to Abraham et al. (1968) myeloid bodies may form as a result of lysosomal enzyme loss and autophagy. They reported that the sequence of events in lysosomes were "ingestion of mitochondria, glycogen, and endoplasmic reticulum (autophagic

vacuoles), followed by the occurrence of intermediate stages of partially disgested mitochondria, with disorganization of membranes, and finally the development of tightly packed whorls of membranes (myeloid bodies), possibly derived from degenerating organelles and cytomembranes." Abraham et al. (1968) reported extensive myeloid body formation resulting from Chloroquine administration to rat liver cells. Extensive myeloid figure development occurs in the presence of several types of congenital "storage" diseases such as Tay-Sachs disease, Neimann-Pick disease and acid mucopolysaccharidosis (Volk and Wallace, 1966).

Lumsden et al. (1972) reported fingerprint-like whorls of smooth surface membranes that were continuous with agranular and granular endoplasmic cisternae in hepatocellular lesions caused by Trypanosoma gambiense. The whorls enveloped lipid droplets, mitochondria, lysosomes, and microbodies.

Steiner et al. (1964) and Tanikawa (1968) considered the whorling of endoplasmic cisternae as a degenerative ergastroplasmic reaction to cell injury.

In the present study myeloid figures (= membranous whorls) were located within membrane-limited vacuoles. These vacuoles appear to be autophagic vacuoles thus indicating that myeloid bodies form from organelle digestion as suggested by Abraham et al. (1968) rather than by expansion of the endoplasmic reticulum as suggested

by Lumsden et al. (1972).

Lipid droplets were regionally numerous and often quite prominent within the trophozoite of S. maiyai. Lom (1969a) reported finding few lipid droplets in Sphaeromyxa cf. magna and Sphaeromyxa sp. from marine fishes. In an earlier study Lom and de Puytorac (1965a) reported numerous lipid droplets in several species of freshwater coelozoic myxosporidians.

The septate desmosomes of S. maiyai appear similar to those occurring between invertebrate epithelial cells. Wood (1959) first described septate desmosomes between the epithelial cells of Hydra as "a series of orientated parallel lamellae arranged perpendicular to the apposed cell surfaces and spanning the intercellular region." Septate desmosomes have been found in numerous phylogenetically separated invertebrate groups: anemones (Grimstone et al., 1958), flatworms (Wood, 1959), annelids (Hama, 1959), insects (Fernandez-Moran, 1958 and Locke, 1961 and 1965), and echinoderm embryos (Balinsky, 1959). Septate desmosomes were observed by Gould (1970) in myxosporidian spores forming junctions between shell valve cells at the level of the sutural line. The two valves were separated by a space of about 400 Å (40 nm), and the septate lamellae showed a periodicity of approximately 80 Å (8 nm). He noted that each valve contained exactly 15 lamellae.

In Sphaeromyxa maiyai the septate desmosomes had a periodicity of approximately 30.6 nm (306 Å) and the shell valve membranes were separated by approximately 11.7 nm (117 Å). Septate desmosomes have not been reported from other myxosporidian spores; however, several figures of Lom (1969) (Figures 23 and 27) indicate that septate desmosomes occurred in Sphaeromyxa cf. magna.

Ultrastructural studies on myxosporidian parasites have illustrated the complex morphological relationships of multicellular spores and the polynuclear syncitial trophic stage. These features, especially the polycellularity of the spore and the striking differences between the capsulogenous cells, valvogenic cells and sporoplasm, separate the Class Heteronucleidea (Lom and Vávra, 1962) (Order Myxosporidea) (Class Isonucleidea, Lom and Vávra, 1962) is either not related to the myxosporidians, or is only very remotely related as indicated by differences between sporogenesis, spore structure and trophozoite structure.

BIBLIOGRAPHY

Abraham, R., R. Hendy and P. Grasso. 1968. Formation of myeloid bodies in rat liver lysosomes after chloroquine administration. Experimental and Molecular Pathology 9:212-229.

Auerbach, M. 1910. Die Cnidosporidien (Myxosporidien, Actinomyxidien, Microsporidien). Eine Monographische Studie. Leipzig, W. Klinkhardt. 261 p.

Awerinzew, S. 1911. Studien uber parasitische. Protozoen. VII. Ueber Sporenbildung bei Myxidium sp. aus der Gallenblase von Cottus scorpius. Archiv fur Protistenkunde 23:199-204.

Balbiani, G. 1863. Sur l'organization et la nature des psorospermies. Comptes Rendus (Hebdomadaires) des Seances de l'Academie des Sciences 57:157-161.

Balinsky, B. 1959. An electron microscope investigation of the mechanism of adhesion of the cells in a sea urchin blastula and gastrula. Experimental Cell Research 16:429.

Butschli, O. 1881. Myxosporidia. Beitrage zur Kenntnis dor Fischpsorospermien. Zeitschrift fur wissenschaftliche Zoologie 35:629-651.

_____ 1887. Mastigophora. p. 1987-1097. In: H. G. Bronn (ed.) Klassen und Ordnungen des Tierreichs. Vol. 1. Verlagshandl, C. F. Wintersche.

Caullery, M. and F. Mesnil. 1905. Recherches sur les Actinomyxidies. Archiv fur Protistenkunde 6:272-388.

Chapman, G. B. and L. G. Tilney. 1959a. Cytological studies of the nematocysts of Hydra. I. Desmoemes, Isorhizas, Cnidocils, and supporting structures. The Journal of Biophysical and Biochemical Cytology 5:69-79.

_____ 1959b. Cytological studies of the nematocysts of Hydra. II. The Stenoteles. The Journal of Biophysical and Biochemical Cytology 5:79-85.

Cheissin, E. M., S. S. Shulman and L. P. Vinnitchenko. 1961. Stroenie spor Myxobolus. Tsitologia 3:662-667.

Cohn, L. 1896. Uber die Myxosporidien von Esox lucius und Perca fluviatilis. Zoologische Jahrbucher Abtheilung fur Anatomie und Ontogenie der Thiere 9:229-272.

Creplin, J.C.H. 1842. Beschreibung der Psorospermien des Kaulbarsches nebst einigen Bemerkungen uber die der Plotze und andere. Archiv fur naturgeschichte 8:61-66.

Davis, H. S. 1916. The structure and development of a Myxosporidian parasite of the squeteague, Cynoscion regalis. Journal of Morphology 27:333-377.

_____ 1923. Studies on sporulation and development of the cysts in a new species of Myxosporidia Lentospora ovalis. Journal of Morphology 37:425-454.

Delage, Y. and E. Herouard. 1896. La cellule et les Protozoaires. p. 251-285. In Traite de Zoologie Concrete. Vol. I. Paris, Schleicher Freres.

Doflein, F. 1898. Studien zur naturgeschichte der Protozoen. III Uber Myxosporidien. Zoologische Jahrbucher Abtheilung fur Anatomie und Ontogenie der Thiere 12:281-350.

_____ 1901. Die Protozoen als parasiten und Krankheitserreger. Jena, Gustav Fischer. 274 p.

Dujardine, M. F. 1845. Histoire naturelle des Helminthes ou vers intestinaux. Paris, Roret. 654 p.

Dunkerly, J. S. 1925. The development and relationships of the Myxosporidia. The Quarterly Journal of Microscopical Science. 69:185-216.

DuPraw, E. J. 1968. Cell and Molecular Biology. New York and London, Academic Press. 739 p.

Emery, C. 1909. Myxosporidia sono protozoi. Monitore Zoologico Italiano 20:247-249.

Erdmann, R. 1917. New facts and views concerning the occurrence of a sexual process in the Myxosporidian life cycle. The American Naturalist 51:719-739.

Fantham, H. B. 1930. Some parasitic protozoa found in South Africa. XIII. The South African Journal of Science 27:376-390.

Fantham, H. B. and A. Porter. 1912. Some effects of the occurrence of Myxosporidia in the gall bladder of fishes. Annals of Tropical Medicine and Parasitology 6:467-481.

Fernandez-Moran, H. 1958. Fine structure of the light perceptors in the compound eyes in insects. Experimental Cell Research 5:586-598.

Georgevitch, J. 1914. Etude du cycle evolutif chez les Myxosporidies. Archives de Zoologie Experimentale et Generale 54:387-409.

_____ 1916. Sur le cycle evolutif de Ceratomyxa herouardi Georgevitch. Comptes Rendus (Hebdomadaires) des Seances de l'Academie des Sciences 163:983-985.

_____ 1917. Recherches sur le developpement de Ceratomyxa herouardi Georgevitch. Archives de Zoologie Experimentale et Generale 56:375-399.

_____ 1919. Etudes sur le developpement de Myxidium gadi Georgevitch. Archives de Zoologie Experimentale et Generale 58:251-289.

_____ 1929. Recherches sur Geratomyxa maenae nov. sp. Archiv fur Protistenkunde 65:106-123.

_____ 1935. Uber diplo und Haplophase im Entwicklungskreise des Myxosporidien. Archiv fur Protistenkunde 84:419-428.

_____ 1936. Uber diplo und haplophase im Entwicklungskreise des Myxosporids Zschokkella rovig nensis Nemeczek. Archiv fur Protistenkunde 84:419-428.

Gilchrist, J. D. F. 1924. A protozoal parasite (Chloromyxum thyrsites, sp. n.) of the Cape sea-fish, the "snoek" (Thyrsites atun Euphr.). Transactions of the Royal Society of South Africa 11:263-273.

Gottschalk, C. 1958. Die Amobosporidien. Eine vergleichende Betrachtung ikrer Entwicklungszyklen unter Berucksichtignung ihrer systematischen Stellung im Tierreich. Zeitschrift fur Wissenschaftlicke Zoologie 160:1-38.

Gould, R. W. 1970. Occurrence of the protozoan fish parasite Ceratomyxa shasta in the Deschutes River basin and the ultrastructure of the spore. Master's thesis. Corvallis, Oregon State University. 51 numb. leaves.

Grasse, P. P. 1960. Les Myxosporidies sont des organismes pluricellulaires. Comptes Rendus (Hebdomadaires) des Seances de l'Academie des Sciences 251:2638-2640.

Grell, K. G. 1956. Protozoologie. Berlin, Gottingen, Heidelberg, Springer Verlag. 284 p.

Grimstone, A. V., R. W. Horne, C. F. A. Pantin and E. A. Robseon. 1958. The fine structure of the mesenteries of the sea anemone Metridium senile. The Quarterly Journal of Microscopical Science 99:523.

Gurley, R. R. 1893. On the classification of the Myxosporidia, a group of protozoan parasites infesting fishes. Bulletin of the United States Fisheries Commission (for 1891) 11:407-420.

_____ 1894. The Myxosporidia or Psorosperms of fishes and the epidemics produced by them. Report of the United States Fisheries Commission (for 1892) 26:65-304.

Hale, L. J. 1965. Biological Laboratory Data. 2nd ed. London, Methuen and Co., Ltd. 147 p.

Hama, K. 1959. Some observations on the fine structure of the giant nerve fibers of the earth worm Eisenia foetida. The Journal of Biophysical and Biochemical Cytology 6:61-72.

Hayat, M. A. 1970. Principles and Techniques of Electron Microscopy: Biological Applications. Vol. I. New York, Van Nostrand Reinhold Co. 412 p.

Hoffman, G. L., R. E. Putz and C. E. Dunbar. 1965. Studies on Myxosoma cartilaginis n. sp. (Protozoa: Myxosporidea) of North American freshwater fishes. The Journal of Protozoology 12:319-332.

Humason, G. L. 1967. Animal Tissue Techniques. 2nd ed. San Francisco, W. H. Freeman and Co. 569 p.

Jurine, L. L. 1825. Histoire abregee des poissons du lac Leman. Memories de la Societe de Physique et d'Histoire Naturelle de Geneve 3:133-232.

Kudo, R. R. 1919. Studies on Myxosporidia. A synopsis of genera and species of Myxosporidia. Illinois Biological Monographs 5:1-265.

_____ 1921. On the effect of some fixatives upon Myxosporidian spores. Transaction of American Microscopical Society 40:161-167.

_____ 1922. On the morphology and life history of a myxosporidian, Leptotheca ohlmacheri, parasitic in Rana clamitans and R. pipiens. Parasitology 14:221-244.

_____ 1966. Protozoology. 5th ed. Springfield, C. C. Thomas. 1174 p.

Labbe, A. 1894. Recherches zoologiques et biologiques sur les parasites endoglobulaire du sang des vertebres. Archives de Zoologie Experimentale et Generale 22:55-258.

Laird, M. 1953. The protozoa of New England intertidal zone fishes. Transactions of the Royal Society of New Zealand 81:79-143.

Leger, L. 1906. Sur une nouvelle maladie myxosporidienne de la truite indigene (Chloromyxum truttae n. sp.) Comptes Rendus (Hebdomadaires) des Seances de l'Academie des Sciences 142:665-666.

Leger, L. and E. Hesse. 1906. Sur la structure de la paroi sporale des Myxosporidies. Comptes Rendus (Hebdomadaires) des Seances de l'Academie des Sciences 142:720-722.

Leveran, A. and F. Mesnil. 1902. Sur la multiplication endogene des Myxosporidie. Comptes Rendus (Hebdomadaires) des Seances et Memoires de la Societe de Biologie 54:469-472.

Lieberkuhn, N. 1854. Notice sur les psorospermies. Bulletins de l'Academie Royale des Sciences, des Lettres, et des Beaux-Arts de Beligique 21:21-23.

Locke, M. 1961. Pore canals and related structures in insect cuticle. The Journal of Biophysical and Biochemical Cytology 19:589-602.

_____ 1965. The structure of septate desmosomes. Journal of Cell Biology 25:166-169.

Lom, J. 1964. Notes on the exteusion and some other festures of myxosporidian spores. Acta Protozoologica 2:321-327.

_____ 1969a. Notes on the ultrastructure and sporoblast development in fish parasitizing Myxosporidia of the genus Sphaeromyxa. Zeitschrift fur Zellforschung und Mikroskopische Anatomie 97:416-437.

_____ 1969b. On a new taxonomic character in Myxosporidia, as demonstrated in descriptions of two new species of Myxobolus. Folia Parasitologica (Praha) 16:97-103.

_____ 1970. Protozoa causing diseases in marine fishes. In: A symposium on diseases of fishes and shellfishes. ed. by Stanislas F. Snieszko, Washington, D.C. American Fisheries Society Special Publication No. 5, p. 101-123.

_____ 1972. On the structure of the extruded microsporidian polar filament. Zeitschrift fur Parasitenkunde 38:200-213.

Lom, J. and J. O Corliss. 1967. Ultrastructural observations on the development of the microsporidian protozoan Plistophora hyphessobryconis Schaperclaus. The Journal of Protozoology 14:141-152.

Lom, J. and G. L. Hoffman. 1971. Morphology of the spores of Myxosoma cerebralis (Hofer, 1903) and M. cartilaginis (Hoffman, Putz and Dunbar, 1965). The Journal of Parasitology 57:1302-1308.

Lom, J. and P. de Puytorac. 1965a. Studies on the myxosporidian ultrastructure and polar capsule development. Protistologica 1:53-65.

_____ 1965b. Observations sur l'ultrastructure des trophozoites de myxosporidies. Comptes Rendus (Hebdomadaires) des Seances de l'Academie des Sciences 260:2588-2590.

Lom, J. and J. Vavra. 1962. A proposal to the classification within the subphylum Cnidospora. Systematic Zoology 11:172-175.

_____ 1963. The mode of sporoplasm extrusion in microsporidian spores. Acta Protozoologica 1:81-90.

_____ 1964. Parallel features in the development of myxosporidian polar capsules and coelenterate nematocysts. Proceedings of the Third European Regional Conference on Electron Microscopy 191-192.

_____ 1965. Notes on the Morphogenesis of the polar filament in Henneguya (Protozoa, Cnidospora). Acta Protozoologica 3:57-60.

Lumsden, R. D., Y. Marciacq and J. R. Seed. 1972. Trypanosoma gambiense: Cytopathologic changes in guinea pig hepatocytes. Experimental Parasitology 32:369-389.

Mavor, J. W. 1916. On the life history of Ceratomyxa acadiensis, a new species of Myxosporidia from the eastern coast of Canada. Proceedings of the American Academy of Arts and Sciences 51:549-578.

Mayer, A. F. 1864. Uber psorospermien, Archiv fur Anatomie Physiologie und Wissenschaftliche Medicin 3:1-264.

Mercier, L. 1906a. Phenomenes de sexualite chez Myxobolus pfeifferi. Comptes Rendus (Hebdomadaires) des Seances et Memoires de la Societe de Biologie 60:427-428.

_____ 1906b. Contribution a l'etude du developpement des spore chez Myxobolus pfeifferi. Comptes Rendus (Hebdomadaires) des Seances et Memoires de la Societe de Biologie 60:763-765.

Miller, D. M. and T. T. Dunagan. 1971. Studies on the rostellar hooks of Macracanthorhynchus hirudinaceus (Acanthocephala) from swine. Transactions of American Microscopical Society 90:329-335.

Morgenthaler, O. 1922. Der Polfaden von Nosema apis. Archiv fur bienenkunde 4:53-60.

Morrison, N. D. and I. Pratt. 1973. Sphaeromyxa maiyai sp. n. (Protozoa: Myxosporidea), coelozoic parasite of the Pacific tomcod, Microgadus proximus. The Journal of Protozoology 20:214-217.

Muller, J. 1841a. Krankhafter hautsusschlag mit speefisch organisierten korperchen (Psorospermien). Bericht uber zur Bekanntmachung geeigneten Verhandlungen der K. Preuss. Akademie der Wissenschaften zu Berlin 4:212-221.

_____ 1841b. Ueber eine eigentumliche krankhafte parasitische Bildung mit spezifisch organisierten Samenkorperchen. Bericht uber zur Bekanntmachung geeigneten Verhandlungen der K. Preuss. Akademie der Wissenschaften zu Berlin 4:246-250.

_____ 1841c. Ueber Psorospermien. Archiv fur Anatomie Physiologie und Wissenschaftliche Medicin 5:477-496.

_____ 1843. Recherches sur une variete remarquable de production parasitique morbide avec des corpuscules seminaux specifiquement organises. Archives de Medecine Comparee 6:219-234.

Naville, A. 1930. Recherches sur la sexualite chez les Myxosporidies. Archiv fur Protistenkunde 69:327-400.

Noble, E. R. 1944. Life cycles in the Myxosporidia. The Quarterly Review of Biology 19:213-235.

Ohshima, K. 1937. On the function of the polar filament of Nosema bombycis. Parasitology 29:220-224.

Parducz, B. 1967. Ciliary movement and coordination in ciliates. International Review of Cytology 21:91-128.

Pearse, A.G.E. 1968. Histochemistry: Theoretical and Applied. Boston, Little, Brown and Co. 759 p.

Reynolds, E. S. 1963. The use of lead citrate at high pH as an electron-opaque stain in electron microscopy. The Journal of Cell Biology 17:208-212.

Robin, C. 1853. Histoire naturelle des vegetaux parasites. Comptes Randus des Seances et Memoires de la Societe de Biologie 5:82-257.

Schaudinn, F. 1900. Untersuchungen uber den Generationswechsel bei Coccidie. Zoologische Jahrbucher Abtheilung fur Anatomie und Onotgenie der Thiere 13:197-292.

Schroder, O. 1907. Beitrage zur Entwicklungsgeschichte der Myxosporidien Sphaeromyxa sabrazesi (Laveran et Mesnil). Archiv fur Protistenkunde 9:359-381.

_____ 1910. Uber die Anlage der Sporocyste (Pansporoblast) bei Sphaeromyxa sabrazesi, Laveran et Mesnil. Archiv fur Protistenkunde 19:1-5.

Schubert, G. 1967. Elektronen-mikroskopische Untersuchungen zeir Sporenentwicklung von Henneguya pinnae Schubert (Sporozoa, Myxosporidea, Myxobolidae). Zeitschrift fur Parasitenkunde 30:57-77.

Shulman, G. 1966. Myxosporidia of the Fauna of the USSR (in Russian). Moscow, Leningrad, Nauka. 506 p.

Spurr, A. R. 1969. A low-viscosity epoxy resin embedding medium for electron microscopy. Journal of Ultrastructural Research 26:31-43.

Steiner, J., K. Miyai, and M. Phillips. 1964. Electron microscopy of membrane-particle arrays in liver cells of ethionine-intoxicated rats. American Journal of Pathology 44:169-190.

Tanikawa, K. 1968. Ultrastructural Aspects of the Liver and its Disorders. Berlin, Springer-Verlag. 612 p.

Thelohan, P. 1892. Observation sur les myxosporidies et essai de classification de ces organismes. Bulletin de la Societe Philomathique de Paris 4:165-178.

_____ 1895. Recherches sur les Myxosporidies. Bulletin Scientifique de la France et de la Belgique 26:100-394.

Tripathi, Y. R. 1953. Studies on parasites of Indian fishes. 1. Protozoa Myxosporidia together with a check list of parasitic protozoa described from Indian fishes. Records of the Indian Museum 50:63-89.

Volk, B. W. and B. J. Wallace. 1966. The liver in lipidosis. American Journal of Pathology 49:203-225.

West, A. F. 1960. The biology of a species of Nosema (Sporozoa: Microsporidia) parasitic in the flour beetle Tribolium confusum. The Journal of Parasitology 46:747-754.

Willis, A. G. 1949. On the vegetative forms and life history of Chloromyxum thyrsites Gilchrist and its doubtful systematic position. The Australian Journal of Scientific Research. Series B, Biological Sciences 2:379-398.

Wood, R. L. 1959. Intercellular attachments in the epithelium of Hydra as revealed by electron microscopy. The Journal of Biophysical and Biochemical Cytology 6:343-345.

Wyatt, E. J. and Ivan Pratt. 1963. Myxobolus insidiosus sp. n., a Myxosporidian from the musculature of Oncorhynchus tshawytscha (Walbaum). The Journal of Parasitology 49:951-955.

APPENDIX

LIST OF FIGURES


A
1

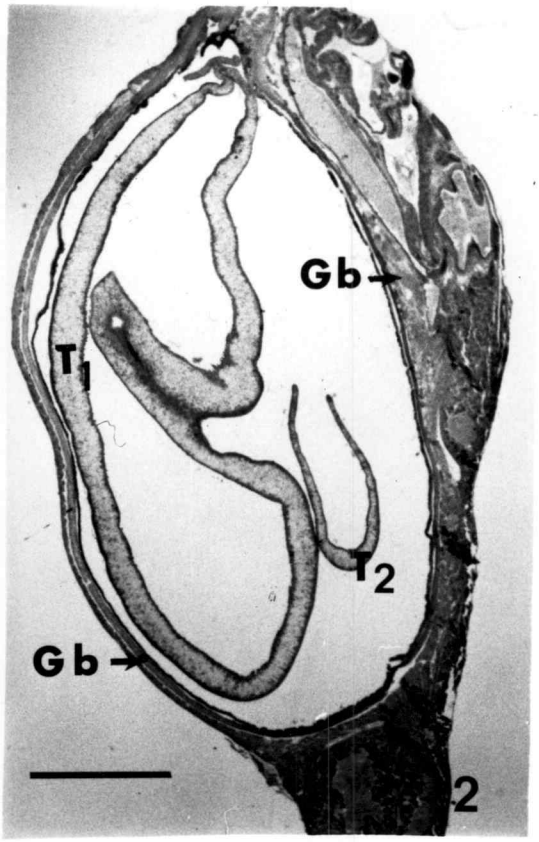
Gb
T1
T2
Gb
2

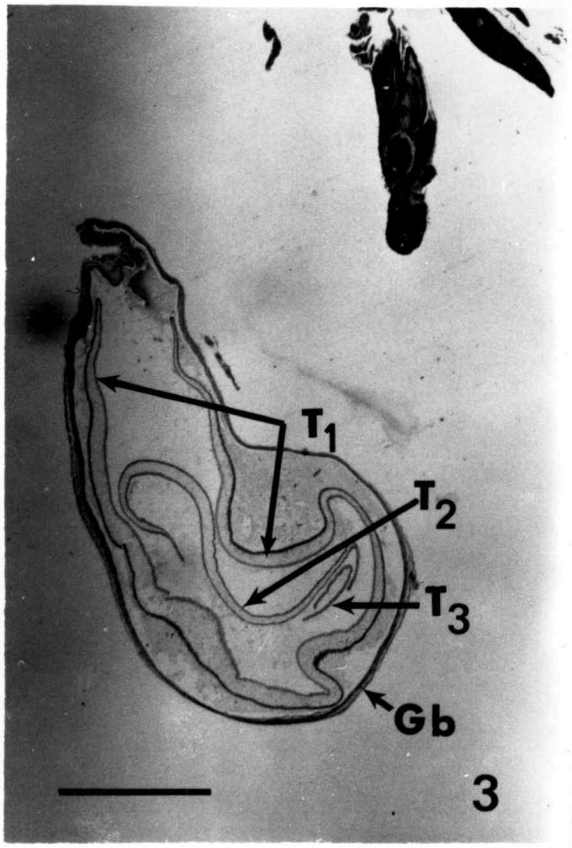
T1
T2
T3
Gb
3

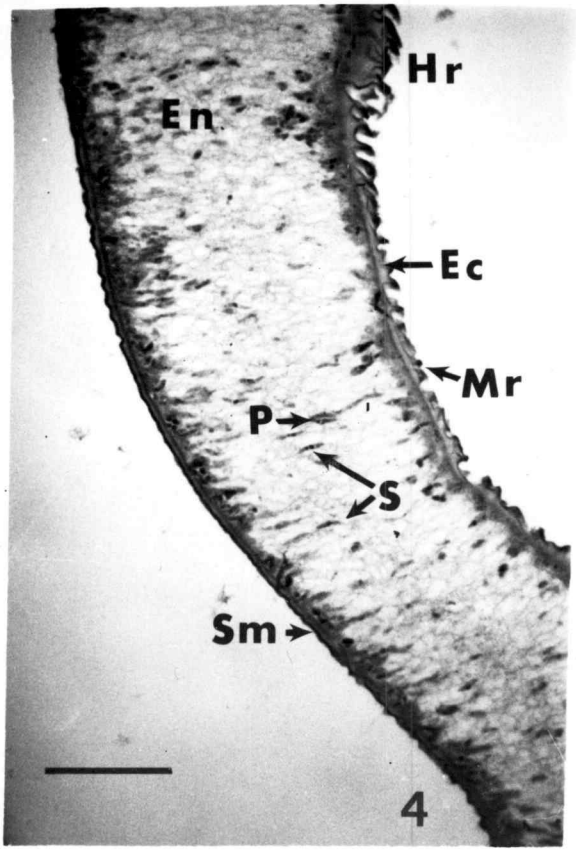
Hr
En
Ec
Mr
P
S
Sm
4

Figure 5. Plasmodial cross section showing the highly rugose inner flexed surface and the thickened ectoplasmic layer, Ec. (Scale = 100 μm; 165x)

Figure 6. Plasmodium in close proximity to the gall bladder mucosal membrane, Gb. Note the relatively smooth outer (= dorsal) surface of the plasmodium, Os. (Scale = 100 μm; 165x)

Figure 7. Cross section showing deep furrows, Fu, of ectoplasm, Ec; almost reaching the outer endoplasmic zone, En. (Scale = 30 μm; 690x)

Figure 8. Cross section of the plasmodial surface showing a thick ectoplasmic zone, Ec; merging with the endoplasmic organelles, En; vacuolated endoplasmic region, V; Alcian blue positive mucoid layer, Ml ; Brush border, Bb; Rugae, R. (Scale = 10 μm; 690x)

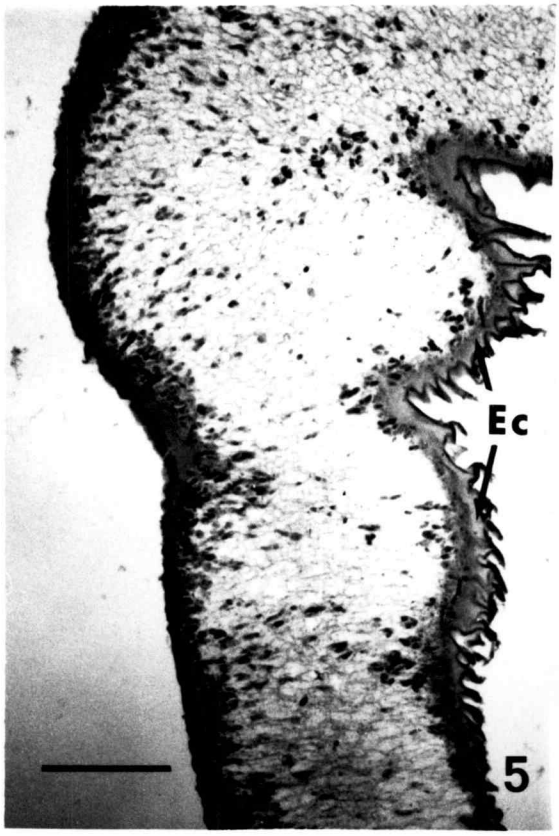
Ec
5

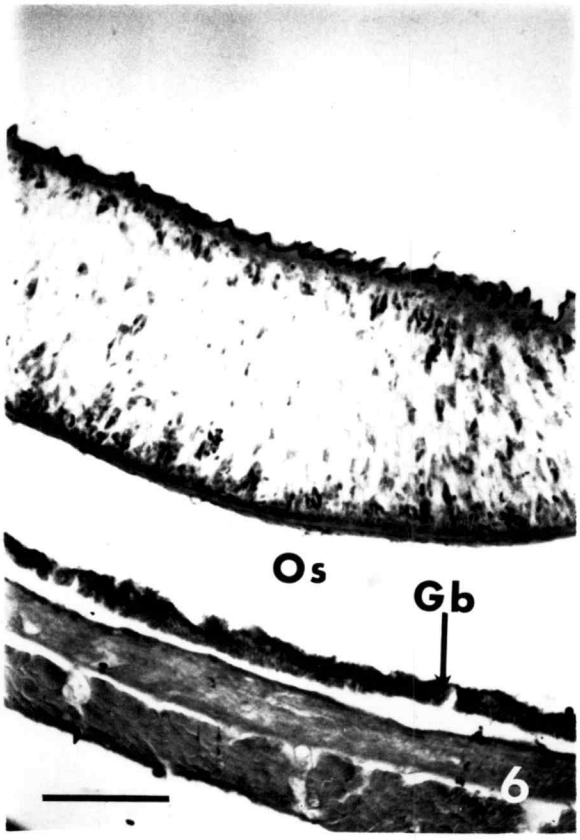
Os
Gb
6


Ec
Fu
En
7

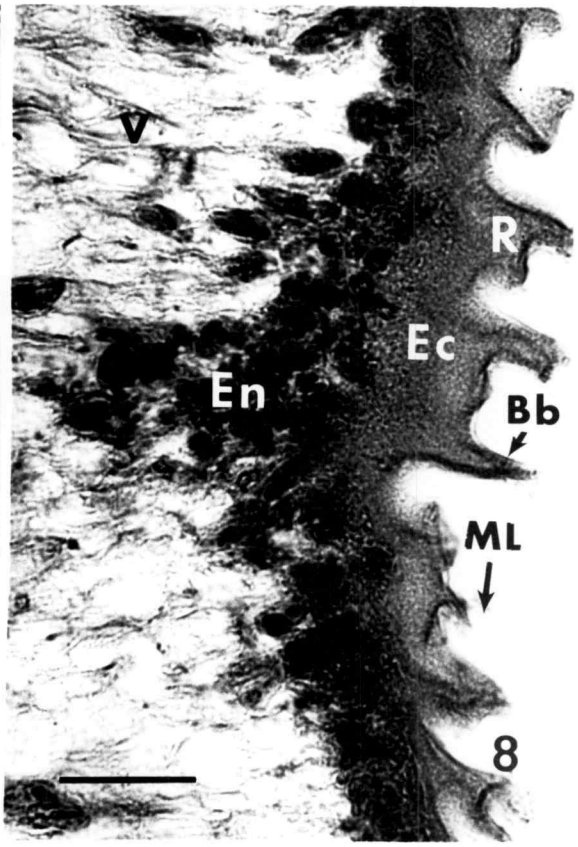
V
R
Ec
En
Bb
ML
8

Figure 9. Cross section of plasmodial surface. Note the position of the spores, S; parallel to each other and approximately perpendicular to the plasmodial surface. Mucoid layer, Ml; Brush border microvilli, Bb; Alveolar layer containing flocculent amorphous material, Af. (Scale = 10 μm; 690x)

Figure 10. Developing sporont, St; of approximately four cell state in the inner endoplasmic region. (Scale = 10 μm; 690x)

Figure 11. Developing sporont, St; in early developmental stage. Deep furrow in ectoplasm, Fu; dense vacuole, Vo; transparent vacuole, Vt. (Scale = 10 μm; 690x)

Figure 12. Cross section of the plasmodial stage showing several sporonts, St; in varying stages of development. (Scale = 10 μm; 690x)

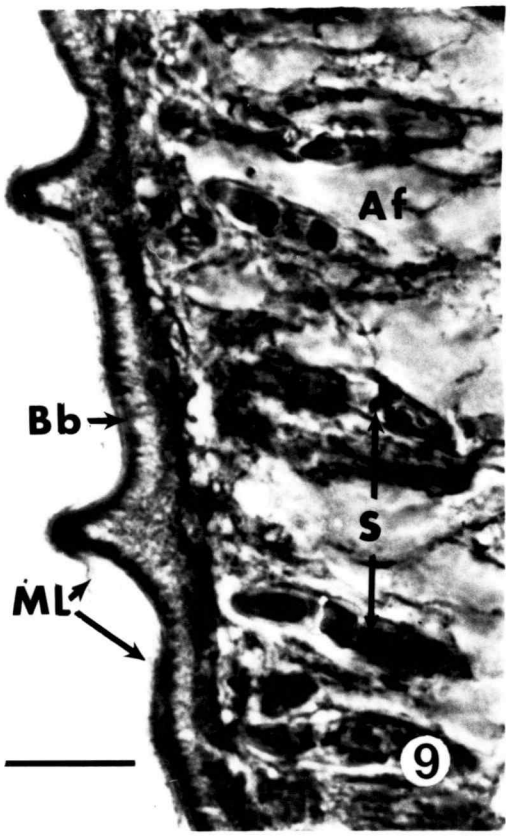
Af
Bb
S
ML
9

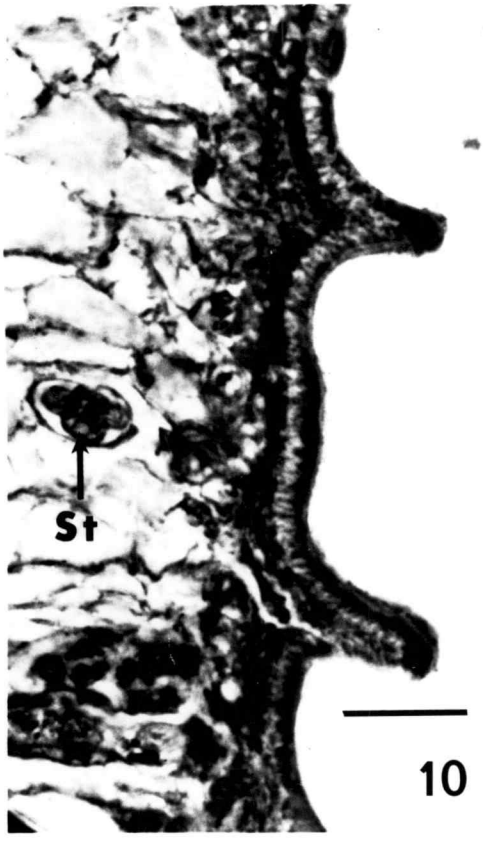
St
10

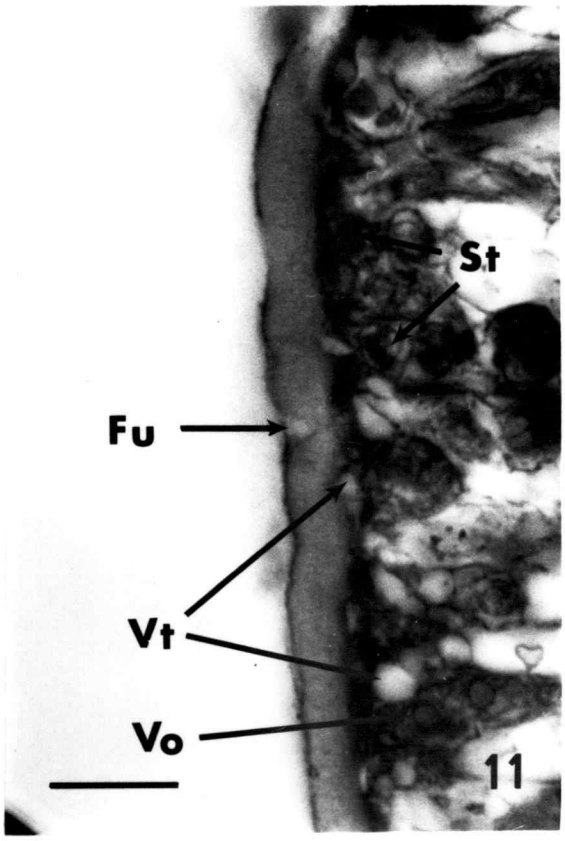
St
Fu
Vt
Vo
11

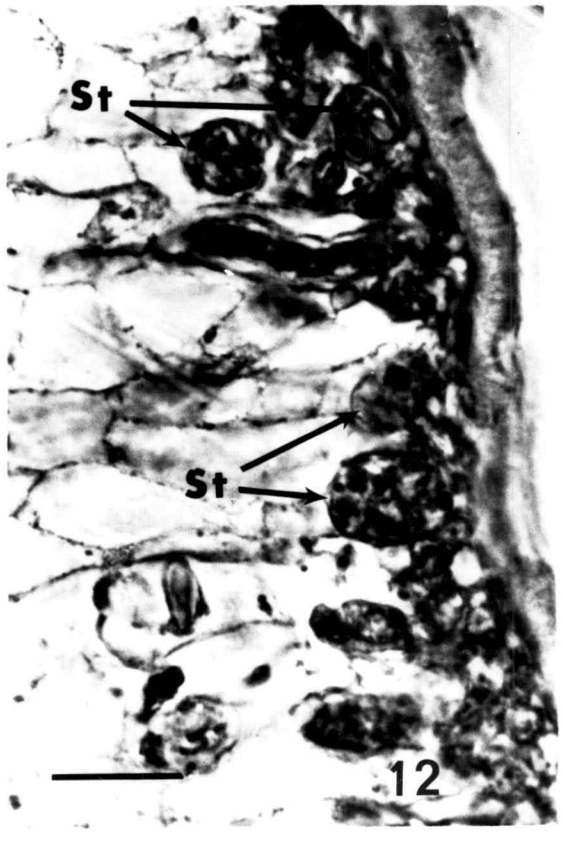
St
St
12

Figure 13. Pansporoblast, P; consisting of two spores, S_1 and S_2; that have developed in a single sporont. (Scale = 10 μm; 690x)

Figure 14. Cross section of thick ectoplasm, Ec; sharply delineated from endoplasm, En. Note the heavy mucoid layer, Ml. (Scale = 10 μm; 690x)

Figure 15. Section of the alveolar endoplasmic zone of the ectoplasm showing the vacuoles, V; several sporoblasts, St; Polar capsule, Pc; and membranes of the vacuoles, Mb; surround the sporoblasts. (Scale = 10 μm; 1700x)

Figures 16-22. Oil immersion photomicrographs of living spores of Sphaeromyxa maiyai embedded in 0.8% ionagar. (Scale = 100 μm; 1700x)

Figure 16. Frontal view of arcuate spore showing bluntly rounded ends, E; Capsulogenous cell, Cc; Capsulogenous cell nucleus, Cn; Sporoplasm, Sp.

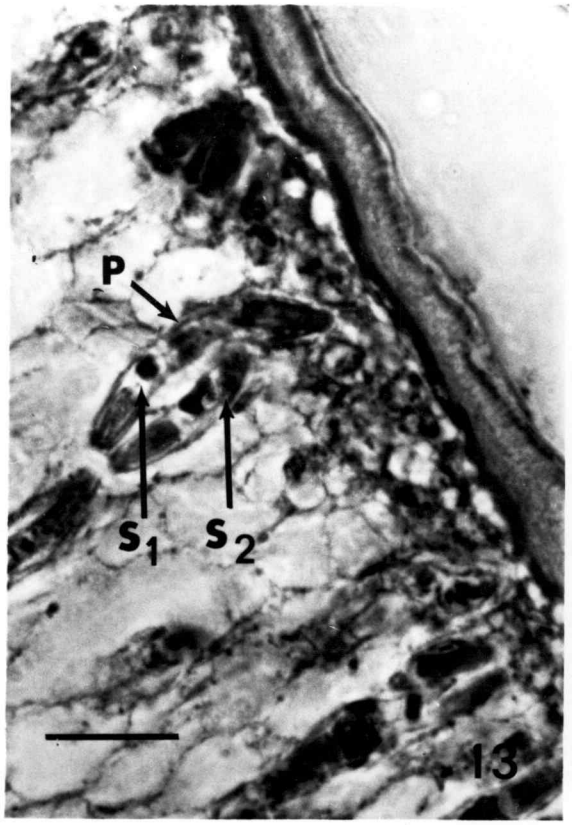
P
S_1
S_2
13

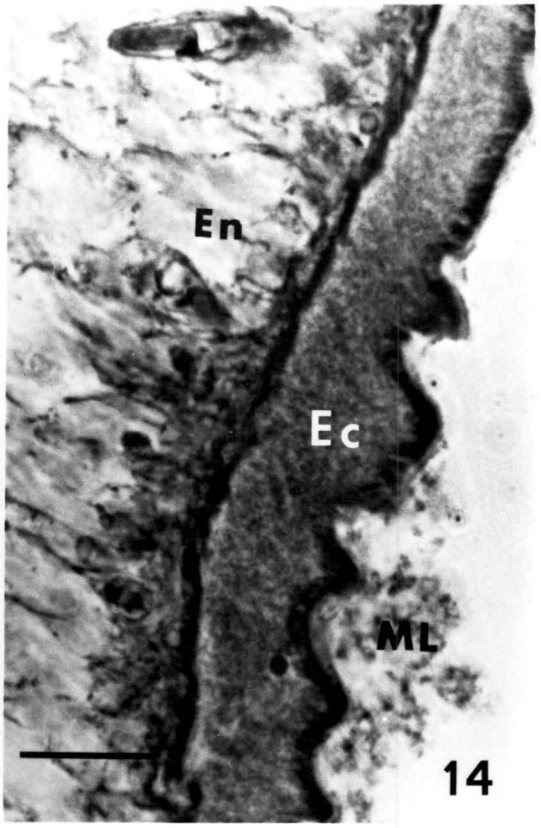
En
Ec
ML
14

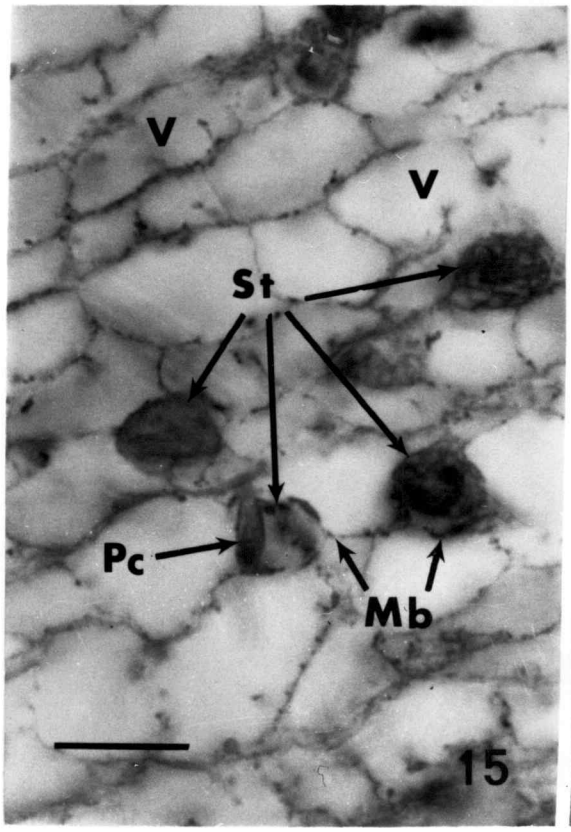
V
V
St
Pc
Mb
15

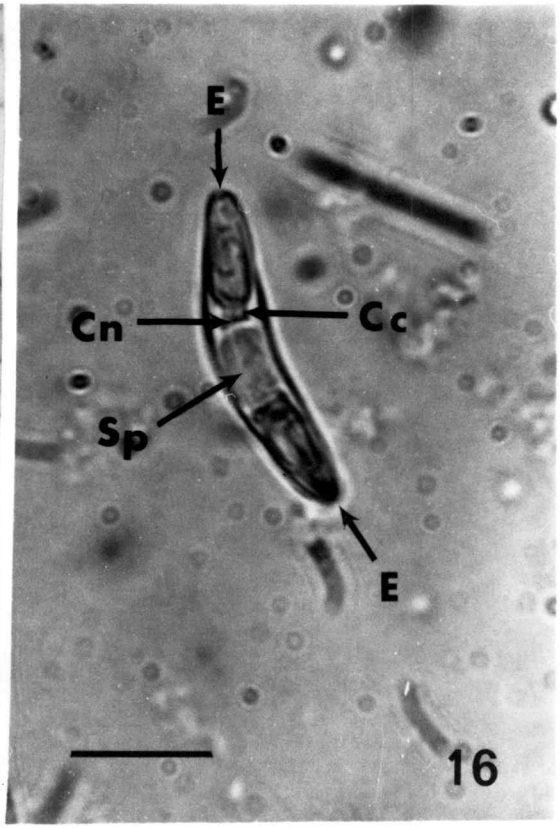
E
Cn
Cc
Sp
E
16

Figure 17. Sutural view of spore showing the sinuous aspect. Note the longitudinally folded polar filament, Pf.

Figure 18. Spore frontal view.

Figure 19. Two spores. A. Frontal view. B. Sutural view showing the sutural line, Sl.

Figure 20. Frontal view of a spore showing the folded Polar filament, Pf; polar filament cap, Pfc; capsulogenous cell, Cc; Capsulogenous cell nucleus, Cn.

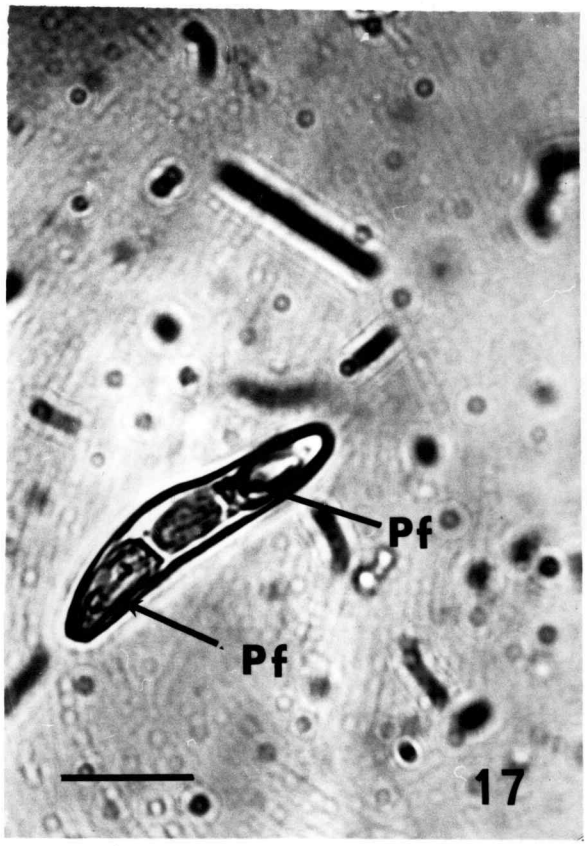
Pf
Pf
17

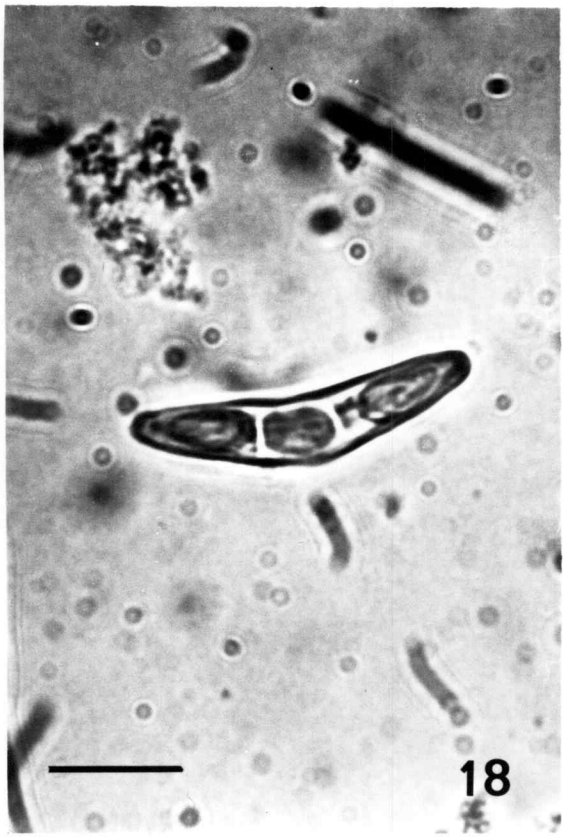
18

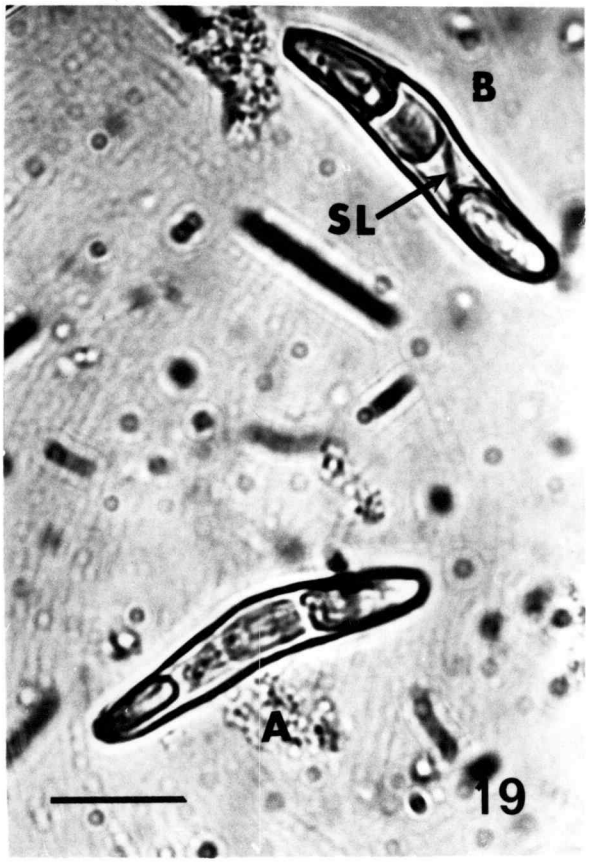
B
SL
A
19

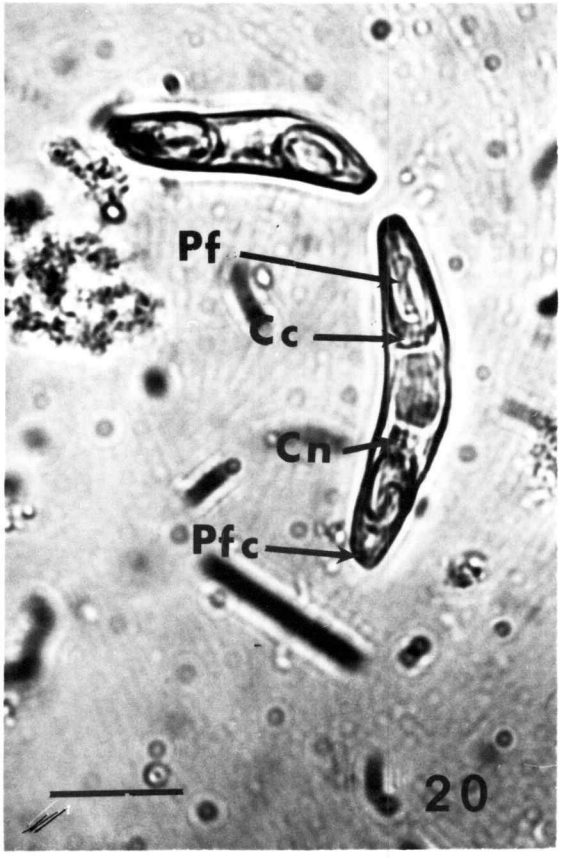
Pf
Cc
Cn
Pfc
20

Figure 21. Frontal view of a spore showing longitudinal striations, Ls.

Figure 22. Sutural view of a spore showing slightly truncated ends, E; sutural line, Sl; and longitudinal striations, Ls.

Figures 23-28. Oil immersion phase contrast photomicrographs of living spores of Sphaeromyxa maiyai embedded in 0.8% ionagar. The spores had been treated with either 5.0% KOH or saturated urea prior to embedment to cause extrusion of the polar filaments. (Scale = 10 μm; 1700x)

Figure 23. Frontal view of spore with partially extruded polar filaments, Pf; Longitudinal striations, Ls; polar capsule, Pc.

Figure 24. Frontal view of a spore with fully extruded polar filaments, Pf; Polar filament cap, Pfc; Pycnotic capsulogenous cell nuclei, Cn; Sporoplasm nuclei, Spn.

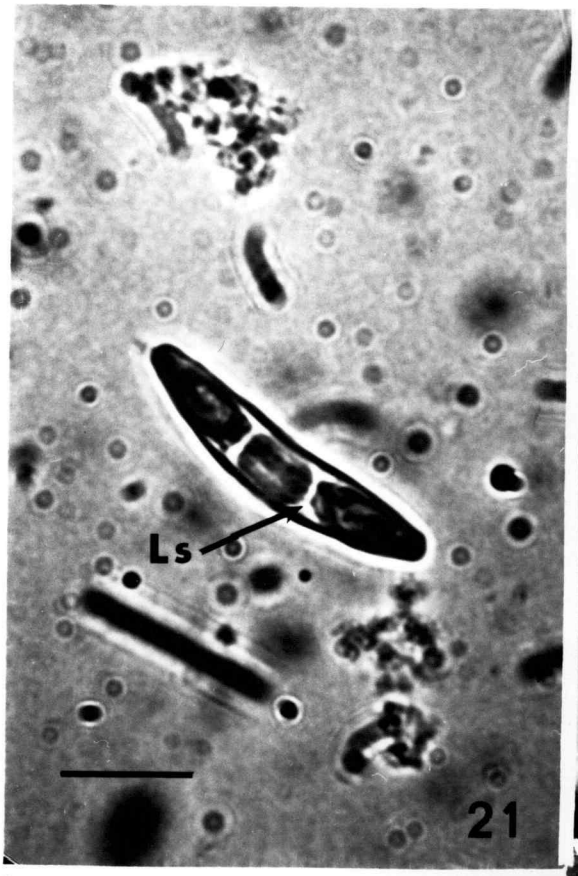
Ls
21

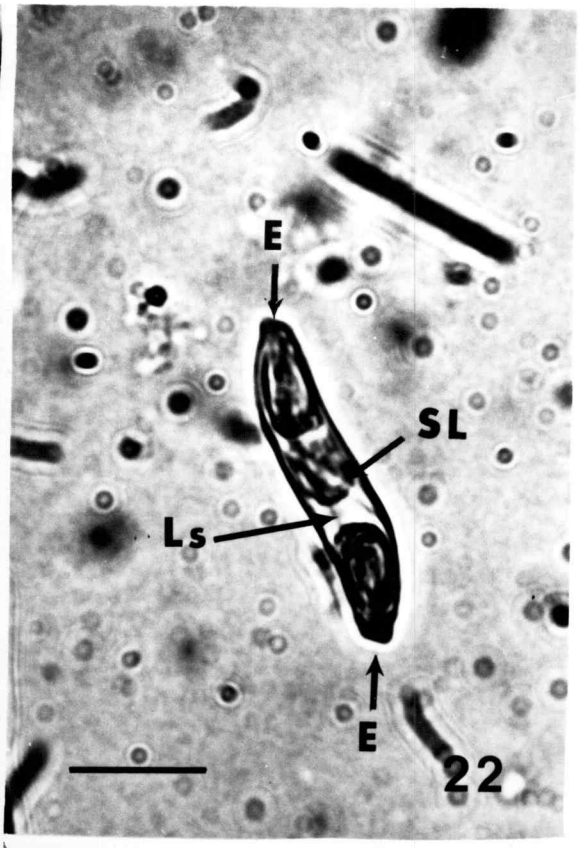
E
SL
Ls
E
22

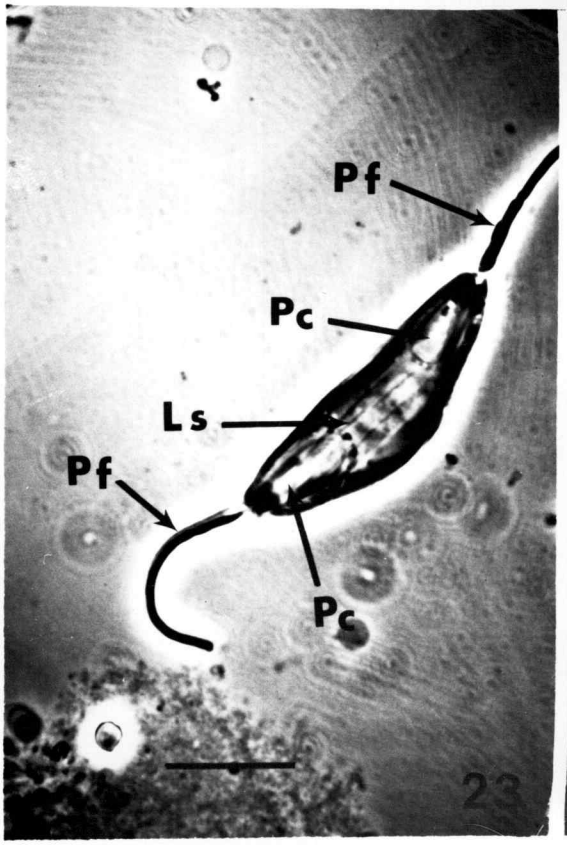
Pf
Pc
Ls
Pf
Pc
23

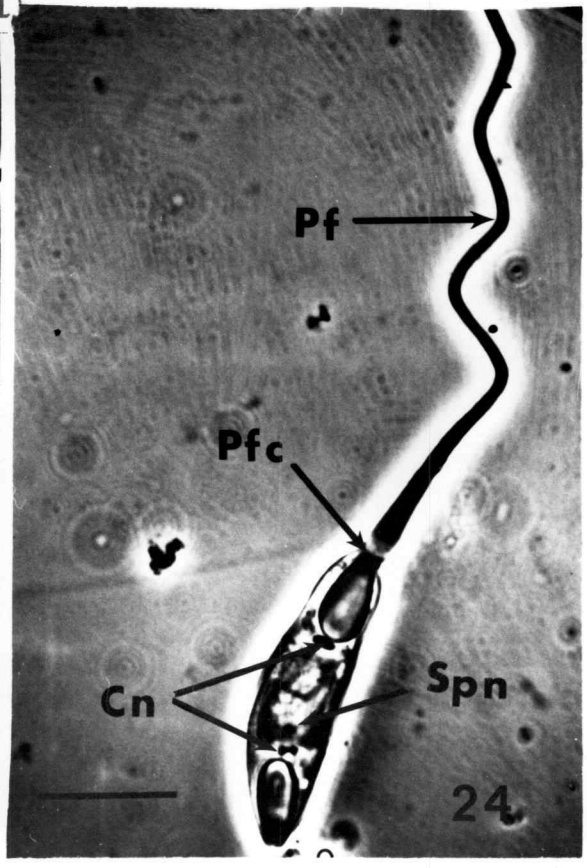
Pf
Pfc
Cn
Spn
24

Figure 25. Spore undergoing lysis along the sutural line, Sl; polar filament cap, Pfc.

Figure 26. Spore with one partially extruded polar filament. Note the optically dense portion of the filament, arrow, Pf_1; entering the base of the filament. The unextruded portion of the filament, Pf; can be seen within the polar capsule. The unextruded polar capsule shows the folded nature of the filament and the distal polar filament cap, Pfc; Sutural line, Sl; Valvulogenic nuclei, Vn.

Figure 27. Polar capsule in the process of being released from a lysed spore. The partially extruded polar filament, Pf_2; showing the capsular portion, Cp; of the filament unfolding into the extruded portion.

Figure 28. Polar capsules liberated from lysed spores. Polar filament cap, Pfc.

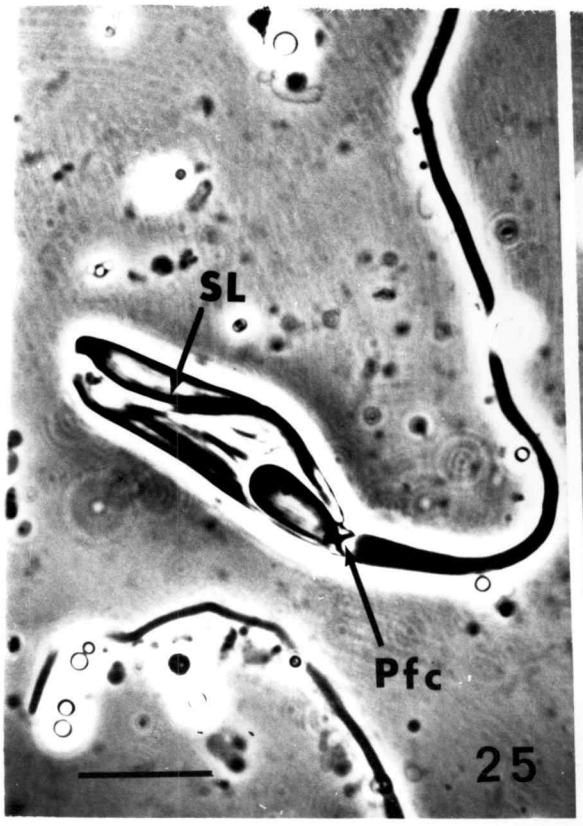
SL
Pfc
25

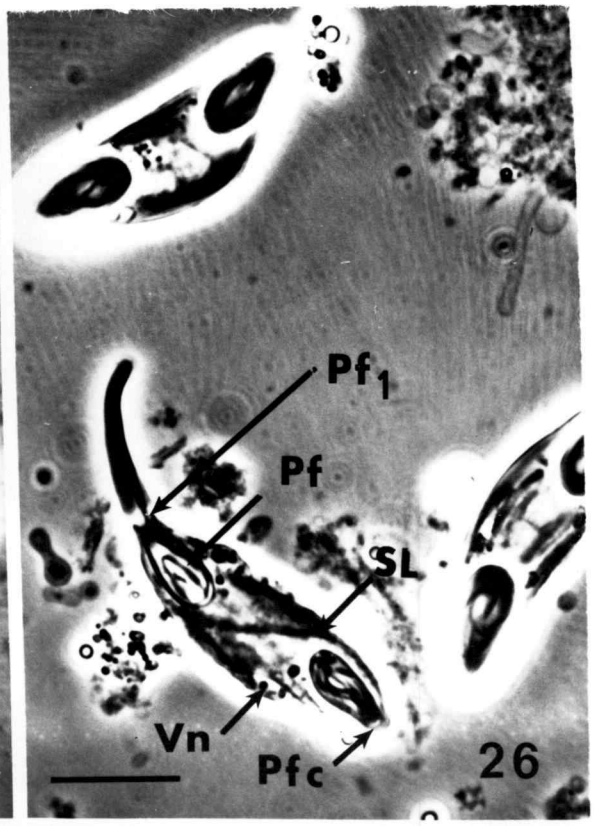
Pf1
Pf
SL
Vn
Pfc
26

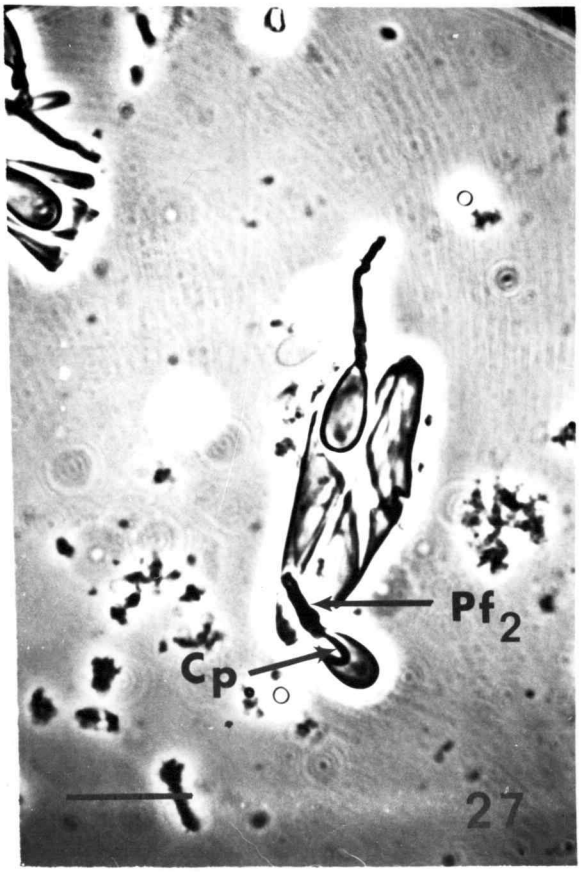
Pf2
Cp
27

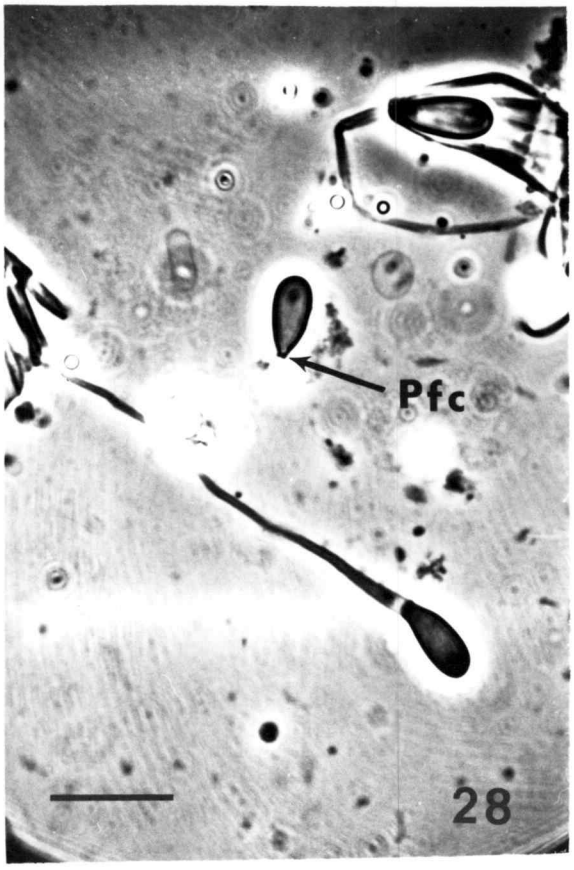
Pfc
28

Figures 29-33. Low magnification stereoscan electron micrographs of air dried plasmodia of Sphaeromyxa maiyai.

Figure 29. Plasmodial stage showing the variance in surface microtopography. Rugose areas, R; Relatively smooth areas, Sm. The large folds, arrows, on the plasmodial surface probably representing drying artifact. (Scale = 1.0 mm; 36.5x)

Figure 30. Enlargement of Figure 29 showing rugosity in more detail. (Scale = 0.5 mm; 91x)

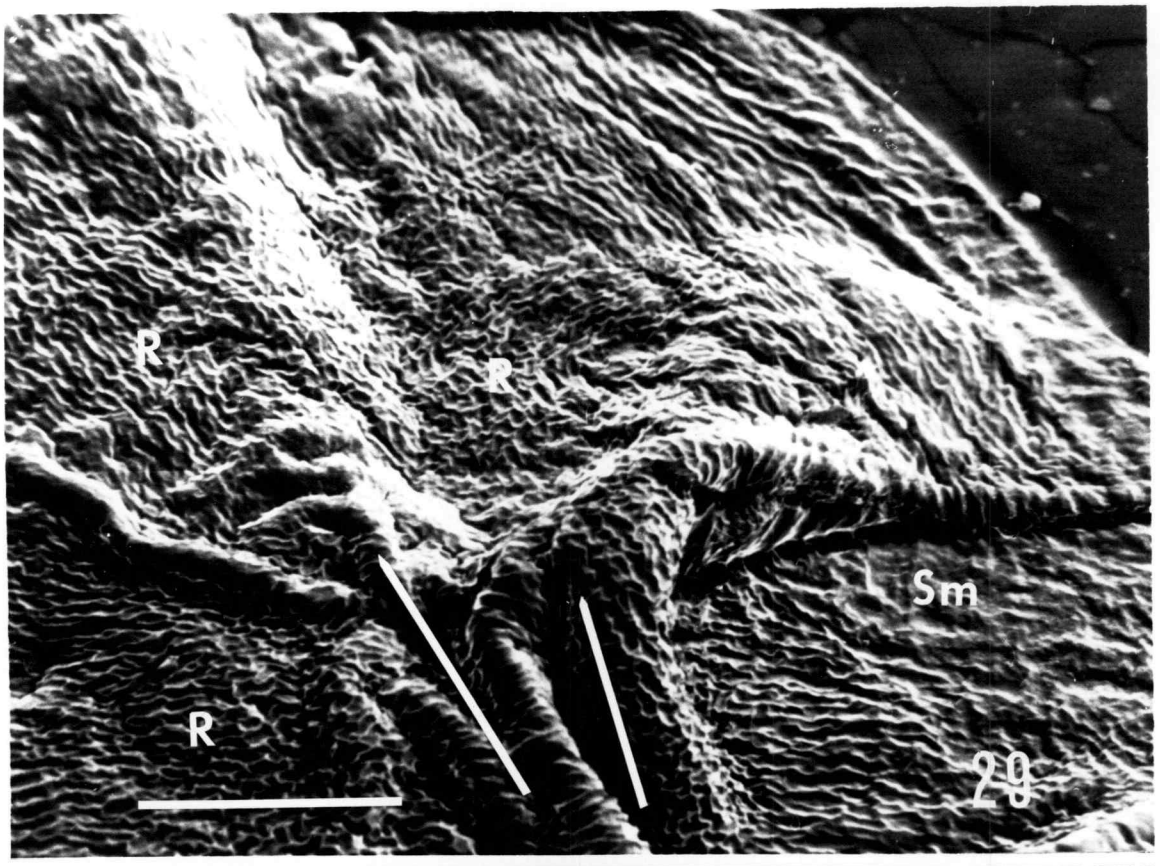
R
R
Sm
R
29

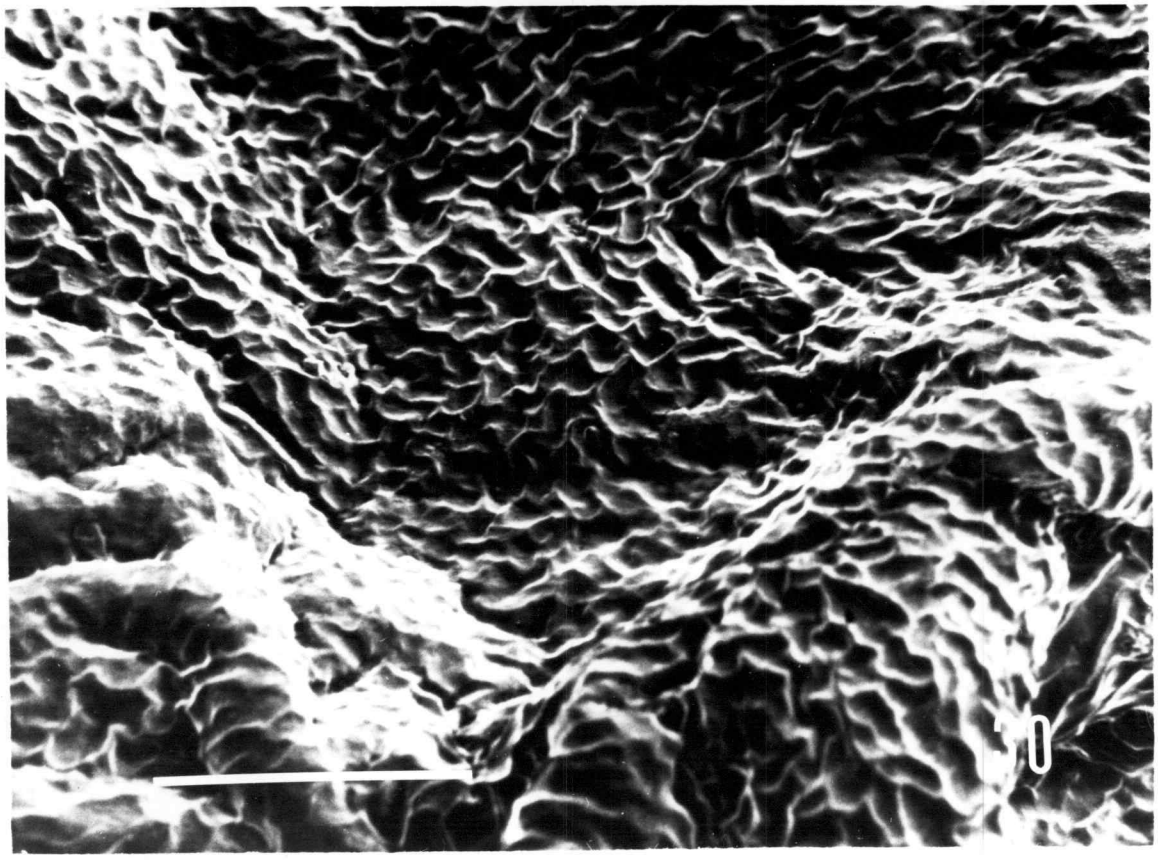
0

Figure 31. Surface of plasmodium showing rugose, R; and relatively smooth, Sm; areas. (Scale = 1.0 mm; 38.8x)

Figure 32. Higher magnification of a smooth surface. (Scale = 100 μm; 370x)

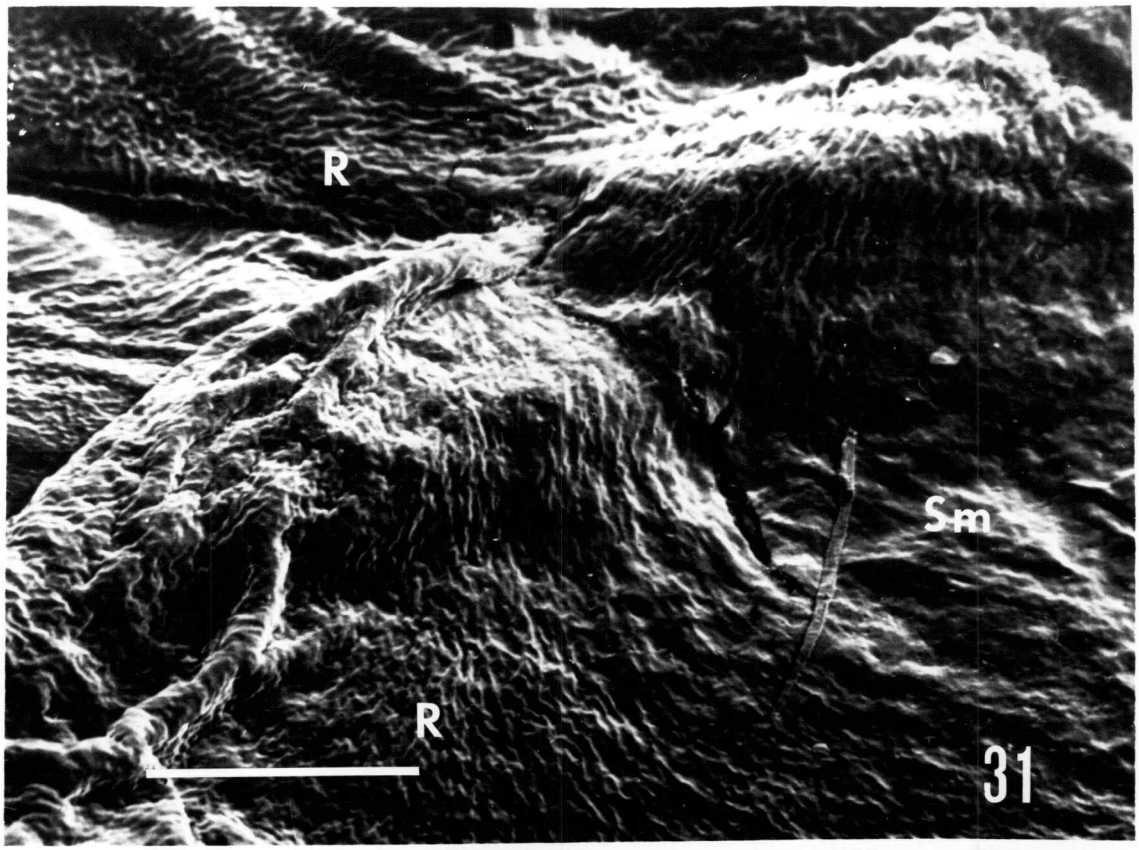
R
Sm
R
31

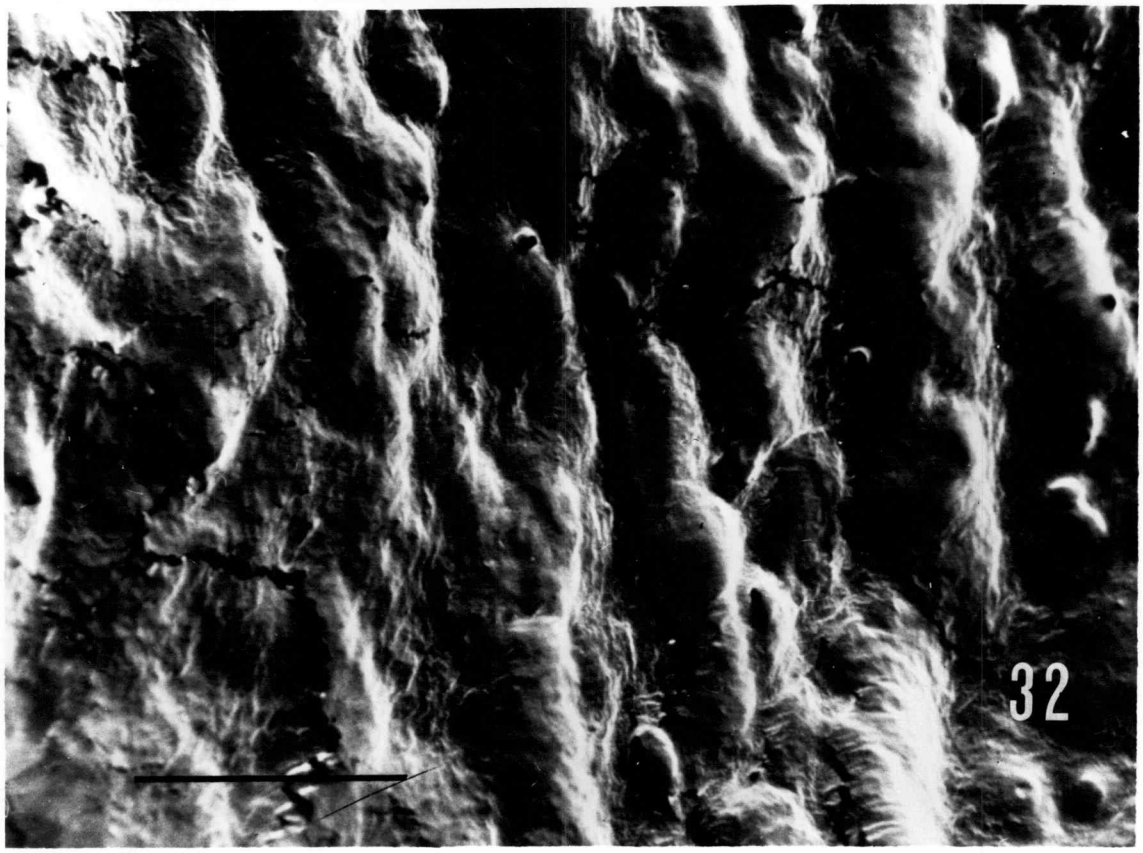
32

Figure 33. Higher magnification of a rugose surface. (Scale = 100 μm; 350x)

Figures 34-37. High magnification stereoscan electron micrographs of critical point dried plasmodial stage of Sphaeromyxa maiyai.

Figure 34. Plasmodium treated with 0.005% EDTA. Note the microvilli, Mv. (Scale = 2.0 μm; 11, 100x)

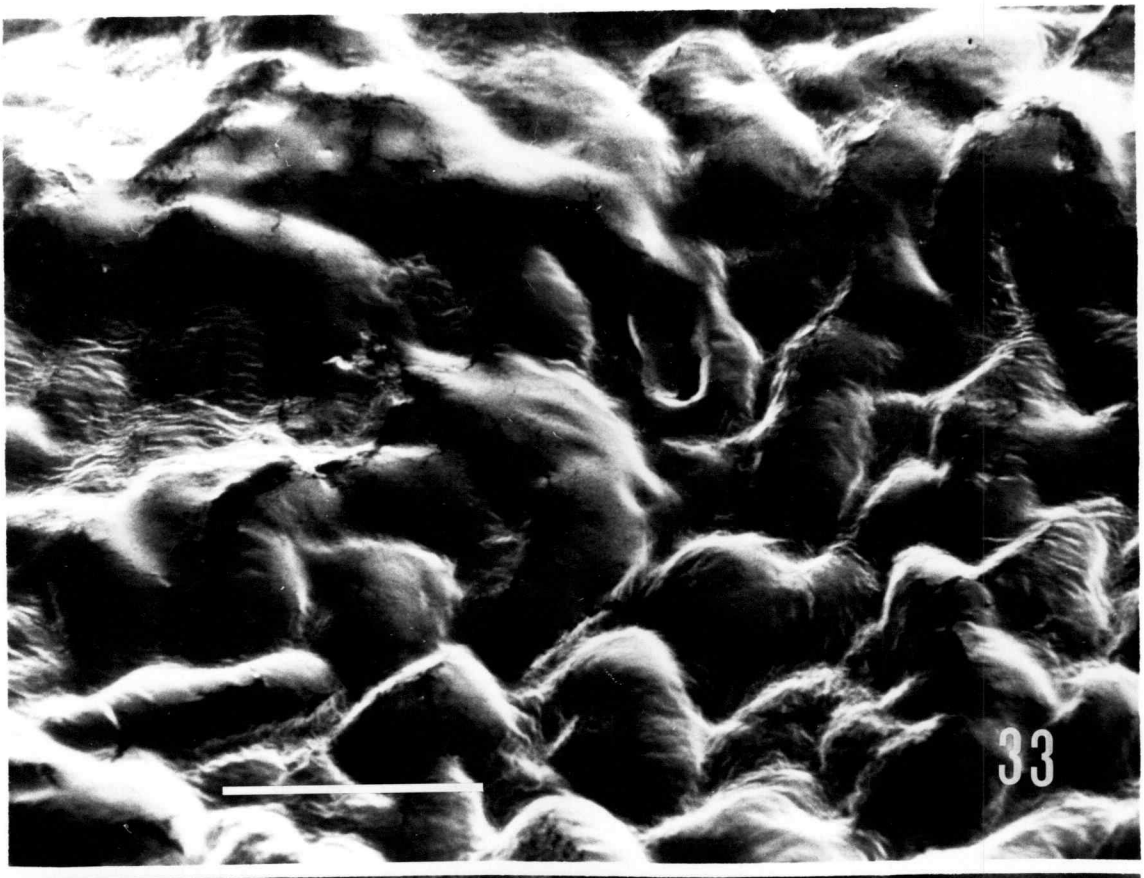
33

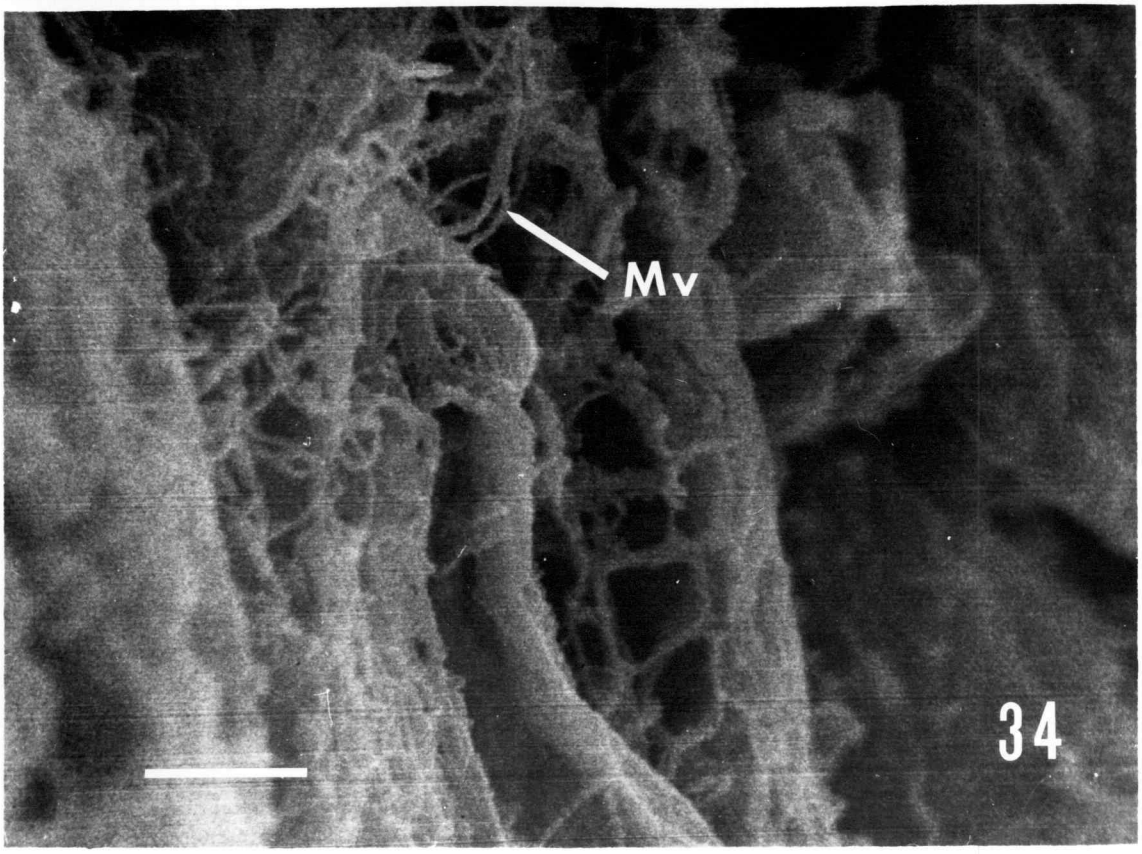
Mv
34

Figure 35. Smooth surface of plasmodium showing small surface depressions and mats of mucoid material. (Scale = 5.0 μm; 4670x)

Figure 36. Finely rugose surface of plasmodium. (Scale = 5.0 μm; 4020x)

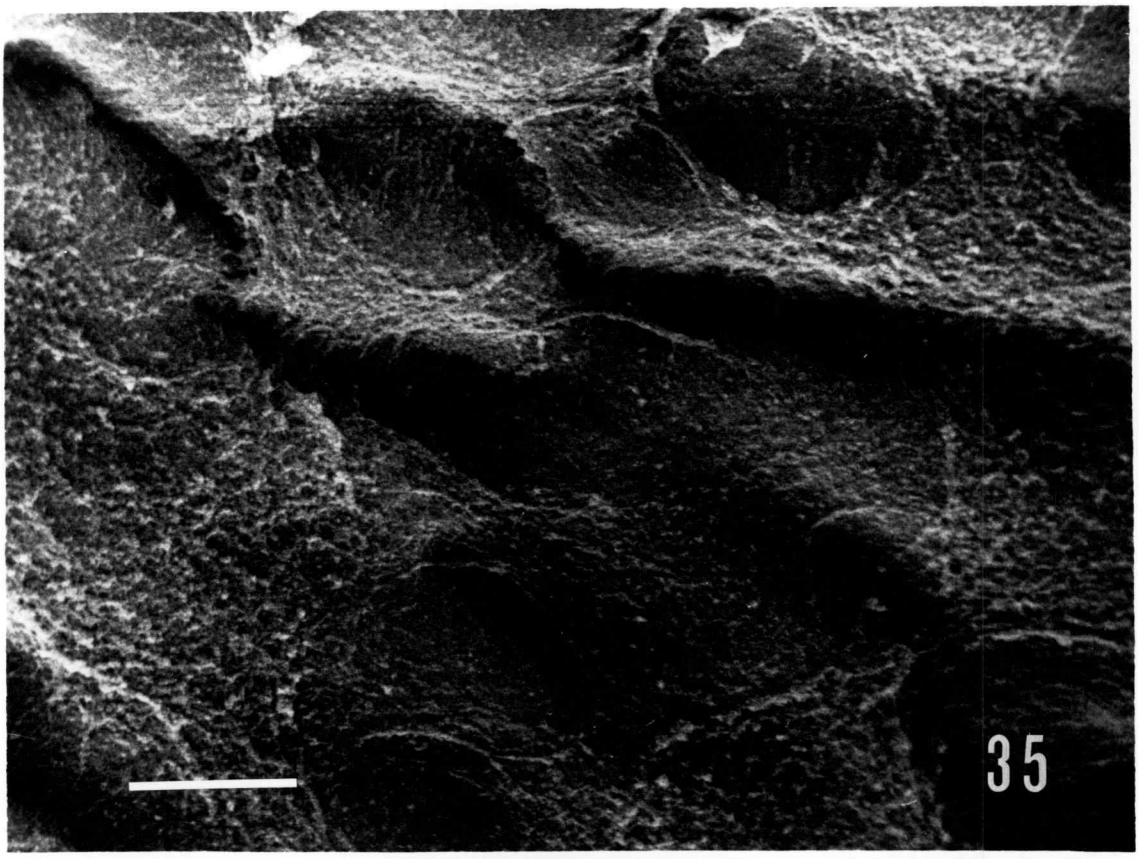
35

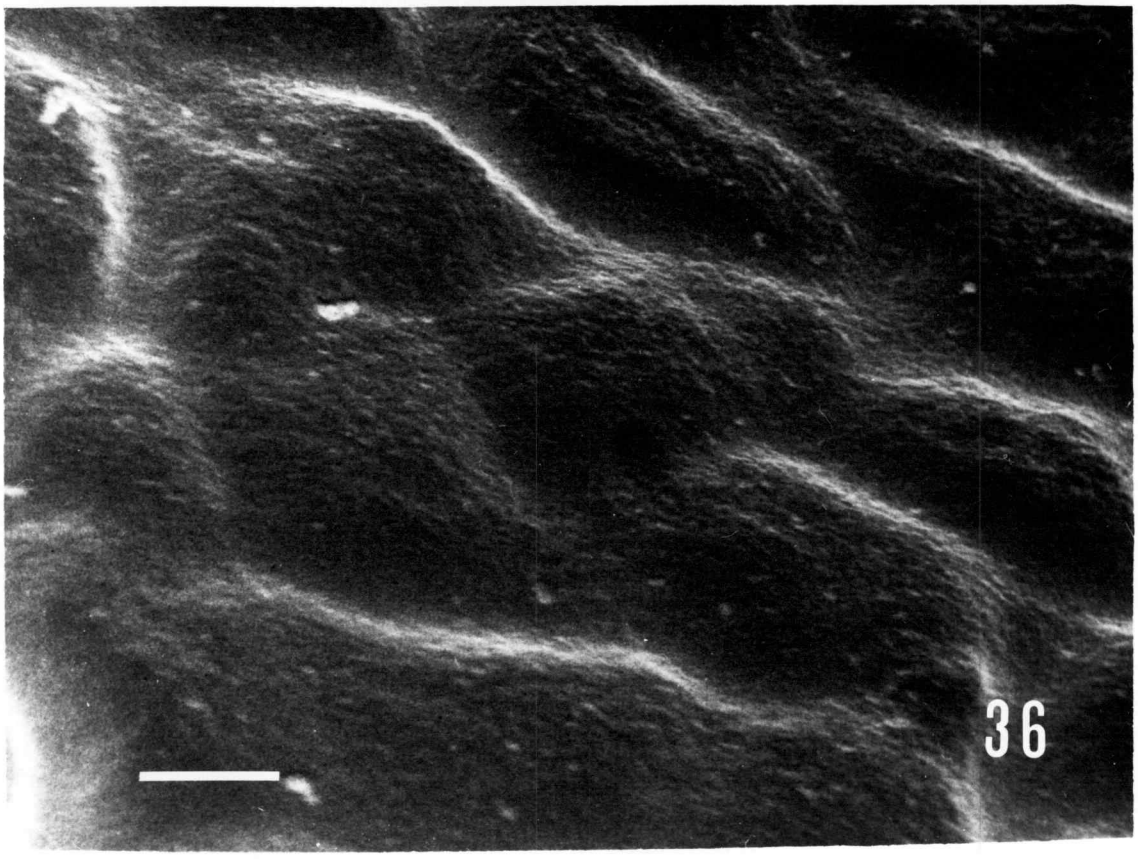
36

Figure 37. Fissure in the mucoid layer of a plasmodium extending deep into the layer and possibly showing microvilli, Mv. (Scale = 20 μm; 1104x)

Figures 38-40. High magnification stereoscan electron micrographs of air dried spores of Sphaeromyxa maiyai.

Figure 38. Spore showing sutural line, Sl; and longitudinal striations, Ls. Note shrinkage over the central sporoplasmic zone, Sp. (Scale = 5.0 μm; 4775x)

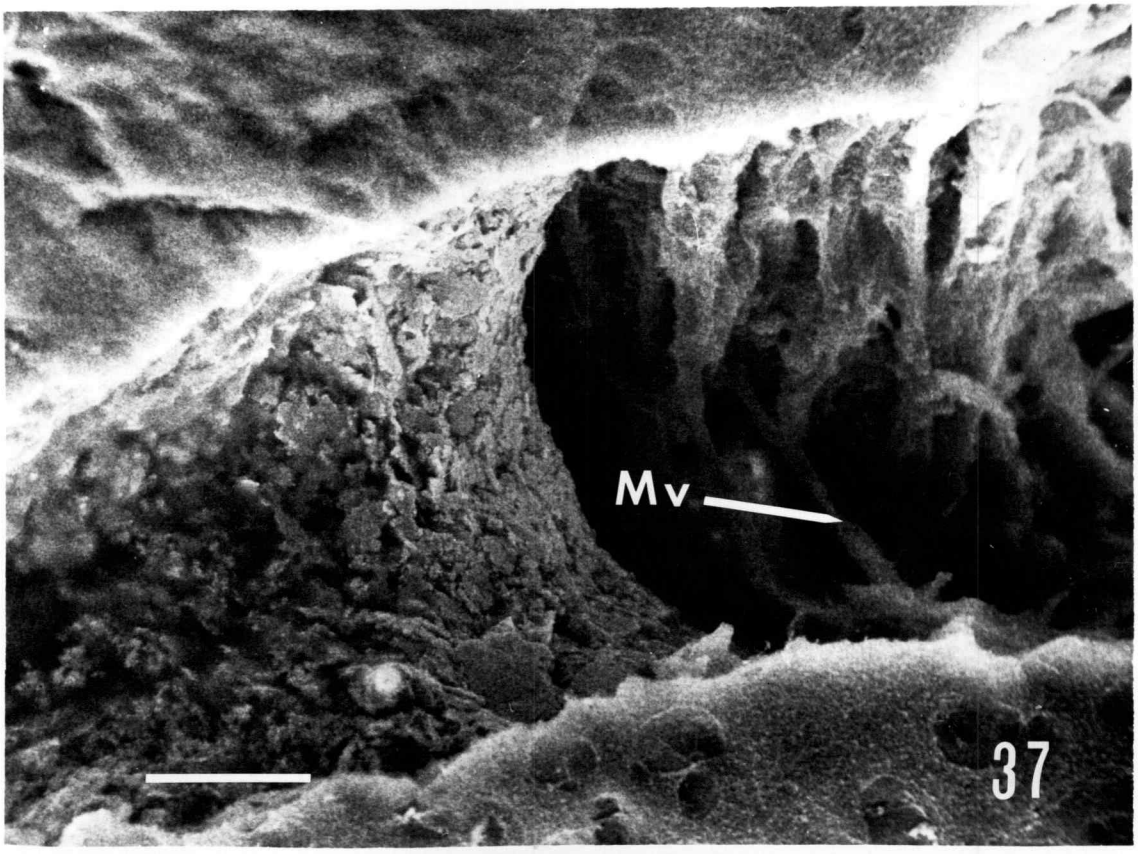
Mv
37

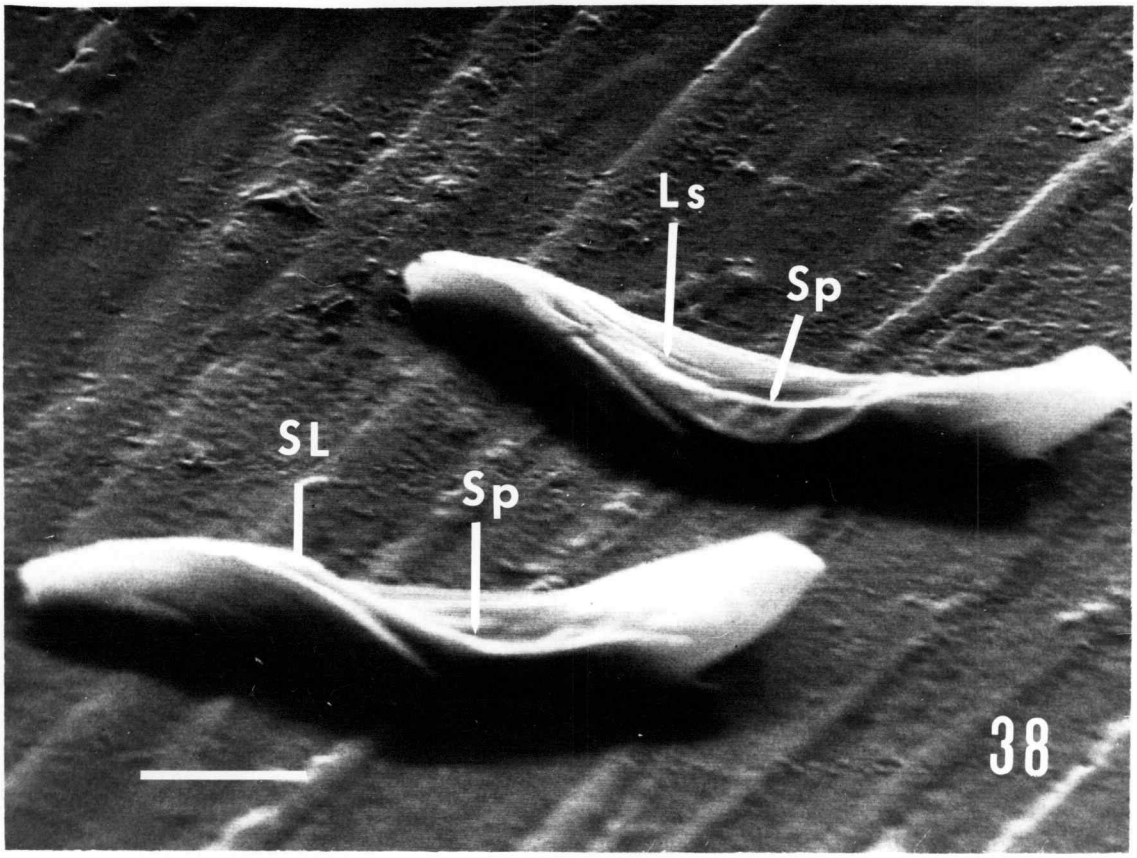
Ls
Sp
SL
Sp
38

Figure 39. Spore showing the spore end, a small indentation, C; representing the center of the unextruded filament, Longitudinal striations, Ls; bulb like swelling, Bs; at spore terminus. Spore shows collapse over sporoplasmic area, Sp. (Scale = 2.0 μm; 14,900x)

Figure 40. Two spores. Spore A shows minimal shrinkage. Spore B shows sutural line, Sl; and parallel longitudinal striations, Ls. (Scale = 5.0 μm; 5050x)

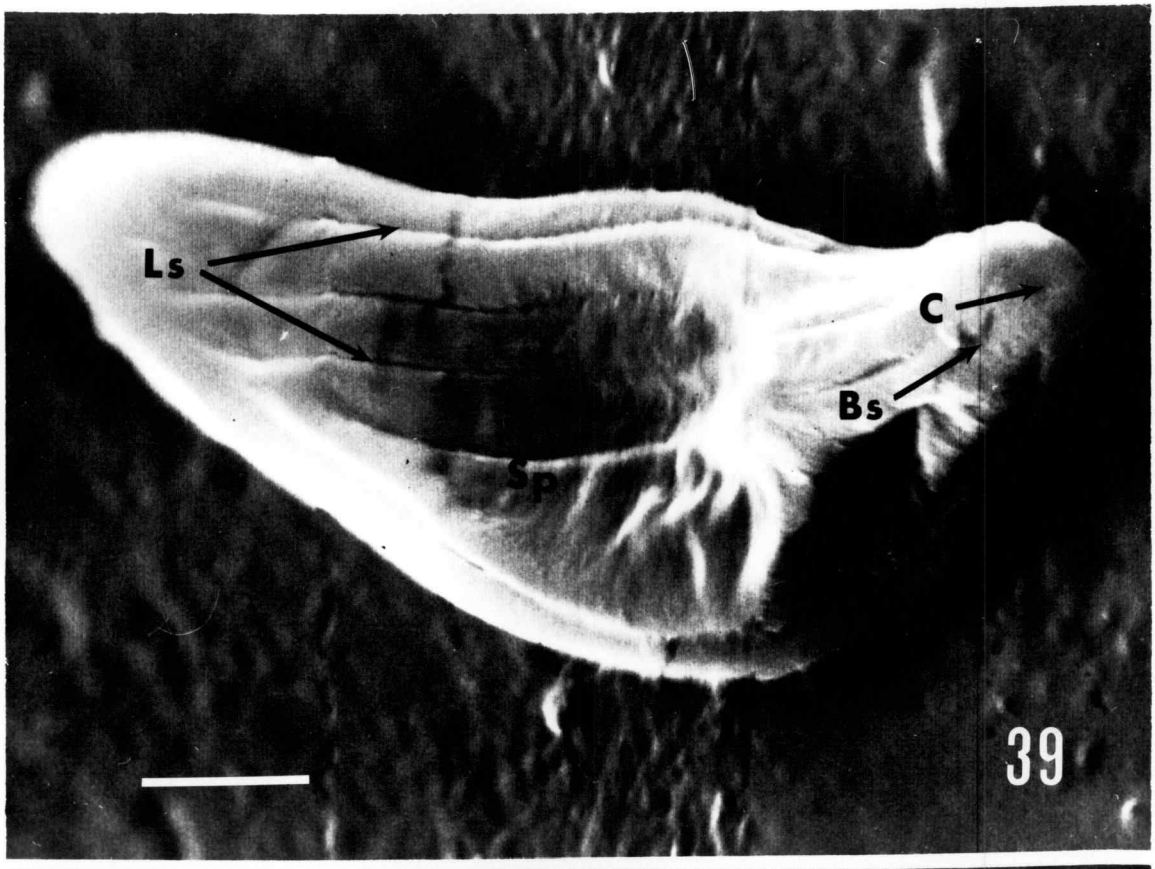
Ls
C
Bs
Sp
39

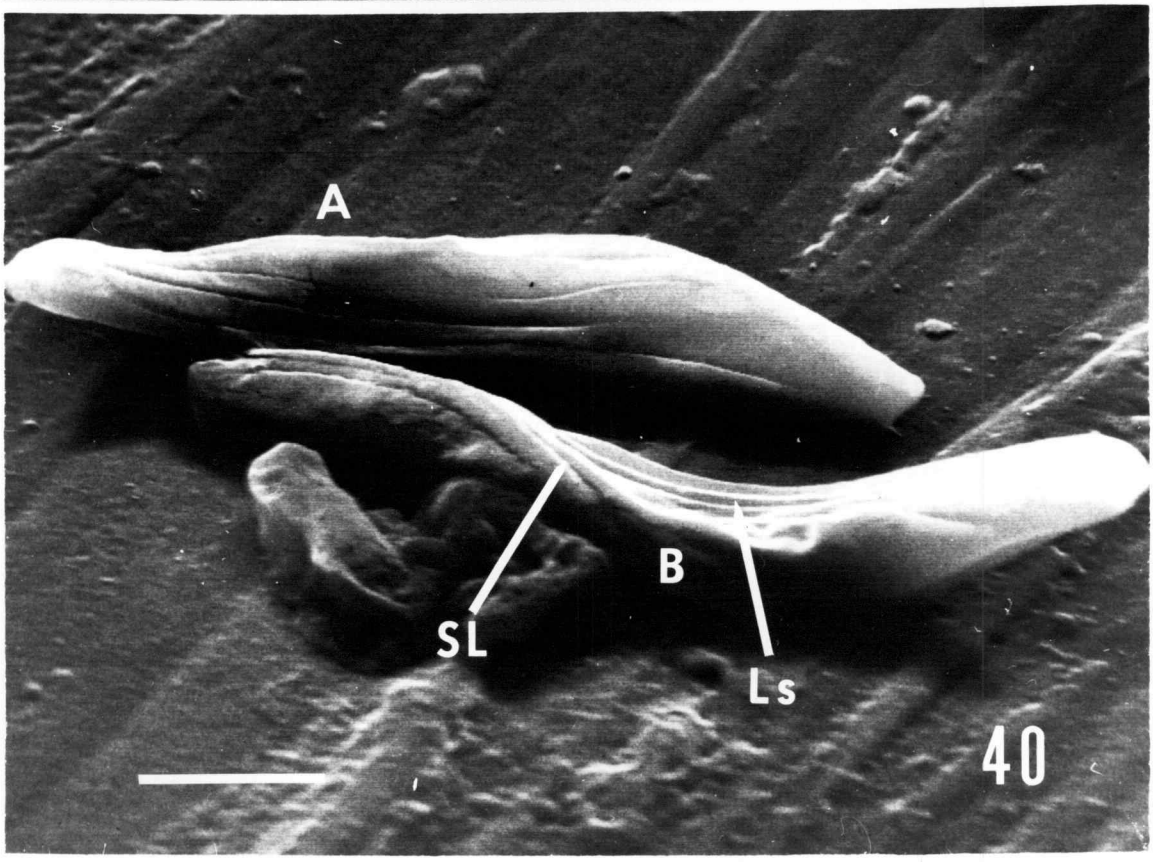
A
B
SL
Ls
40

Figure 41. Critical point dried spore showing minimal shrinkage. (Scale = 4 μm; 9730x)


41

Figures 42-46. High magnification stereoscan electron micrographs of critical point dried spores with extruded polar filaments.

Figure 42. Spores of two species of myxosporidians. Elongated form = Sphaeromyxa maiyai; disc shaped form = Myxosoma sp. Note the structurally rigid proximal portion of the polar filament, Pf_1; and the more pliable apparently adhesive distal portion, Pf_2. (Scale = 6.0 μm; 4300x)

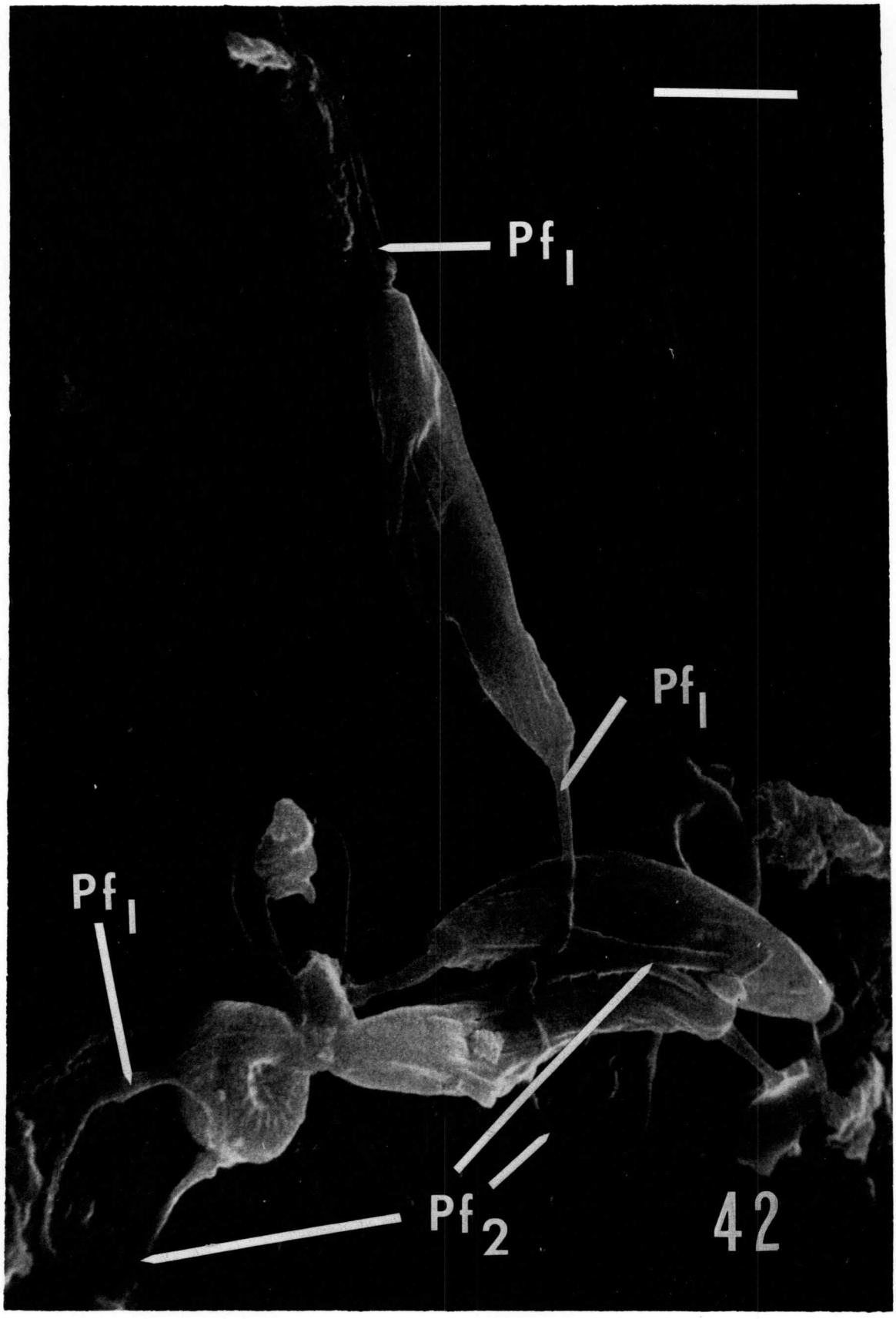
Pf1
Pf1
Pf1
Pf2
42

Figure 43. Spore terminus showing an extruded polar filament. Note the bulb like swelling, Bs; forming the terminal region of the spore; the indistinct junction between the filament and the bulb, J; and the longitudinal groove in the filament, Lg. (Scale = 1.0 μm; 21,195x)

Figure 44. Extruded polar filament showing the point of filament emergence from the polar capsule, J; and the corrugated polar filament, Cpf. (Scale = 2.0 μm; 11,250x)

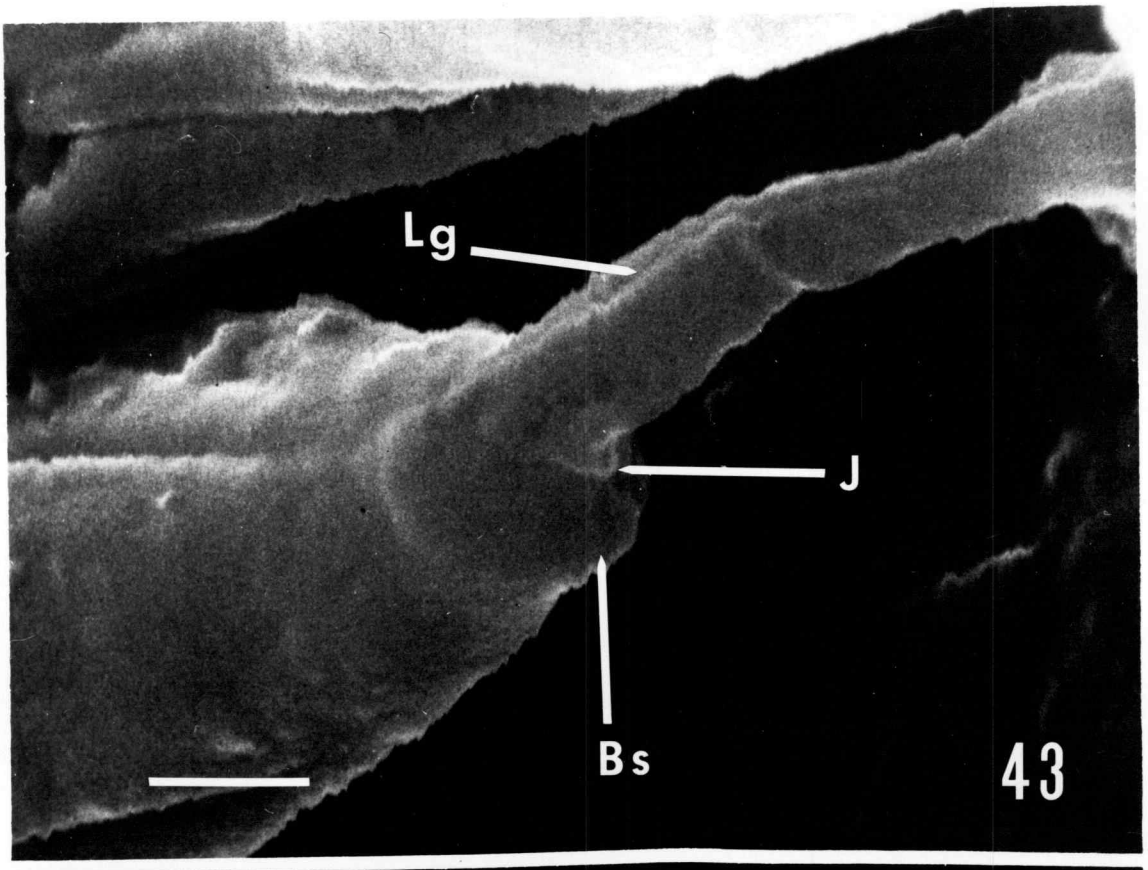
Lg
J
Bs
43

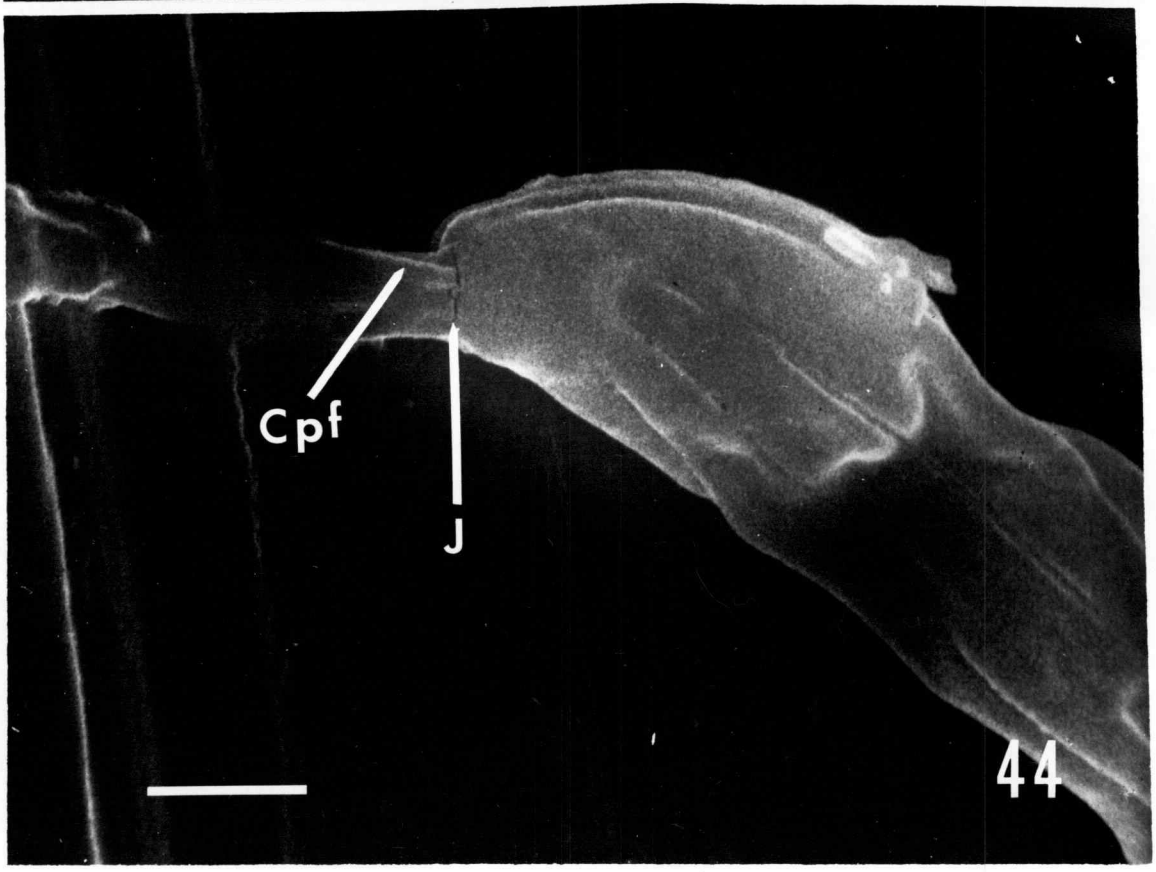
Cpf
J
44

Figure 45. Polar filaments showing apparent artifactual blebs, arrow. (Scale = 2.0 μm; 11, 450x)

Figure 46. Unfolding tip of a polar filament showing the inner filament surface folding over itself to become the definitive outer polar filament surface. (Scale = 2.0 μm; 11, 100x)

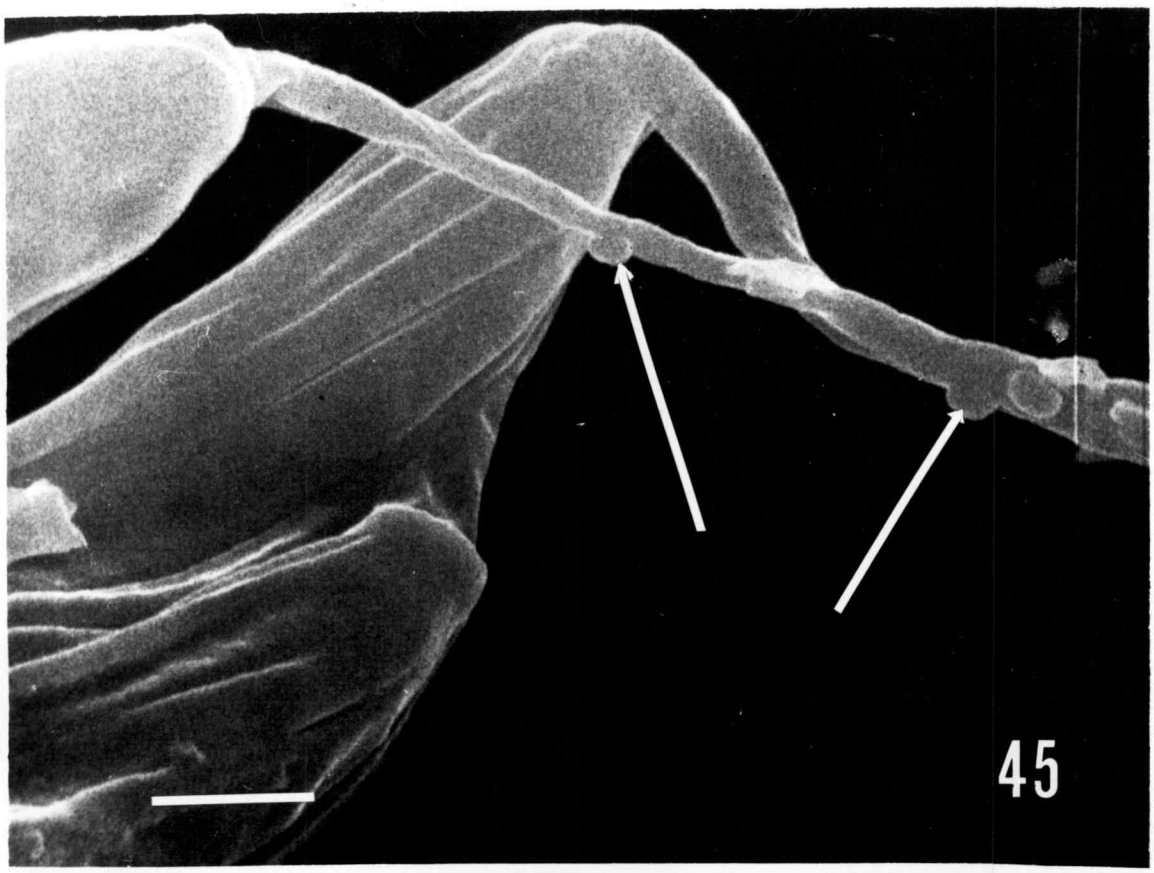
45

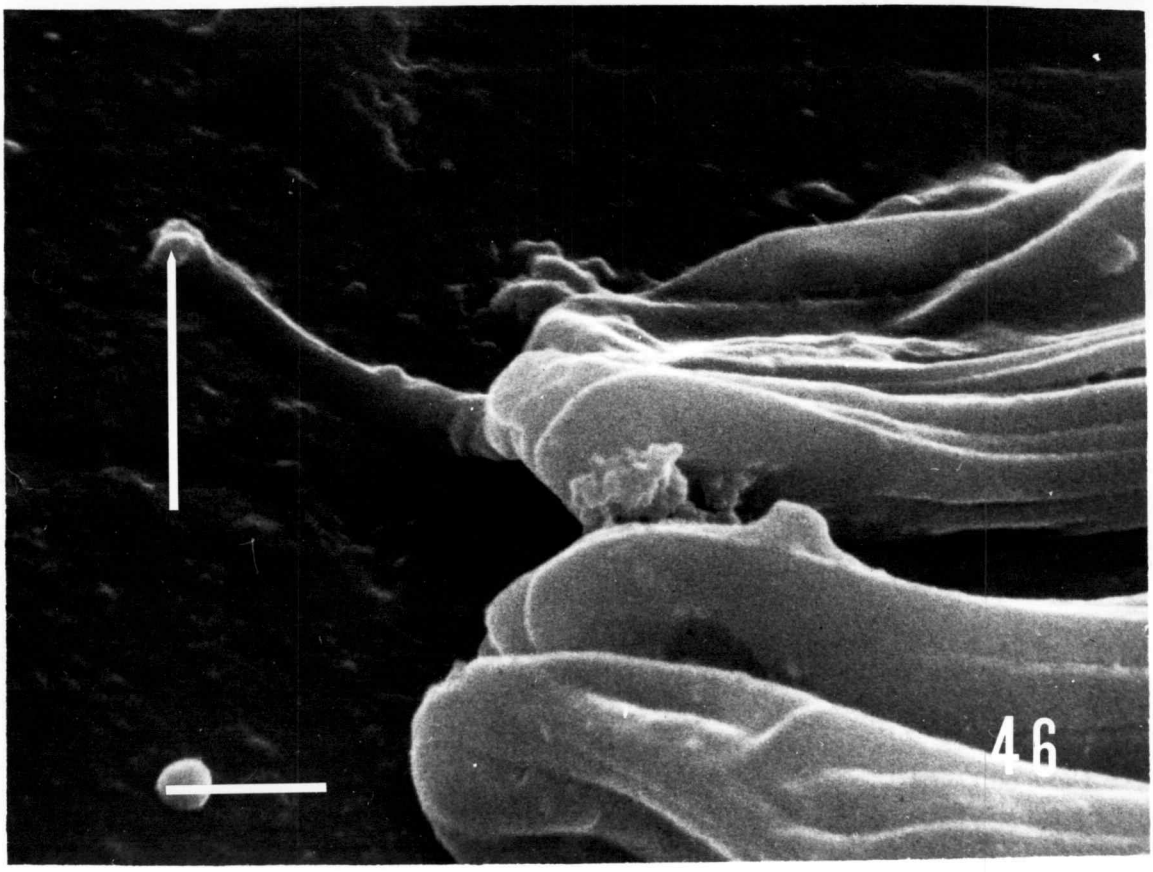
46

Figures 47-99. Transmission electron micrographs of the plasmodium of Sphaeromyxa maiyai.

Figure 47. Cross section showing the general organization of the plasmodium. Notice the sharp separation between the relatively homogenous ectoplasm and the organelle-rich endoplasm. Mucoid layer (= glycocalyx), ML; Ectoplasm, Ec; Vacuoles, V; Endoplasm, En; Glycogen deposits, G; layer of microtubules, Mt; Autophagic vacuoles, Av; Lipid inclusion bodies, L; Mitochondria, M; Developing sporoblasts, St. (Scale = 1.0 μm; 12,750x)

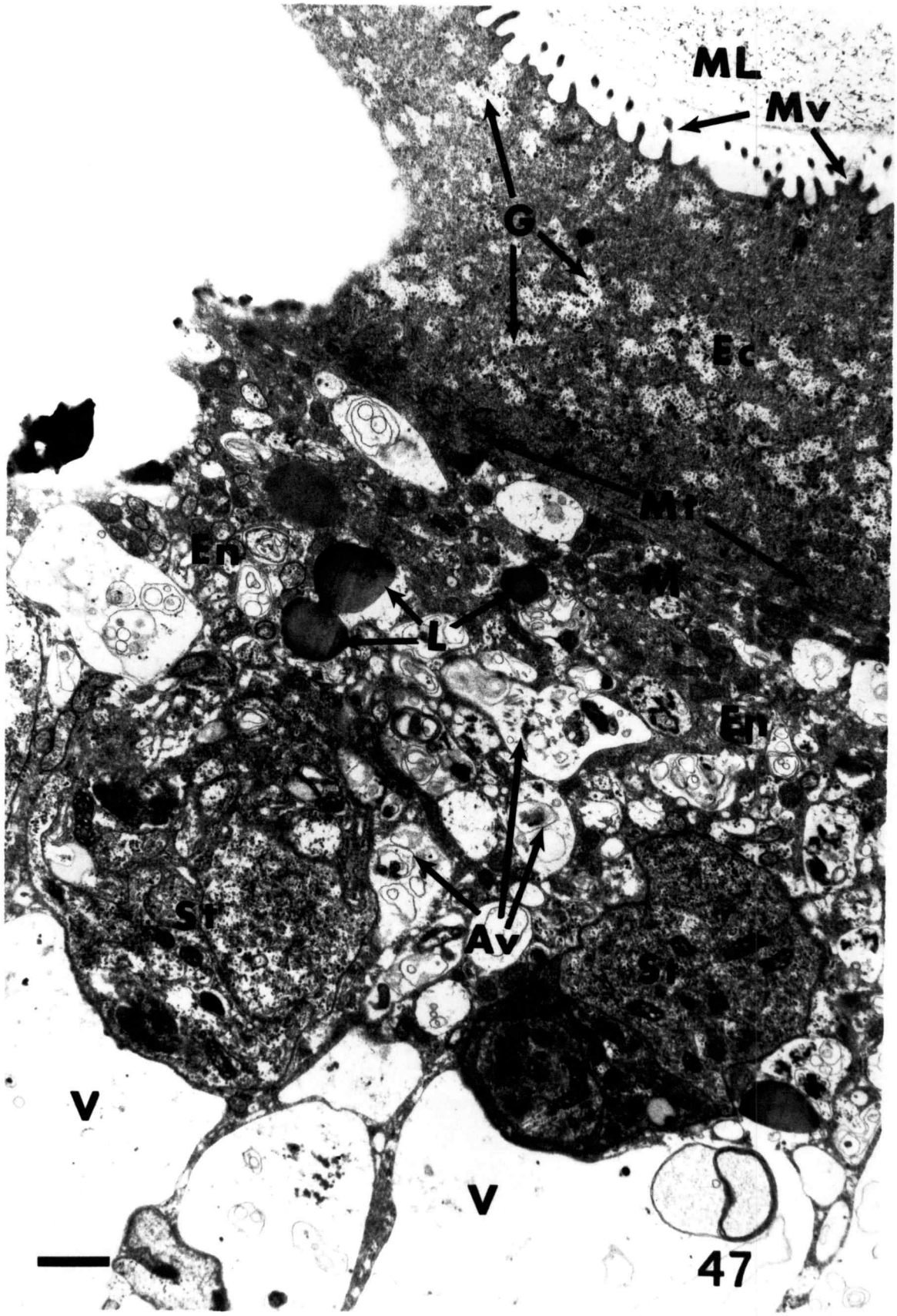
ML
Mv
G
Ec
Mt
M
En
L
En
Av
St
St
J
V
V
47

Figure 48. Cross section showing developing sporoblasts in the endoplasm adjacent to the endoplasmic-ectoplasmic junction. Rugae, R; Ectoplasmic-endoplasmic junction, EE; Polar capsule within the capsulogenous cell, Pc; Enveloping cell of the sporoblast, EvC. (Scale = 1.0 μm; 11,000x)

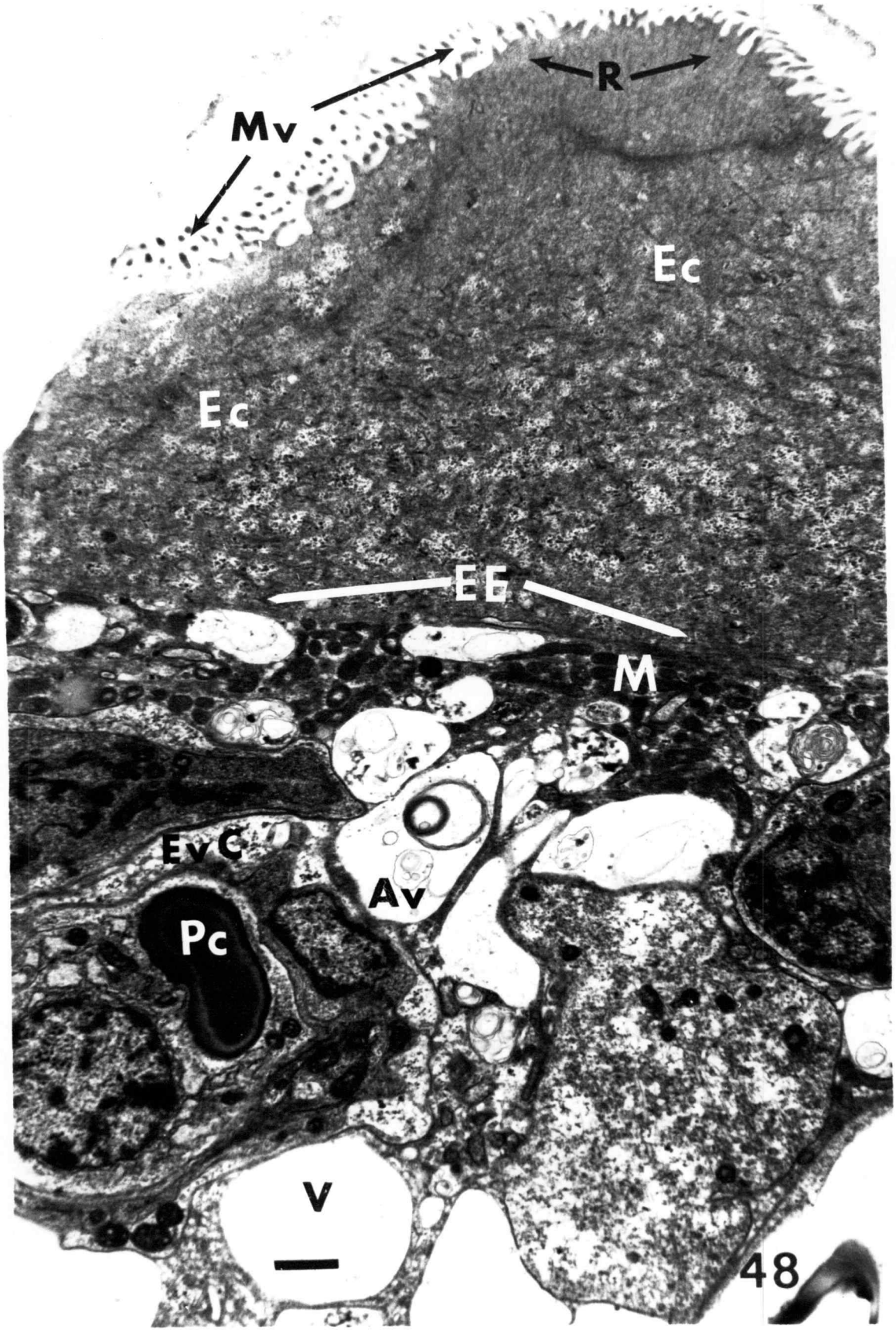
Mv
R
Ec
Ec
EE
M
EvC
Av
Pc
V
48

Figure 49. Cross section showing a diffuse or Type II ectoplasmic-endoplasmic junction. Ectoplasmic vacuoles, EcV; Mitochondria, M; Vegetative nucleus, VgN; Sporoblast, St; Enveloping cell of sporoblast, EvC; Enveloped cell, EnC; Pseudopodial extensions of the outer enveloping cell, Ps; Ectoplasm, Ec; Endoplasm, En; Alveolar layer of the endoplasm, Av; Lipid inclusion bodies, L. (Scale = 2 μm; 7550x)

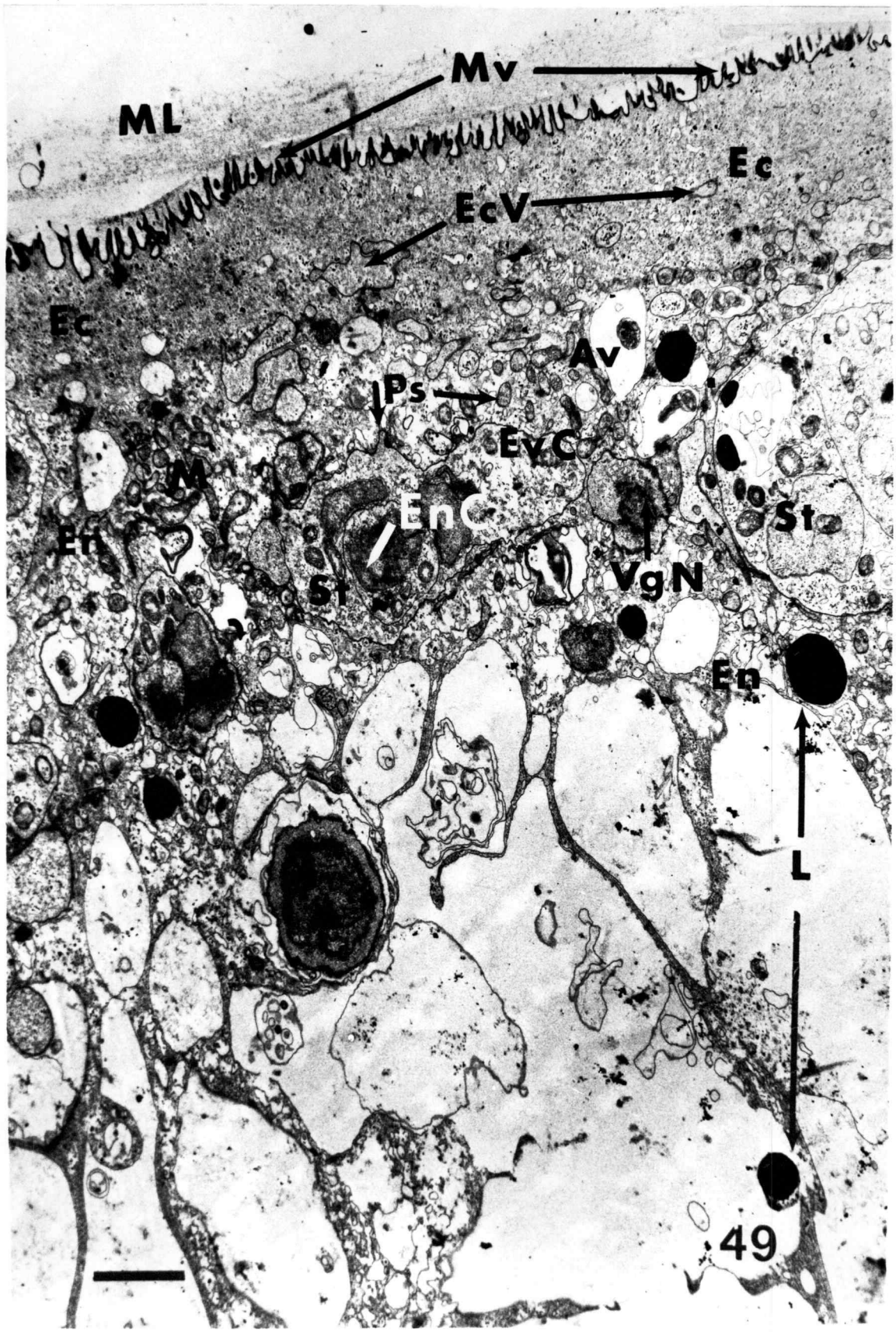
Mv
ML
Ec
EcV
Ec
Av
Ps
EvC
M
EnC
St
Et
St
VgN
En
L
49

Figure 50. Cross section showing several sporoblasts within the endoplasm. Also large ectoplasmic vacuoles in communication with the plasmalemma. Sporoblast, St; Pseudopodia, Ps; Lipid inclusion bodies situated along the ectoplasmic-endoplasmic junction, L. (Scale = 2.0 μm; 8900x)

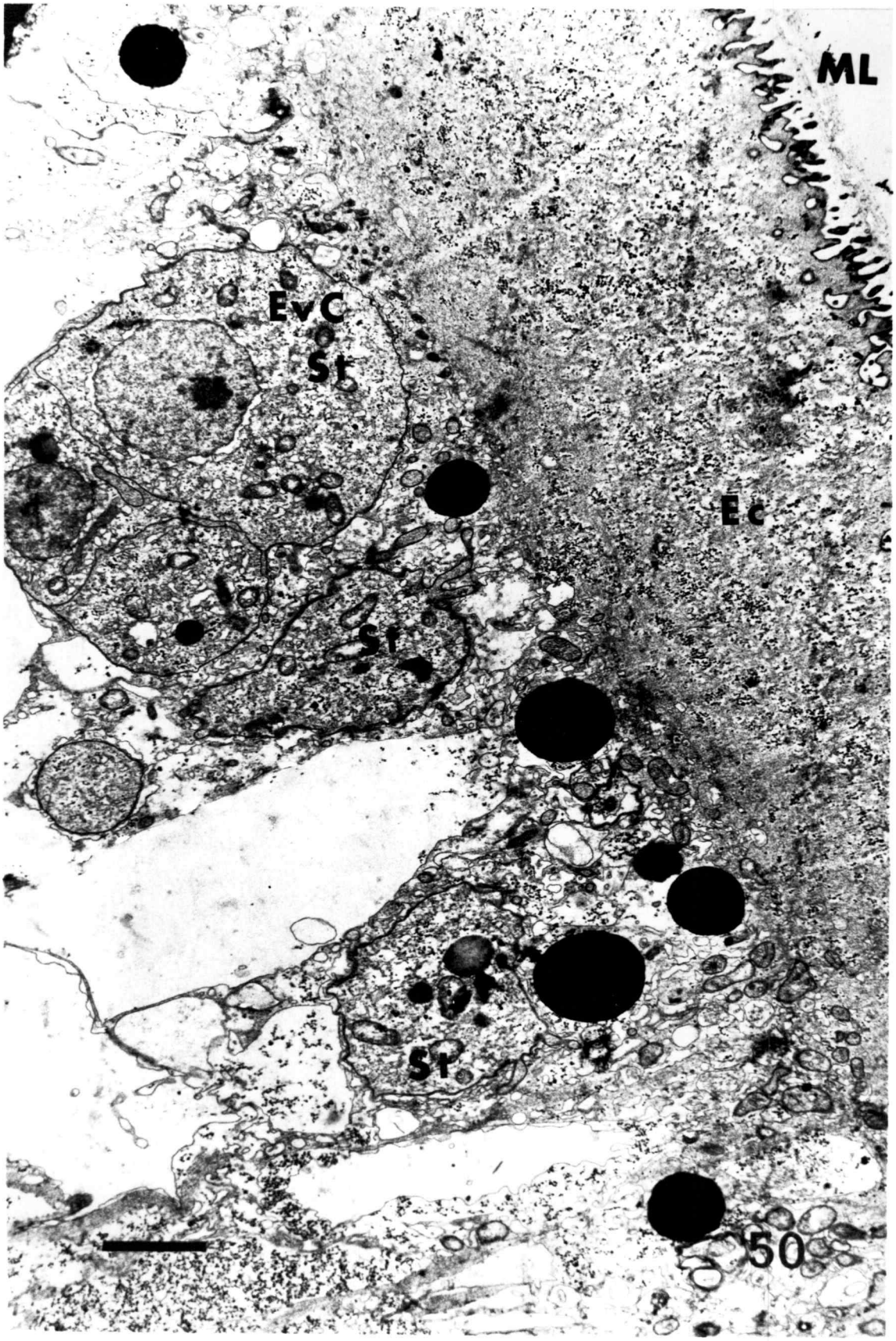
ML
EvC
St
Ec
St
St
50

Figure 51. Cross section of the ectoplasmic surface showing the bilamminate configuration of the glycocalyx. A microtubular layer is seen near the ectoplasmic-endoplasmic junction. Plasmalemma, PL; Outer layer of the glycocalyx, MLO; Inner layer of the glycocalyx, MLI; Alpha glycogen aggregates, G; Microtubules, Mt; Mitochondria, M; Dense inclusion bodies, DI. (Scale = 1.0 μm; 24, 600x)

Figure 52. Cross section of the outer ectoplasmic zone showing the filamentous glycocalyx, microfilaments, and a pinocytotic vesicle forming at the plasmalemma. Pinocytotic vesicle, PV; Plasmalemma (unit membrane), Pl; Alpha glycogen aggregates, G; Vesicles of the agranular endoplasmic reticulum, Ag; Microfilaments extending from the microvilli into the outer ectoplasm, F; Dense areas of glycocalar material along the microvillar apices, ML. (Scale = 0.5 μm; 63, 000x)

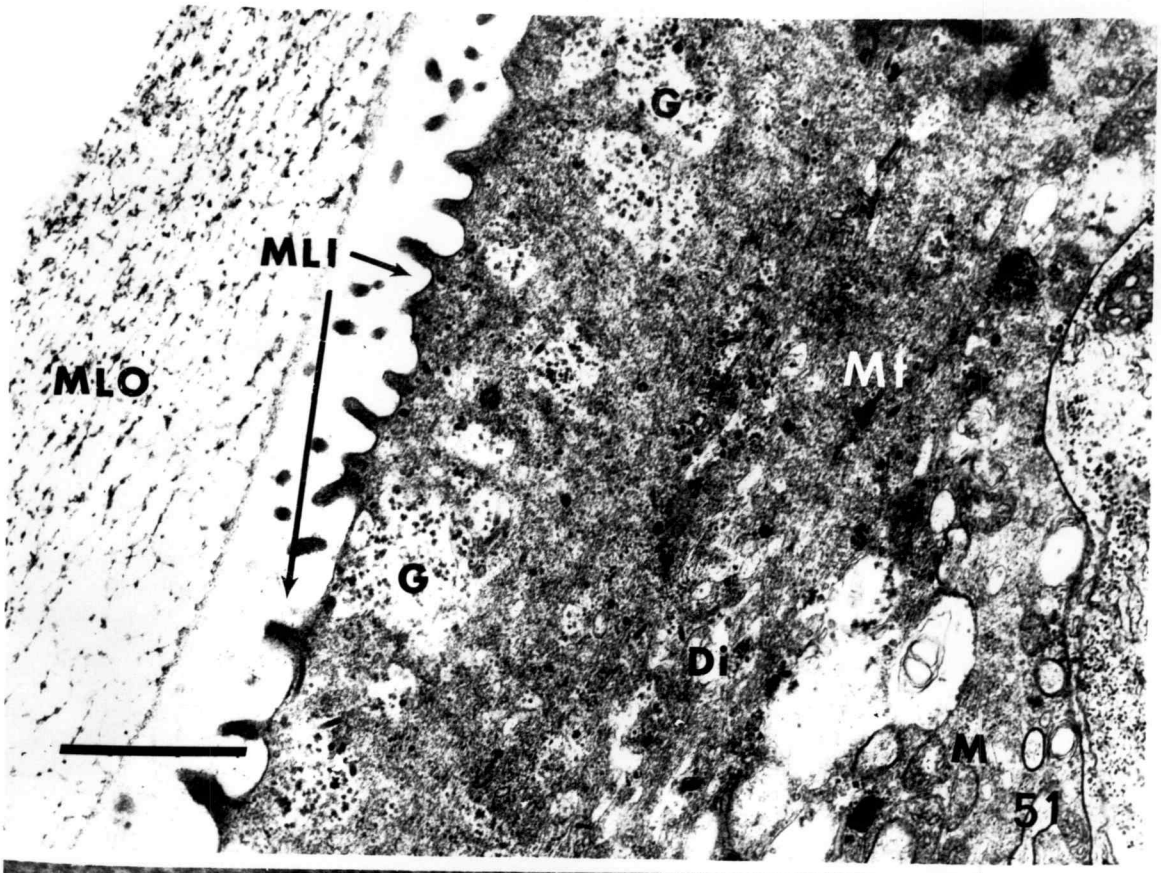
G
MLI
MLO
Mf
G
Di
M
51

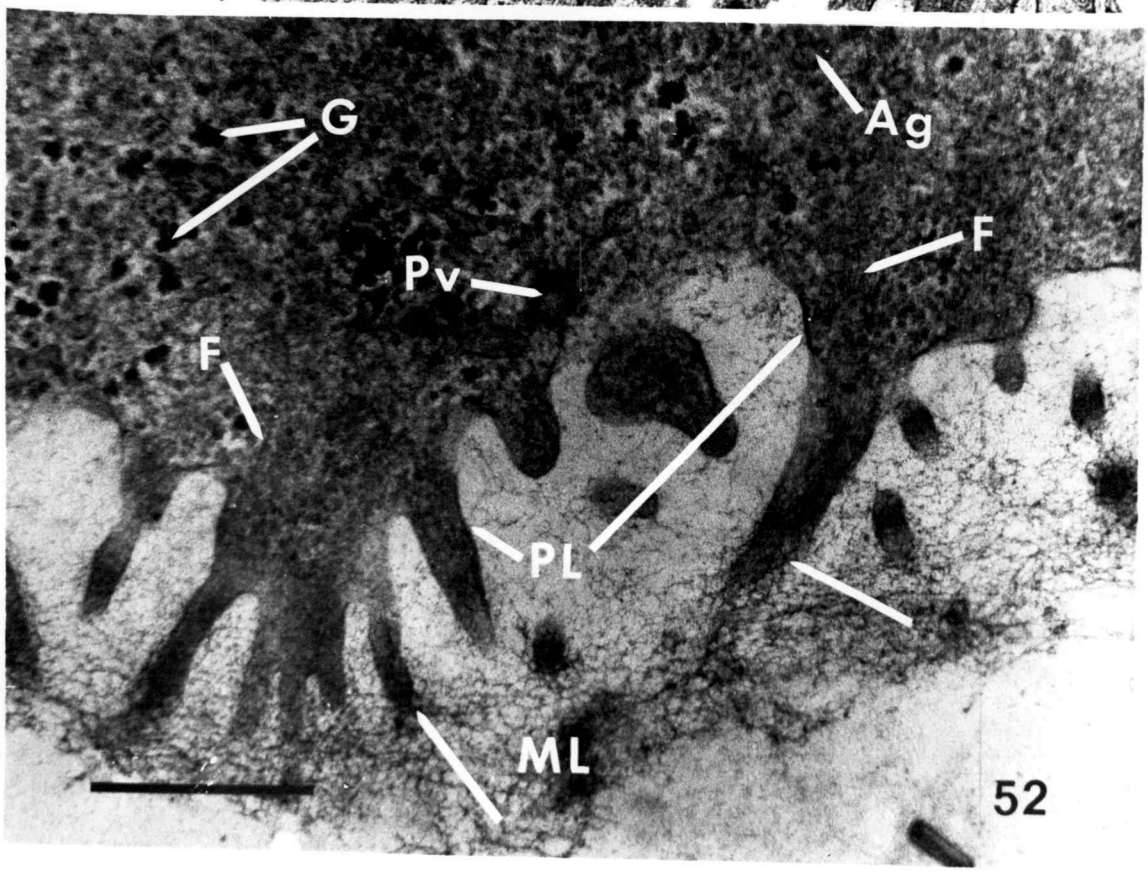
G
Ag
F
Pv
F
PL
ML
52

Figure 53. Cross section of the outer ectoplasm showing a region of relatively high concentration of agranular endoplasmic reticulum. Vesicles of the agranular endoplasmic reticulum, Ag; Microfilaments, F; Alpha glycogen granules, G; Pinocytotic vesicles, Pv. (Scale = 0.5 μm; 51, 700x)

Figure 54. Cross section of the external ectoplasmic region and the investing glycocalar layer. Microfilaments, F; Plasmalemma, Pl; Glycocalar filaments, ML. (Scale = 0.1 μm; 184, 000x)

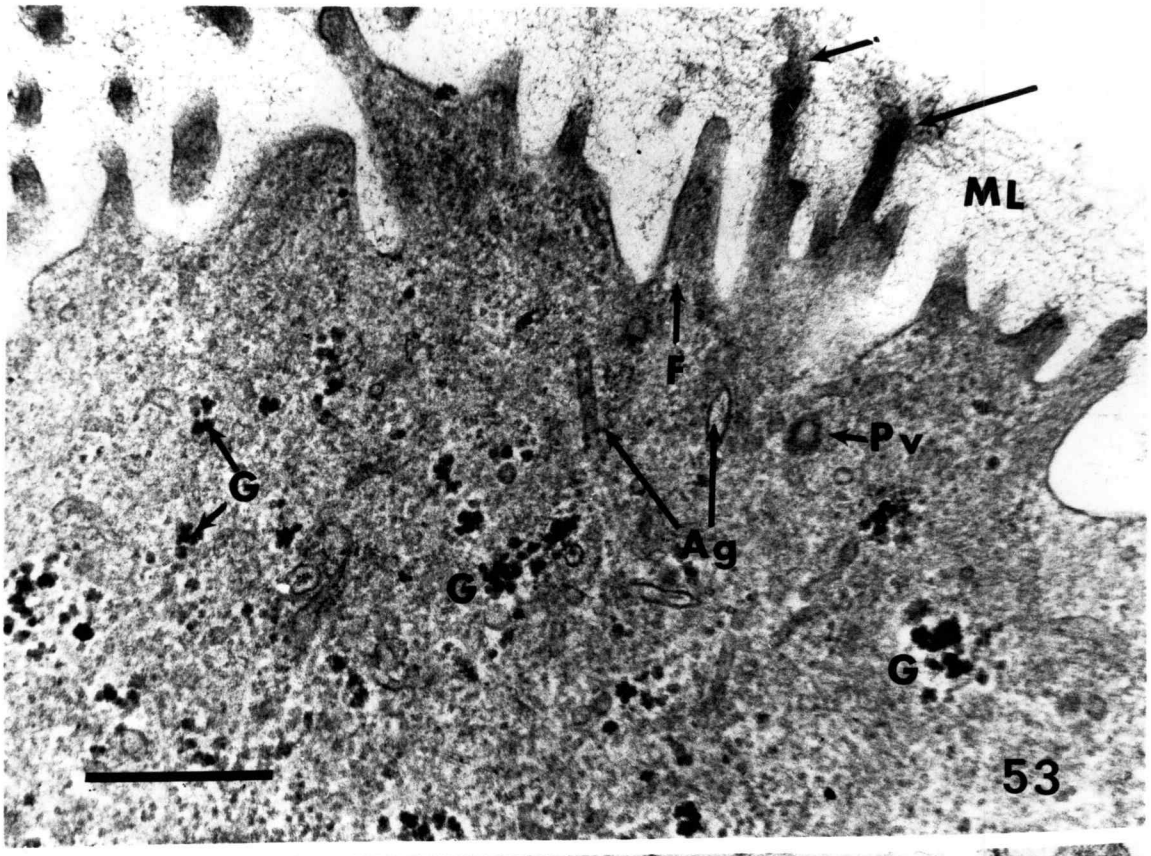
ML
F
Pv
G
G
Ag
G
53

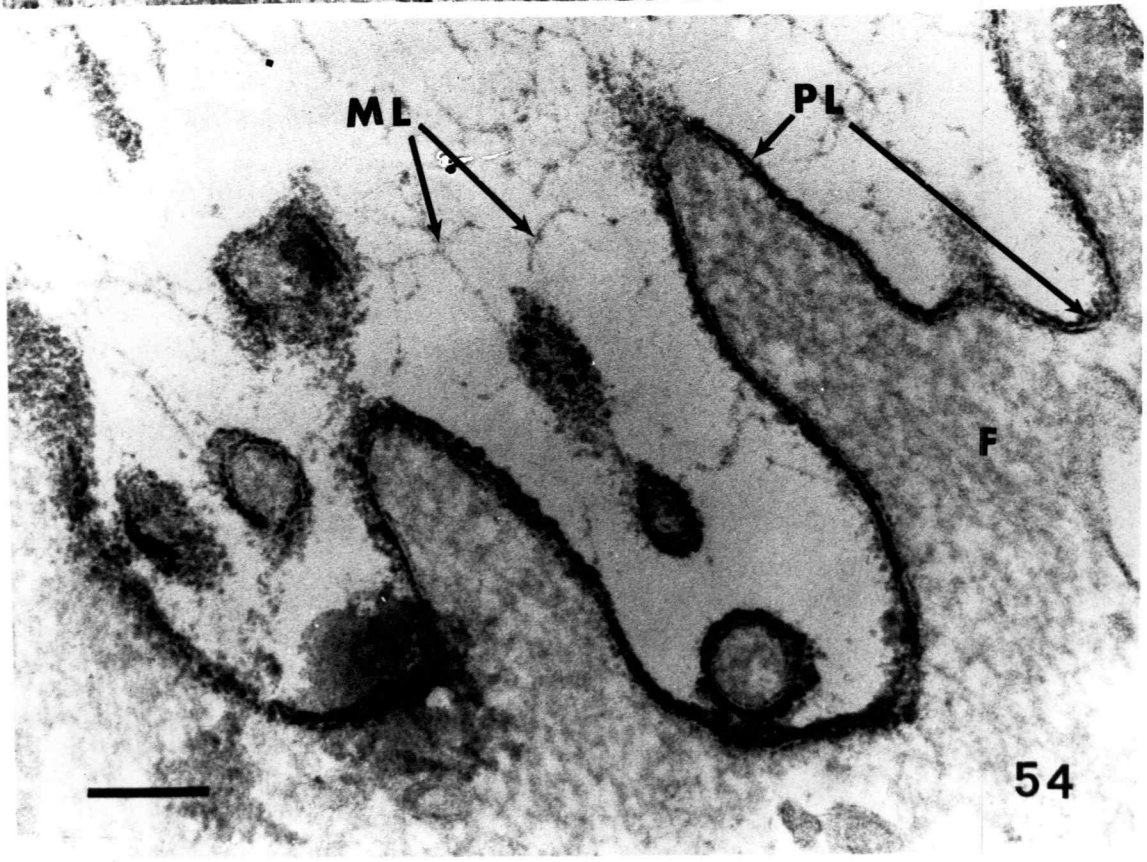
ML
PL
F
54

Figure 55. Cross section of the ectoplasm showing a sharp separation between the ectoplasmic-endoplasmic layers. Microtubules, Mt; Vesicles of the agranular endoplasmic reticulum, Ag; Dense inclusion bodies, DI; Endoplasmic-ectoplasmic junction, EE; Ribosome like particles, Rb. (Scale = 0.5 μm; 30, 100x)

Figure 56. Section of the endoplasm showing an early sporoblast and a high regional density of autophagic vacuoles and residual bodies. Sporoblast, St; Autophagic vacuoles, Av; Myelin-like figures, Mw; Microtubules, Mt; Pseudopodial extensions from sporoblast, Ps; Glycogen, G. (Scale = 0.5 μm; 30, 100x)

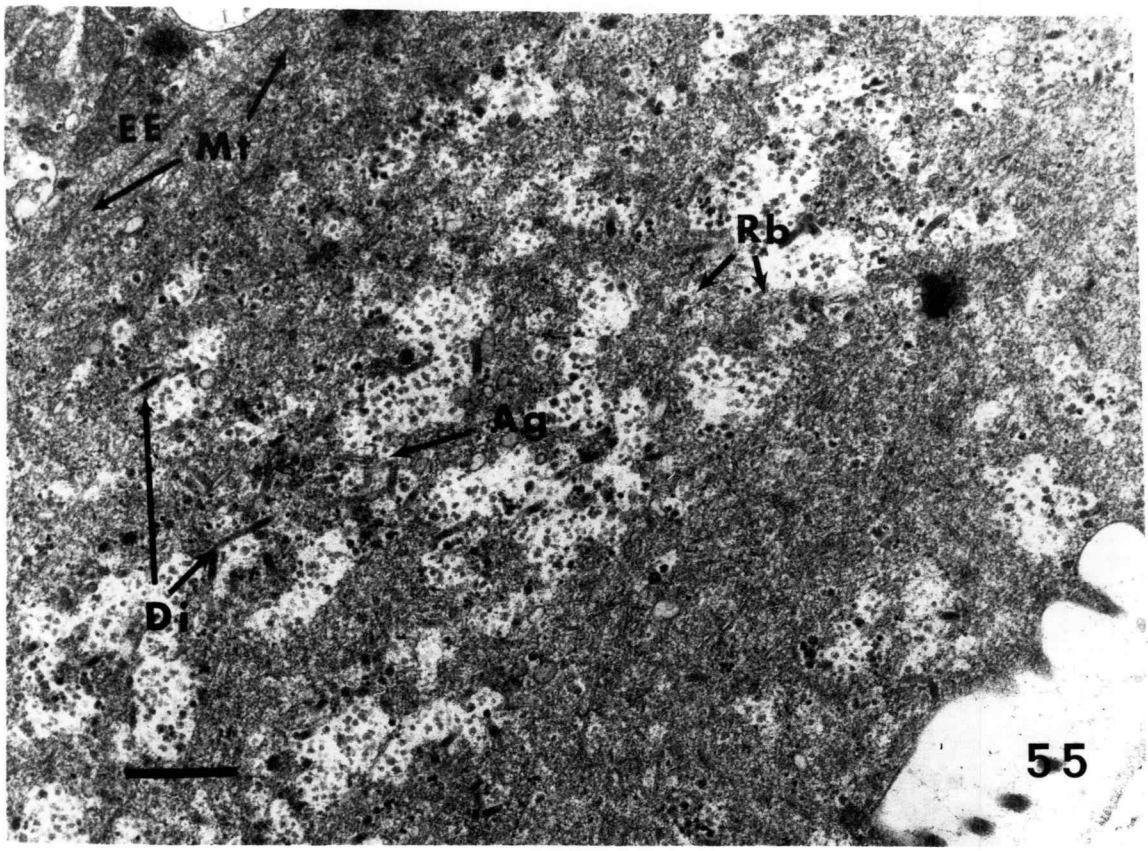
EE
Mt
Rb
Ag
Di
55

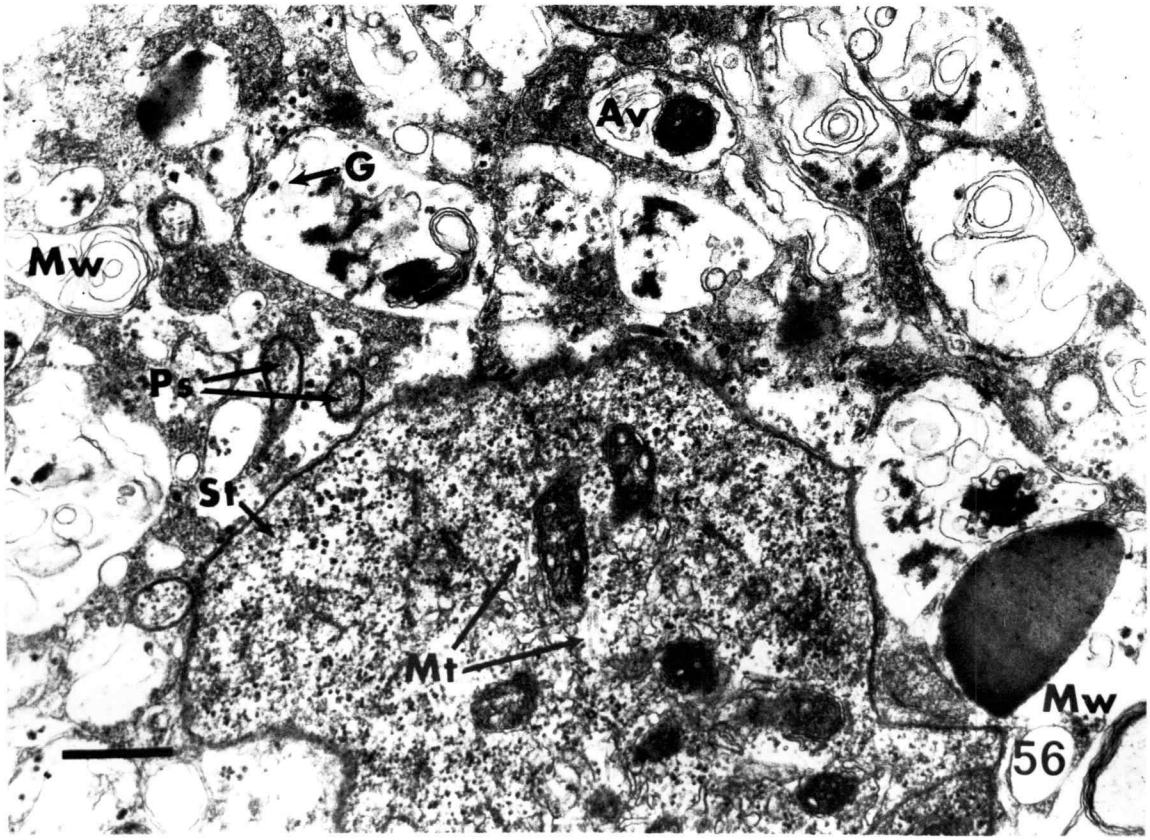
Av
G
Mw
Ps
Sf
Mt
Mw
56

Figure 57. Cross section of the external ectoplasmic region. Glycocalyx, ML; Alpha glycogen aggregates, G; Agranular endoplasmic reticulum, Ag. (Scale = 0.5 μm; 51,700x)

Figure 58. Cross section of the ectoplasmic surface showing dense inclusion bodies and the unit membrane structure of the plasmalemma. Dense inclusion bodies, DI; Plasmalemma, PL; Tips of sinuous microvilli, TMv. (Scale = 0.1 μm; 101,500x)

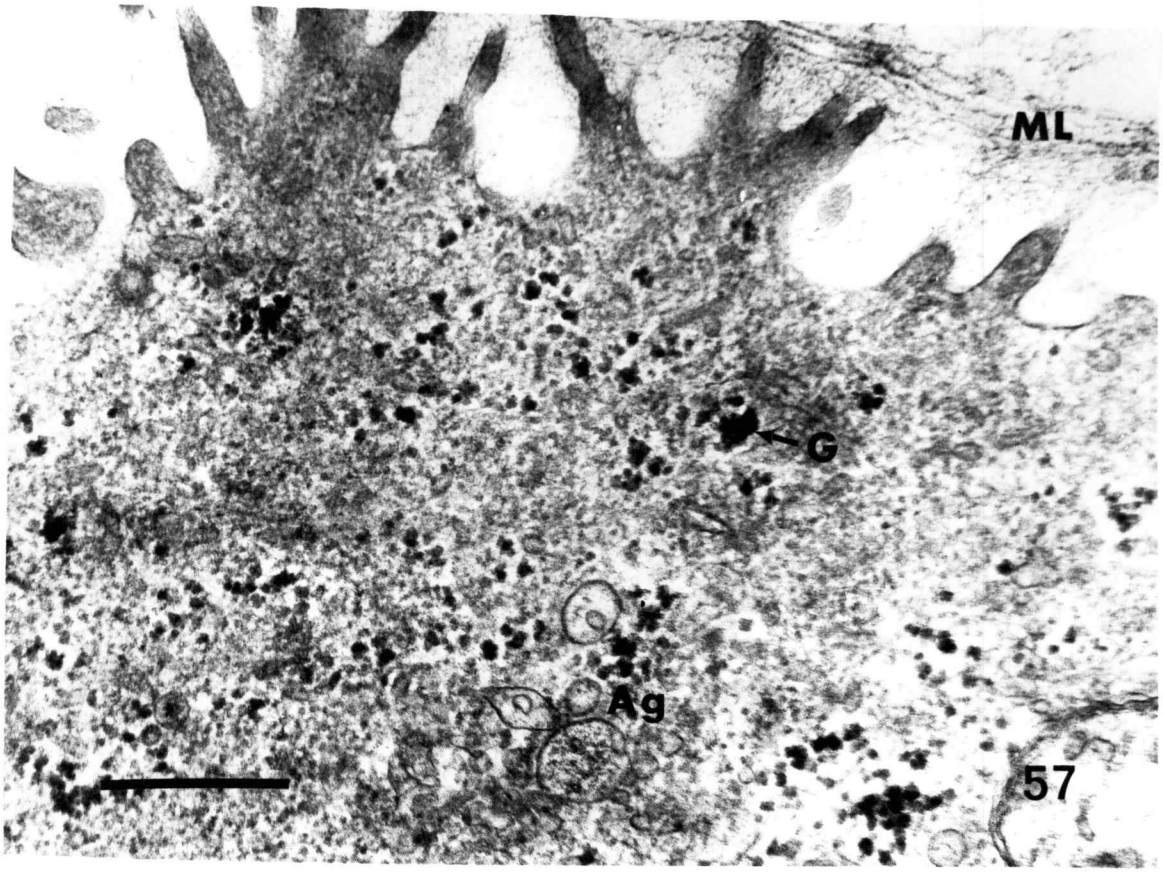
ML
G
Ag
57

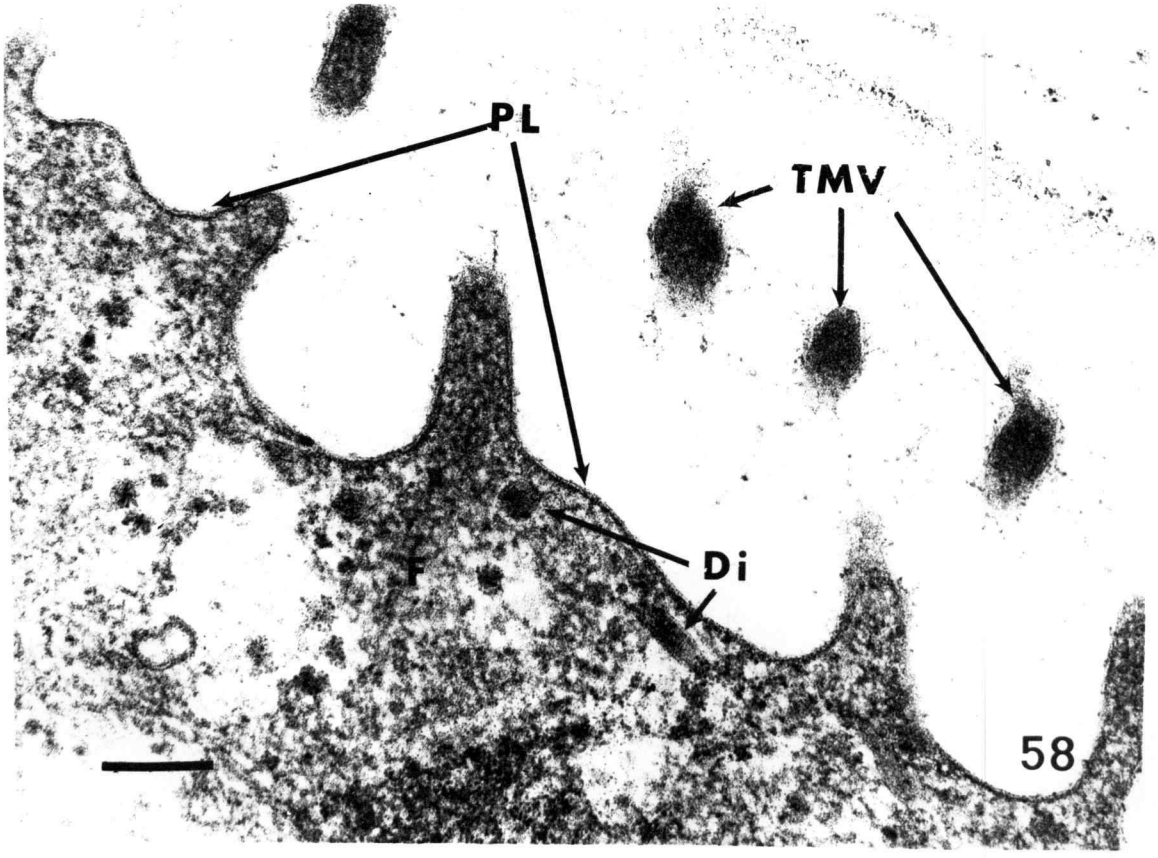
PL
TMV
F
Di
58

Figure 59. Large vacuoles in the ectoplasm. Phagocytotic vacuoles, PVa. (Scale = 0.5 μm; 30, 100x)

Figure 60. Heavily vacuolated area within the ectoplasm. Phagocytotic vacuole, PVa; Pinocytotic vesicles, PV; Microtubules, Mt. (Scale = 0.5 μm; 51, 700x)

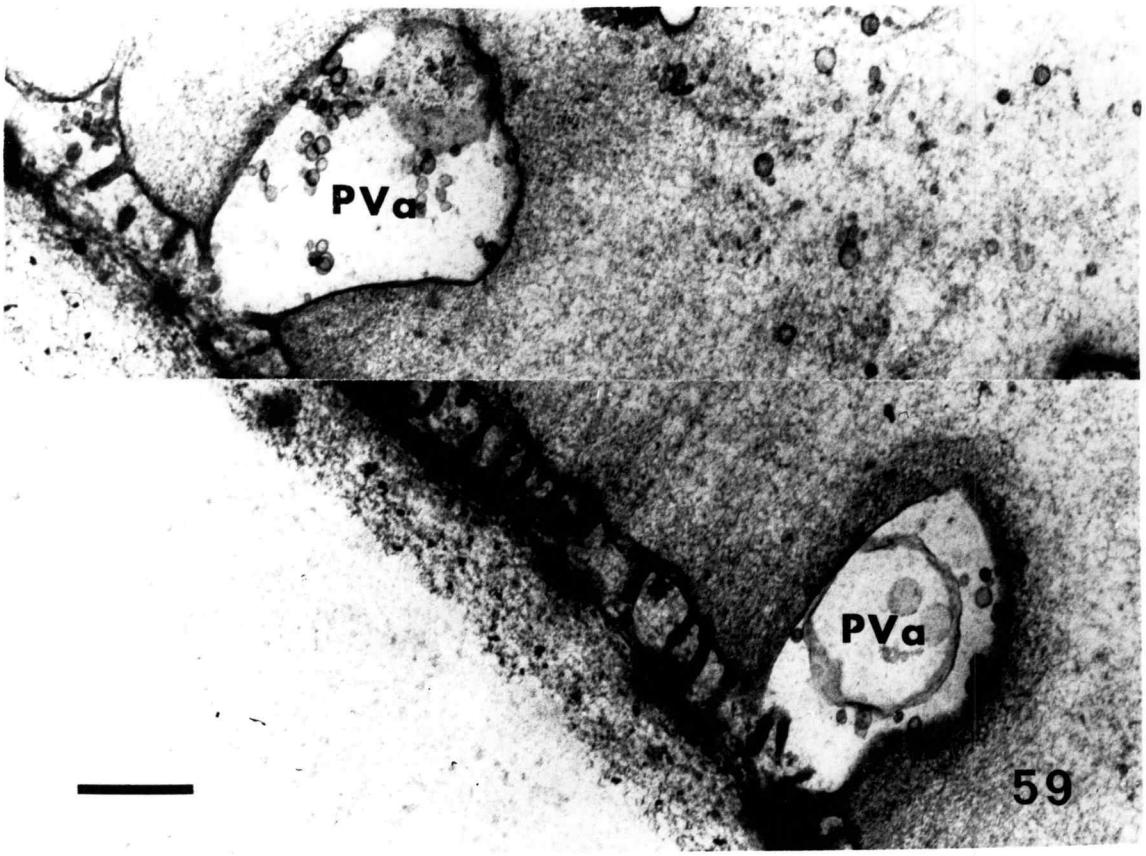
PVa
PVa
59

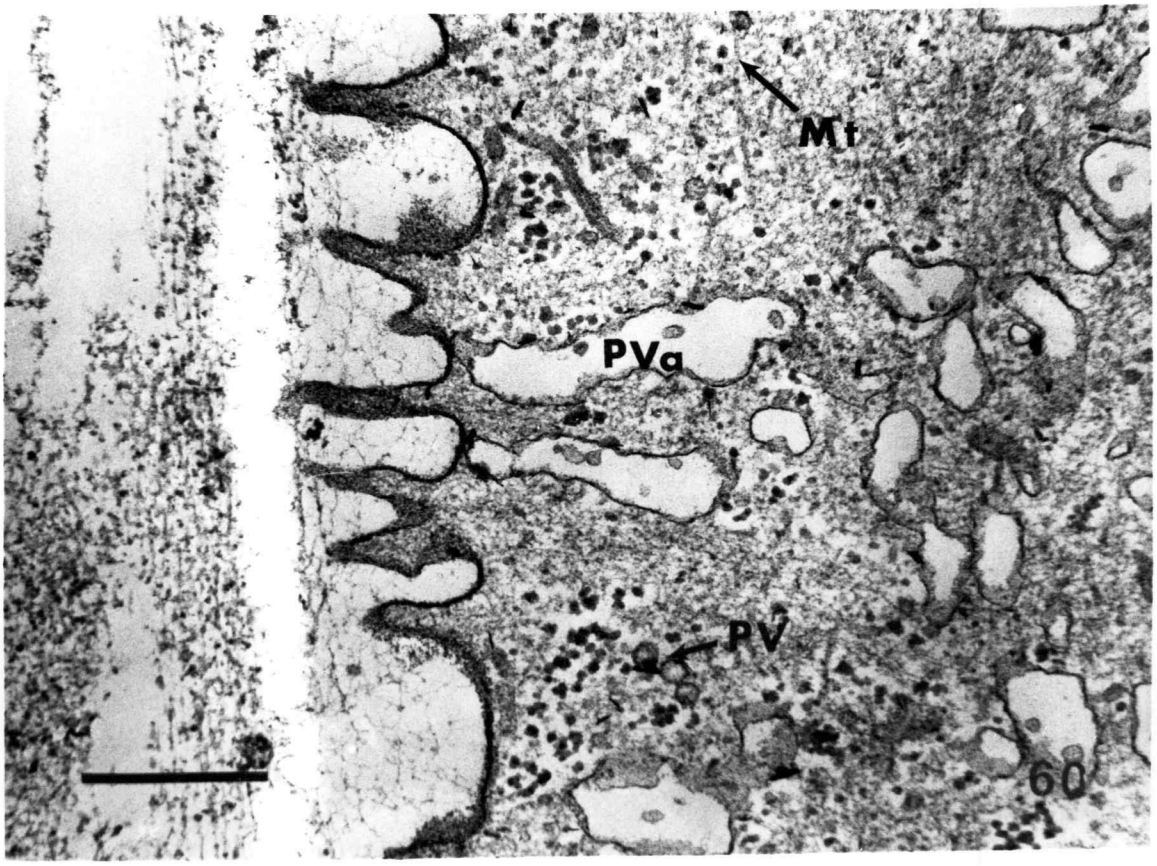
Mt
PVa
PV
60

Figure 61. Tangential section of the ectoplasmic surface showing the circular profile of the microvilli, MV. (Scale = 0.25 μm; 63, 000x)

Figure 62. Cross section showing the ectoplasm and the outer aspects of the endoplasm. Ectoplasm, Ec; Vacuoles, V; Vegetative nucleus, VgN; sinuous microvilli, MV; Golgi apparatus, Gc. (Scale = 1.0 μm; 15, 750x)

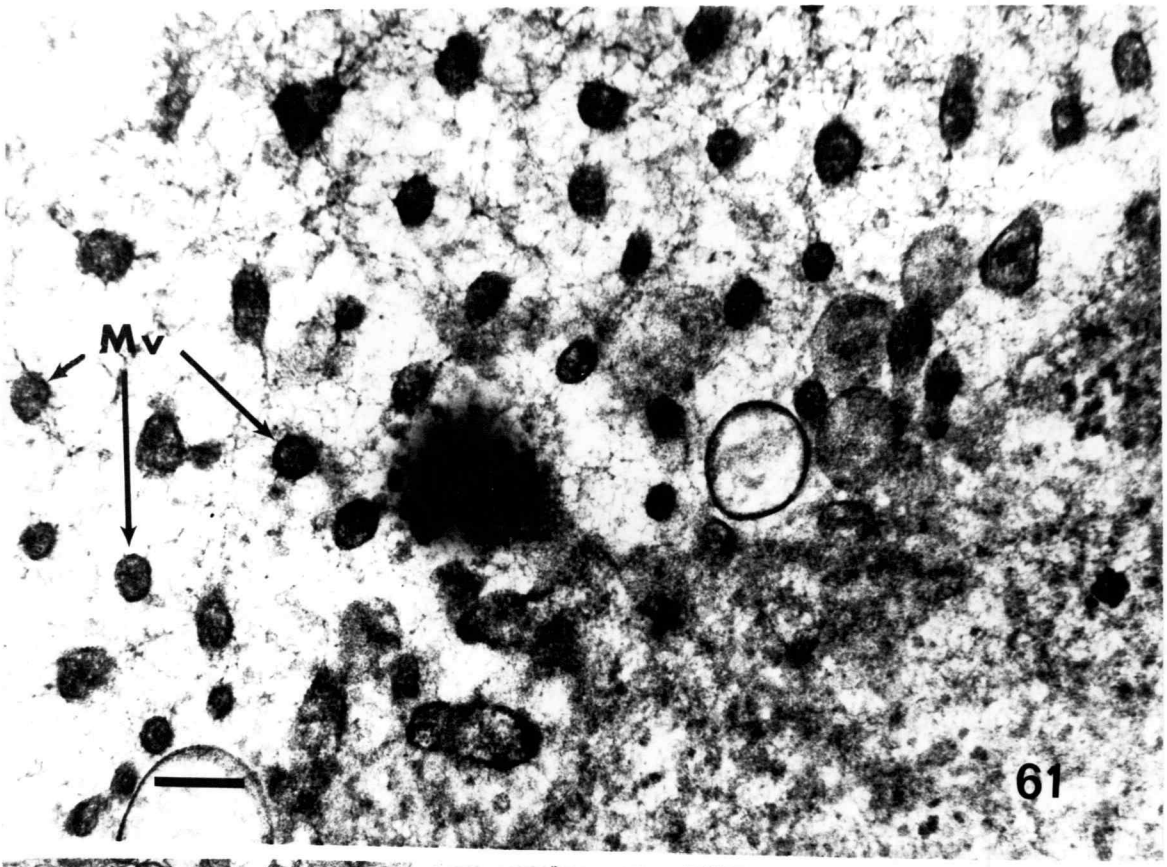
Mv
61

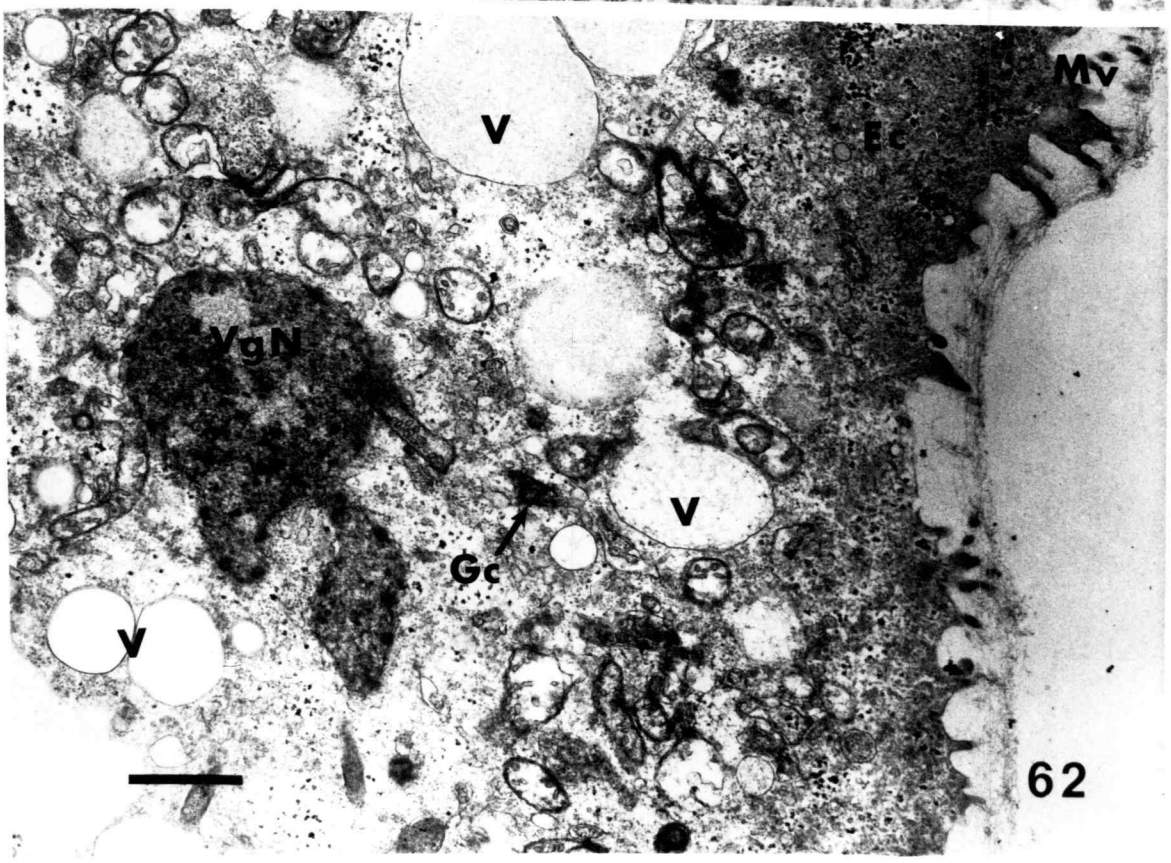
V
Mv
VgN
V
Gc
V
62

Figure 63. Cross section of ectoplasm showing dense inclusion bodies and microfilaments within the microvilli. Dense inclusion bodies, Di; Pinocytotic vesicles, Pv; Microfilaments, F; Glycogen aggregates, G. (Scale = 0.2 μm; 101,500x)

Figure 64. Cross section of the ectoplasm and endoplasm. Glycogen aggregates, G; Agranular endoplasmic reticulum, Ag; Pseudopodia of enveloping cell of the sporoblast, Ps; Endoplasmic-ectoplasmic junction, EE; Lipid droplets, L. (Scale = 1.0 μm; 11,500x)

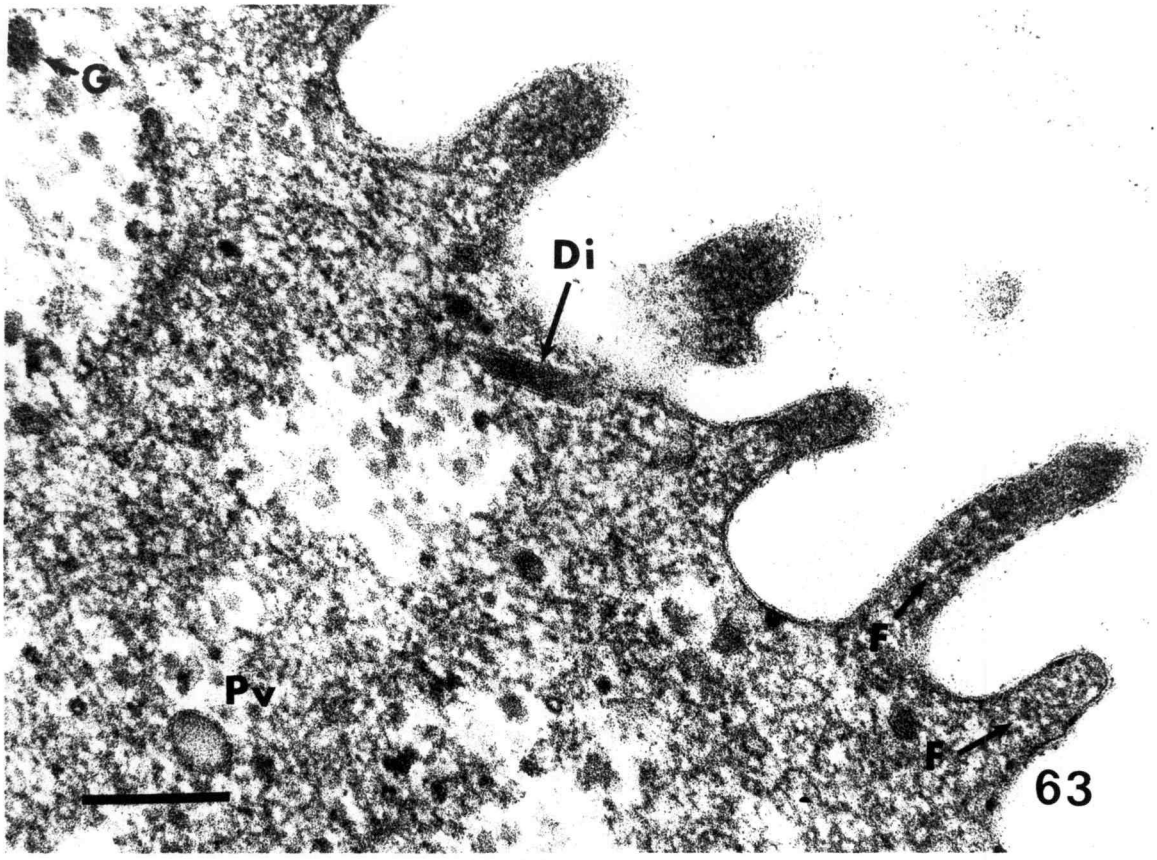
G
Di
F
Pv
P
63

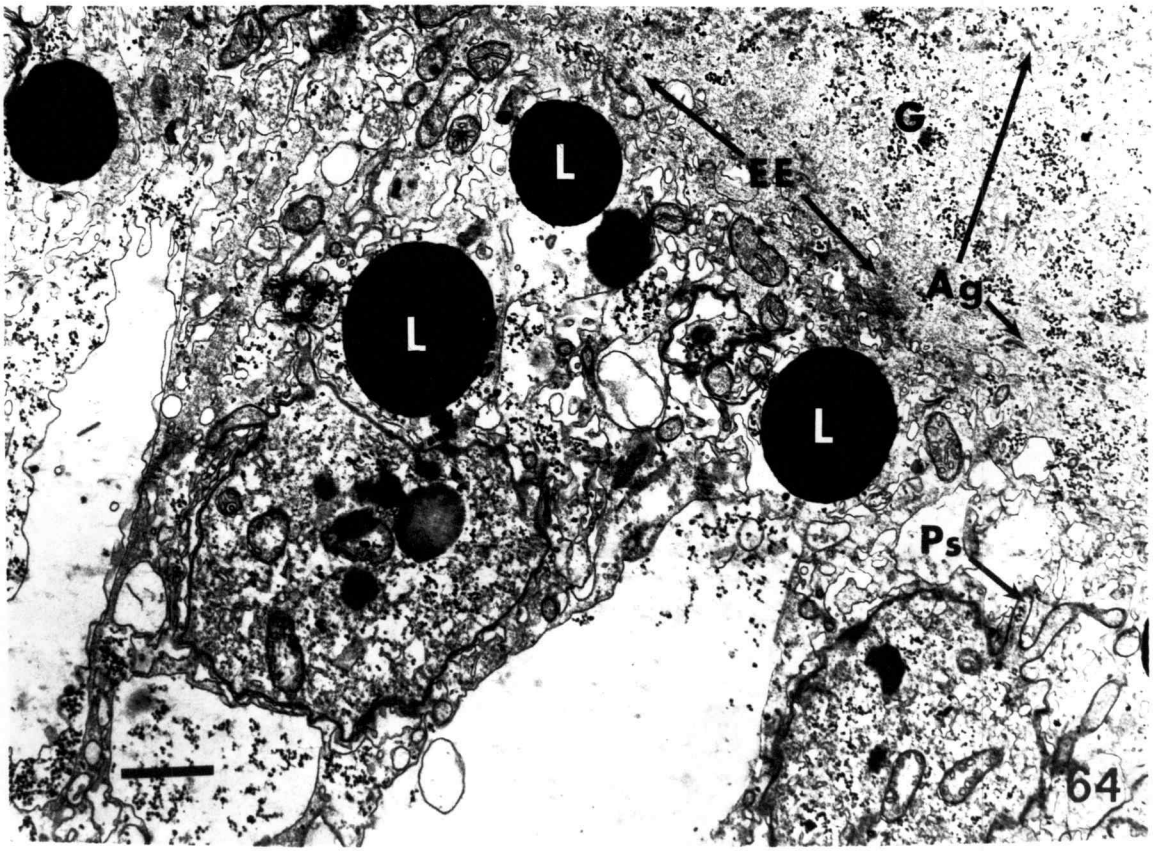
L
EE
G
Ag
L
L
Ps
64

Figure 65. Developing sporoblast within the ectoplasm. Enveloping cell of the sporoblast, EvC; Enveloped cell, EnC; Nucleus, N; Microtubuli, Mt; Pseudopodial extensions of the enveloping cell of the sporoblast, Ps. (Scale = 1.0 μm; 24, 600x)

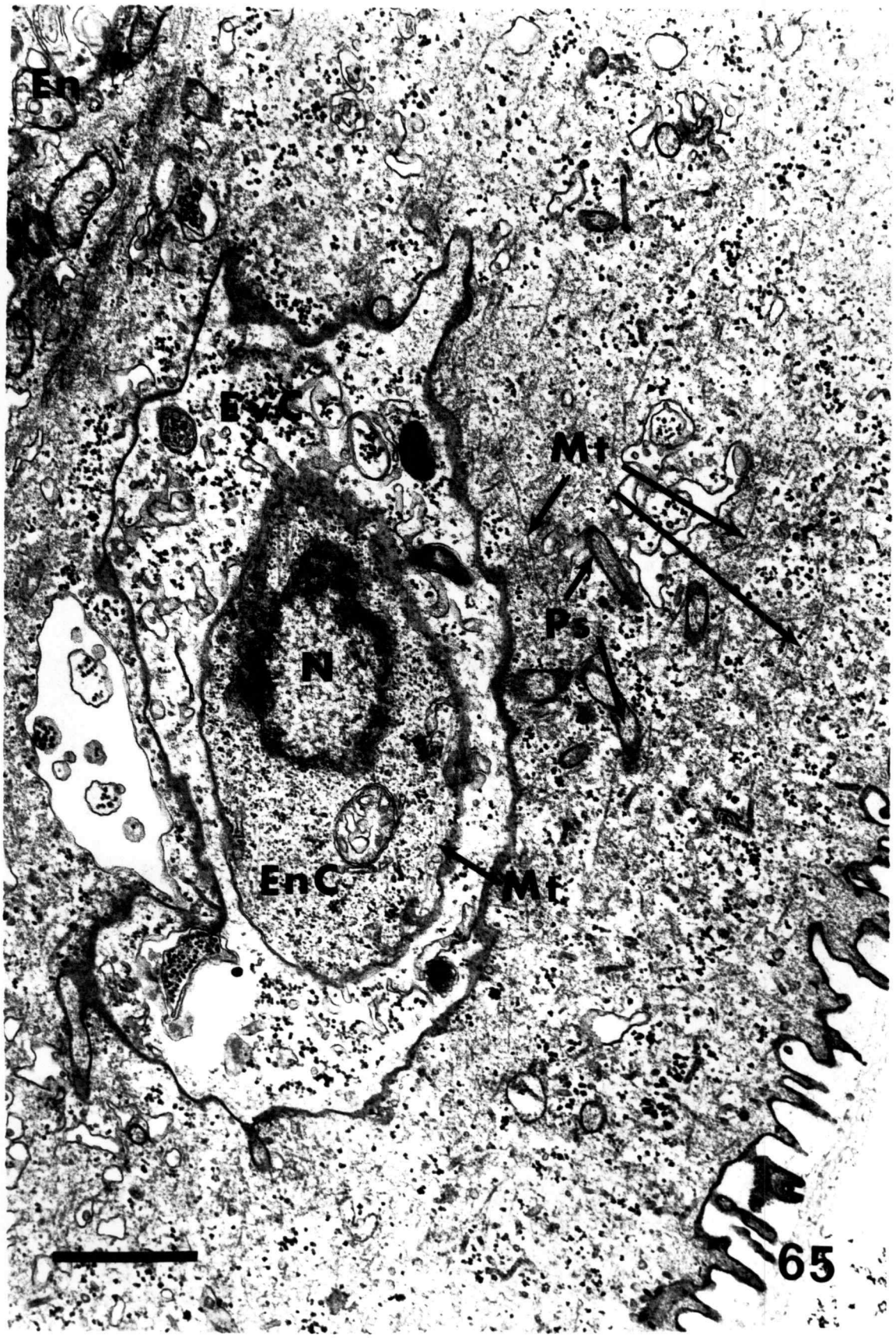
En
Mt
Ps
N
EnC
Mt
65

Figure 66. Cross section showing a thick Glycocalyx and the characteristic distinct separation of developing sporoblasts from the ectoplasm. Glycocalyx, ML; Sporoblast in the 2 cell stage, St; Enveloping cell, EvC; Pseudopodia of the enveloping cell, Ps. (Scale = 2.0 μm; 7550x)

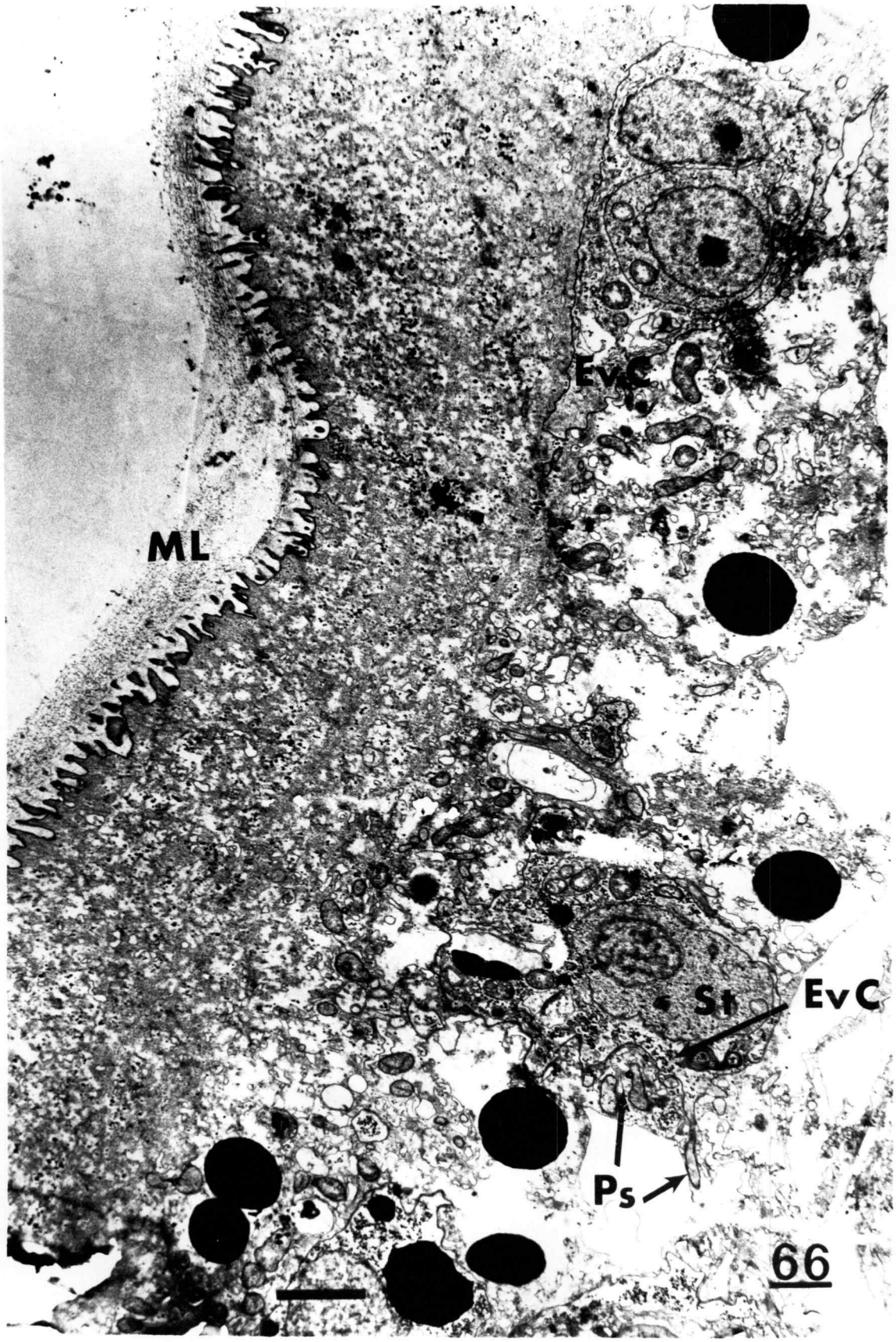
EvC
ML
Si
EvC
Ps
66

Figure 67. Endoplasmic mitochondrion illustrating the typical goblet-shaped myxosporidian cristae, Cr; Autophagic vacuole containing degenerating glycogen aggregates, Av. (Scale = 0.5 μm; 51, 700x)

Figure 68. Oblique section through a developing sporoblast showing the large vacuole and double membranes surrounding the sporoblast. Shell valve Cells, Sv; Polar capsule premordium, PP; Capsulogenous cells, CC; Capsulogenous cell nucleus, Cn; lipid inclusion bodies within the limiting vacuole, L; Mitochondria, M; Double membrane of limiting vacuole, DM; Suture line and septate desmosomes, SL; Microtubules of the shell valve capsulogenous cells, Mt; Rough endoplasmic reticulum, RER. (Scale = 1.0 μm; 18, 600x)

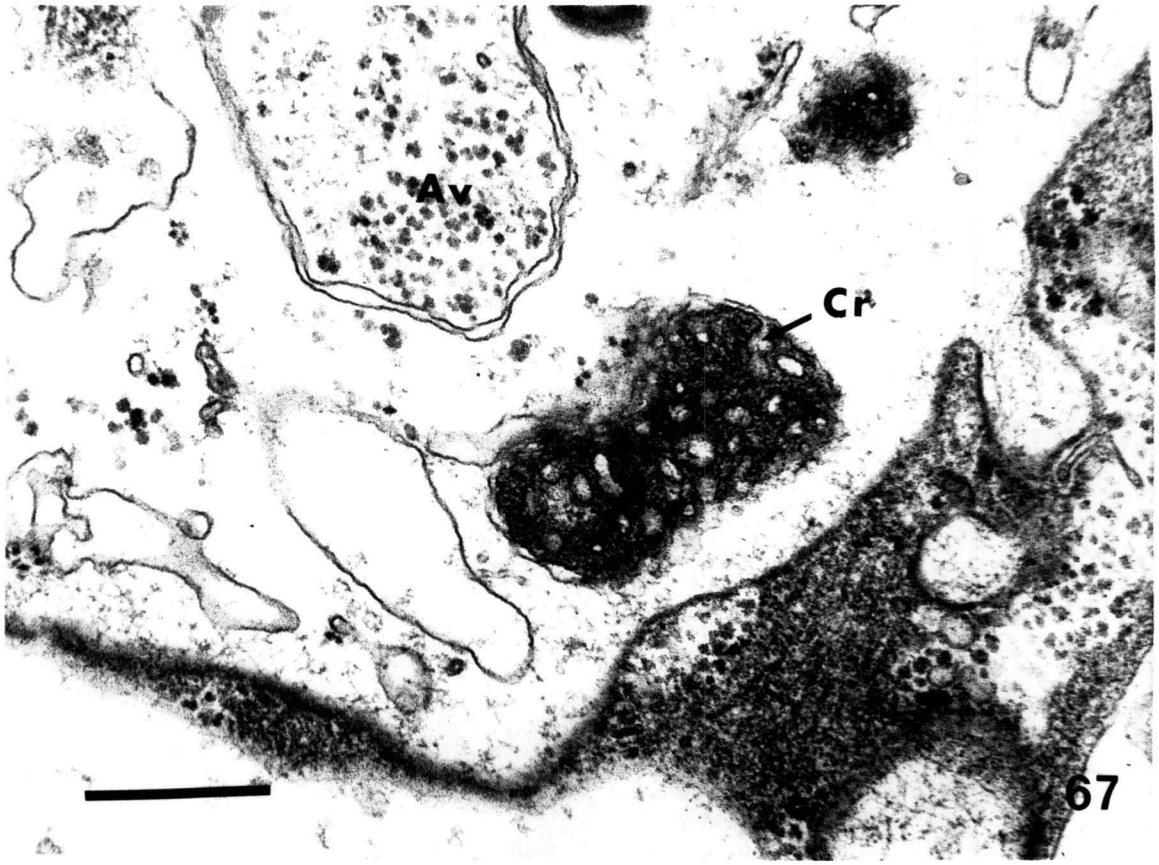
Av
Cr
67

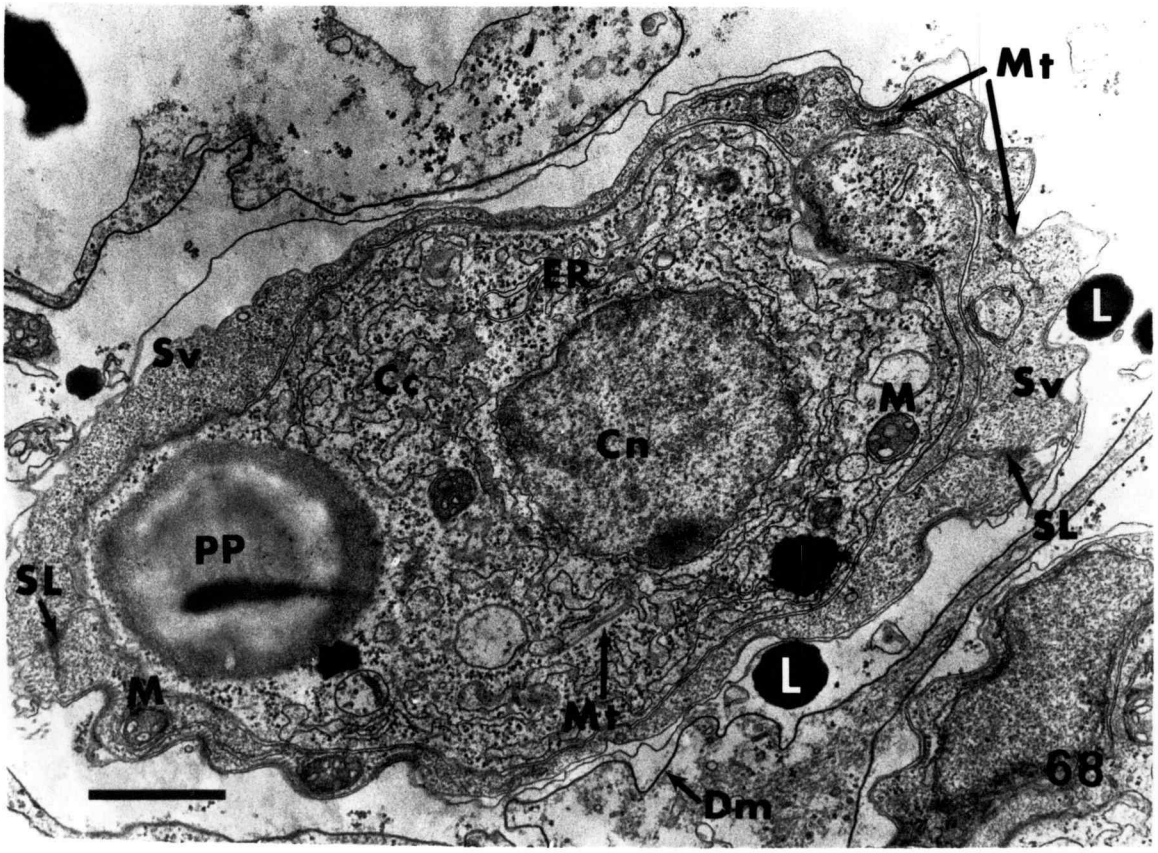
Mt
ER
L
Sv
Cc
M
Sv
Cn
SL
PP
SL
L
M
Mt
68
Dm

Figure 69. Cross section of the endoplasmic region showing the double membranes DM surrounding the developing sporoblast. Pseudopodial extensions of the developing sporoblast composed of double membranes, Ps. (Scale = 0.25 μm; 63, 000x)

Figure 70. Low power electron micrograph of the endoplasmic region showing an area of high lipid accumulation. Lipid, L. (Scale = 2.0 μm; 5640x)

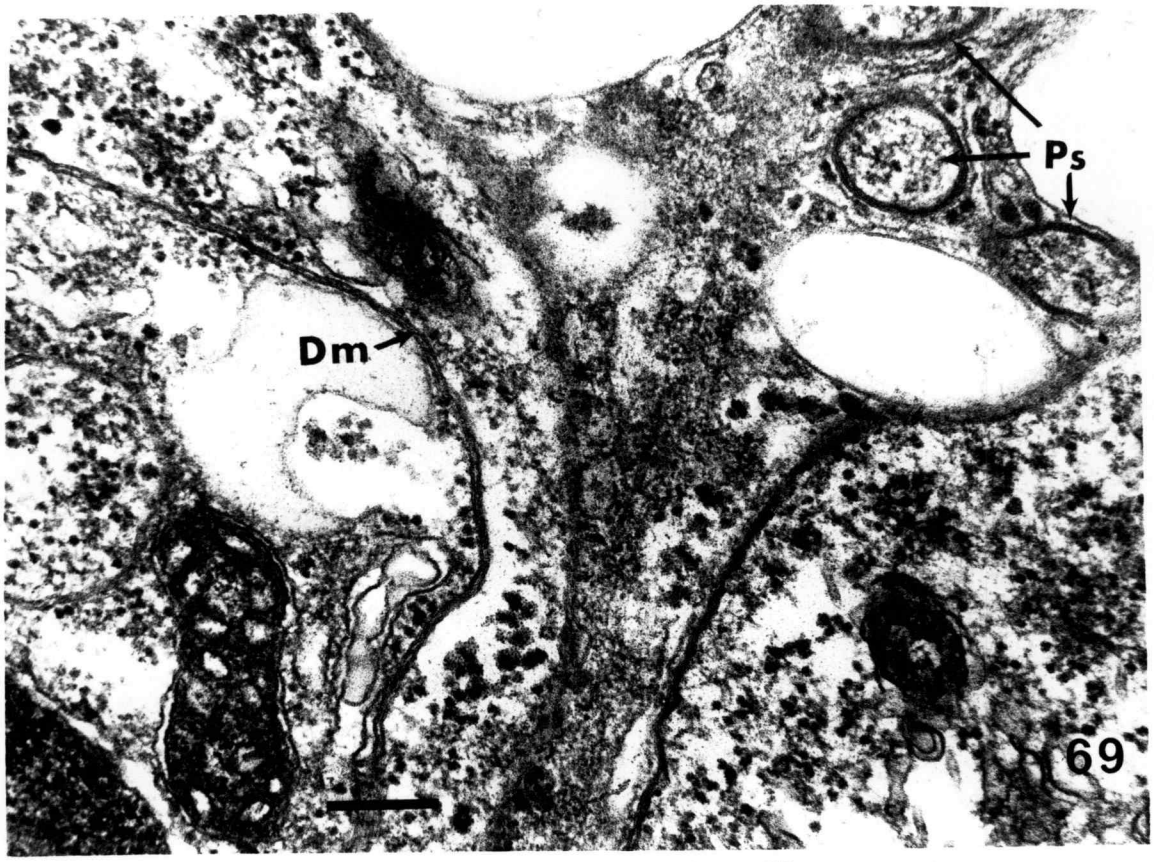
Ps
Dm
69

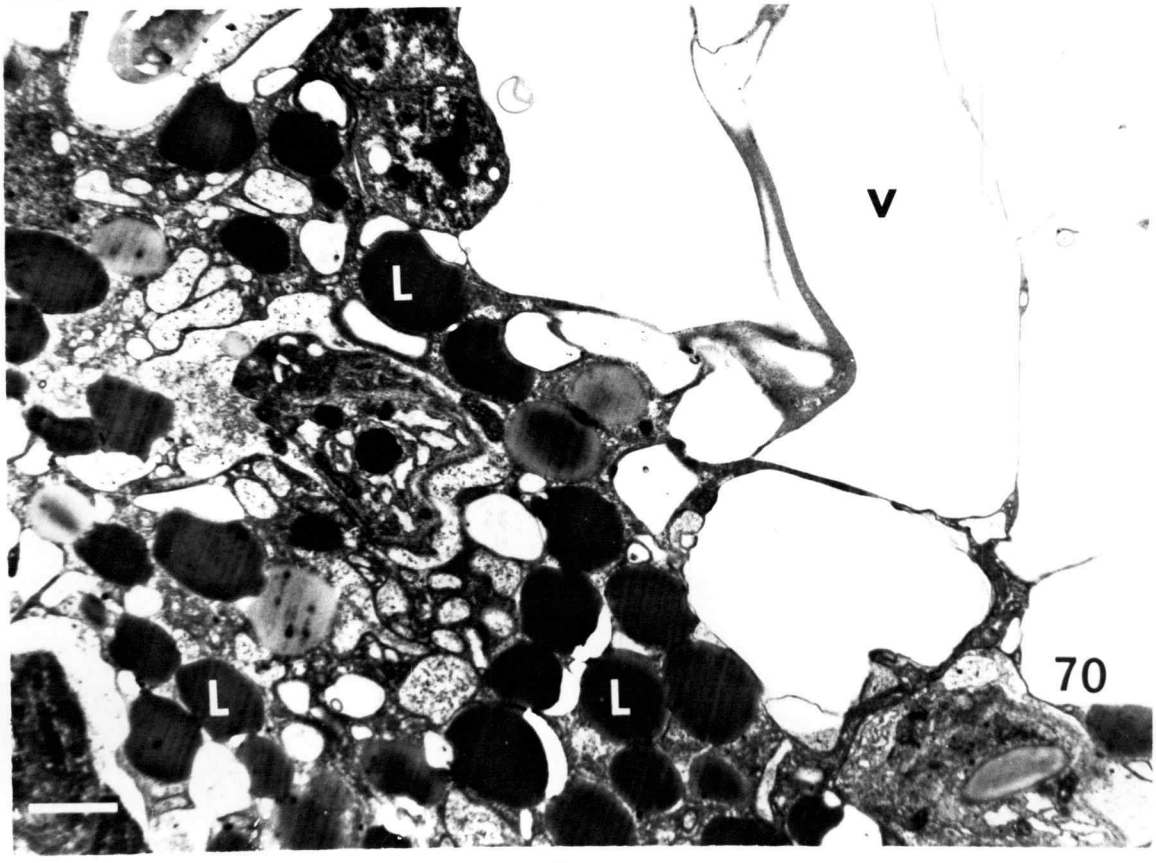
V
L
L
L
70

Figure 71. Cross section of the endoplasm in the region of the ectoplasmic-endoplasmic junction showing the dense accumulation of mitochondria immediately beneath the junction and the membranous (myeloid figures) whorls within vacuoles. Mitochondria, M; Ectoplasmic-endoplasmic junction, EE; Membranous whorls, MW; Vacuoles, v. (Scale = 1.0 μm; 24, 600x)

Figure 72. Cross section of the endoplasmic region showing an early sporoblast and a well developed membranous whorl. Sporoblast, St; Membranous whorl, MW; Double membrane surrounding the developing sporoblast, DM; Pseudopodial extensions of the sporoblast, Ps. (Scale = 1.0 μm; 24, 600x)

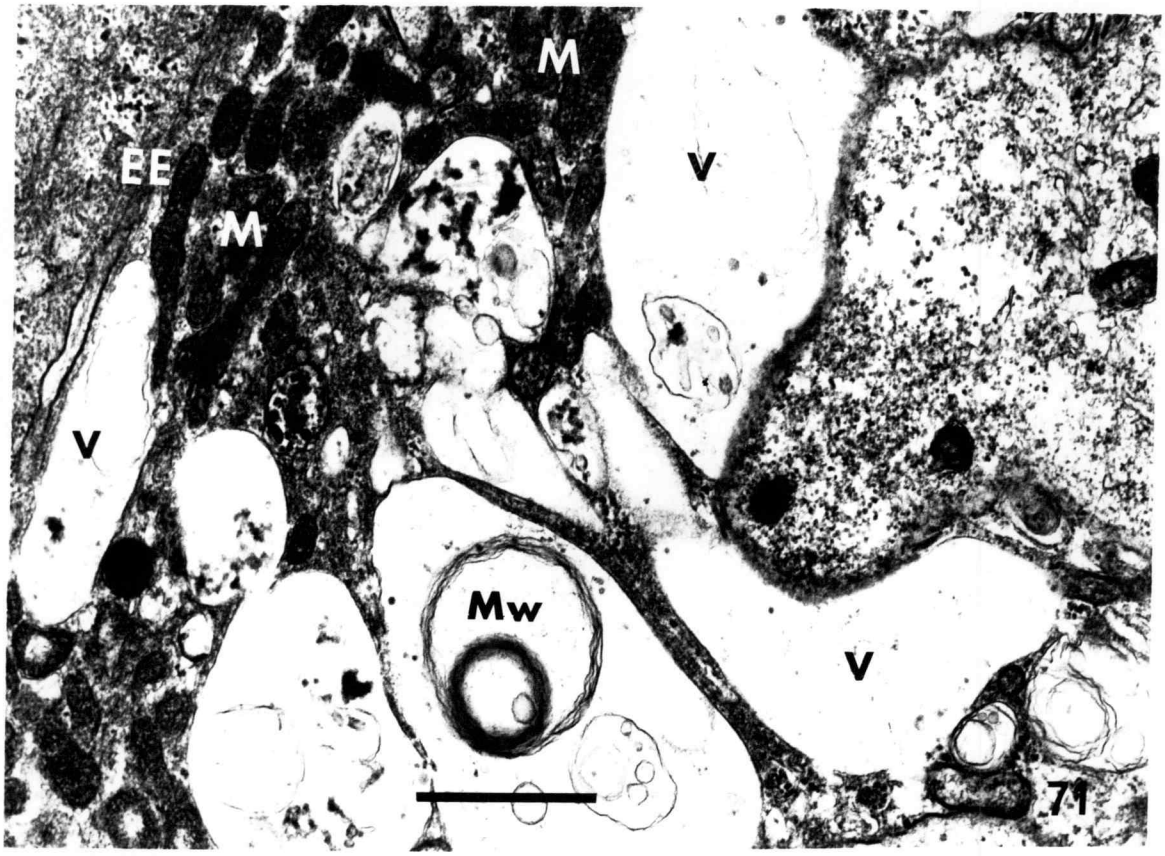
M
EE
M
V
V
Mw
V
71

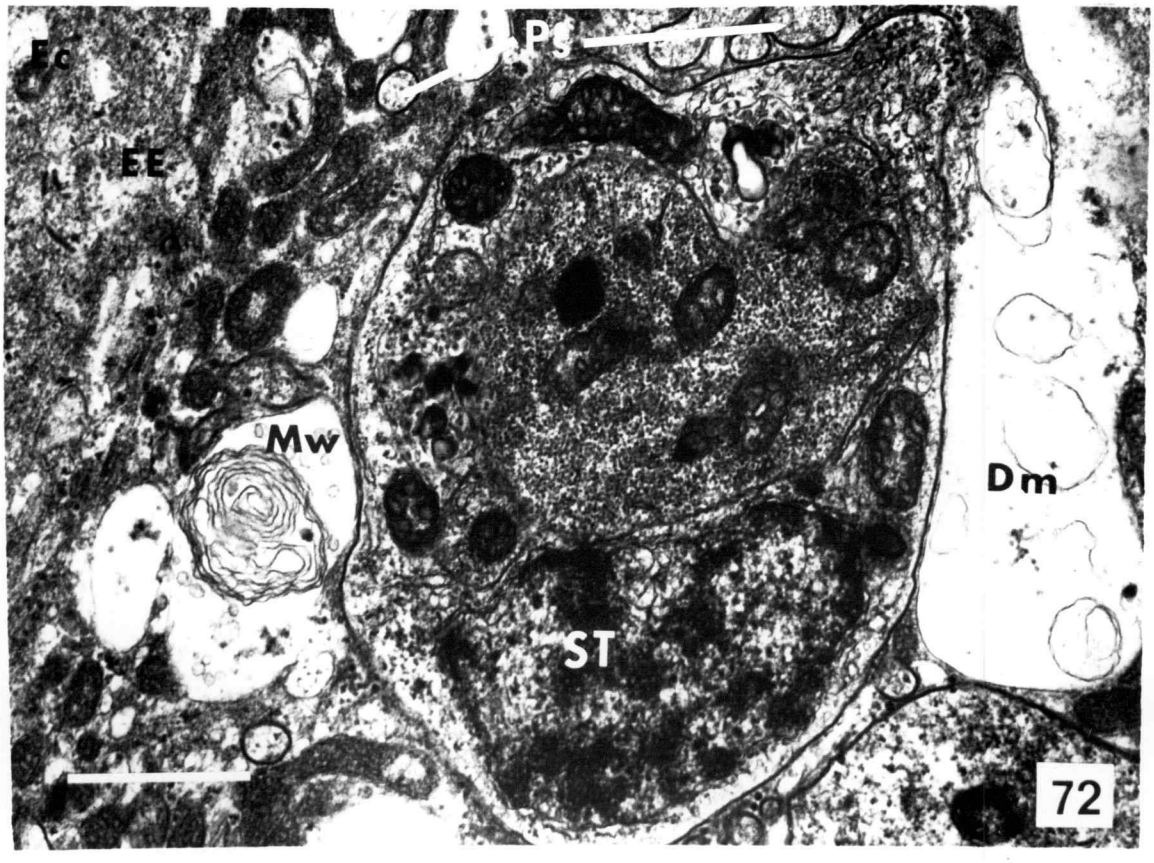
Ec
EE
PJ
Mw
Dm
ST
72

Figure 73. Highly developed myeloid body within a developing sporoblast. Myeloid figure, Mf; Sporoblast, St; Sporoblast membrane, Stm. (Scale = 1.0 μm; 18,600x)

Figure 74. High power electron micrograph of an alveolar partition within the central zone of the endoplasm showing the internal microtubules, Mt; and the limiting unit membrane, UM; Endoplasmic vacuoles, V. (Scale = 0.25 μm; 79,000x)

Figure 75. Oblique section through a fairly mature spore. Alveolar partition, Ap; Microtubules within the alveolar partitions, Mt; Shell valve cell, SV; Longitudinal striations of the spore, Ls; Capsulogenous cell, CC; Sporoplasm, Sp; Sporoplasm nucleus, SpN. (Scale = 1.0 μm; 15,750x)

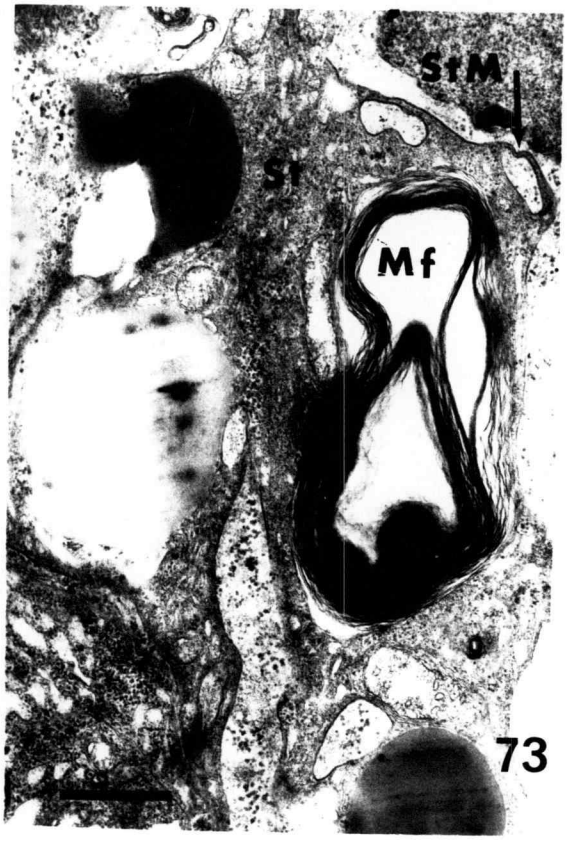

73

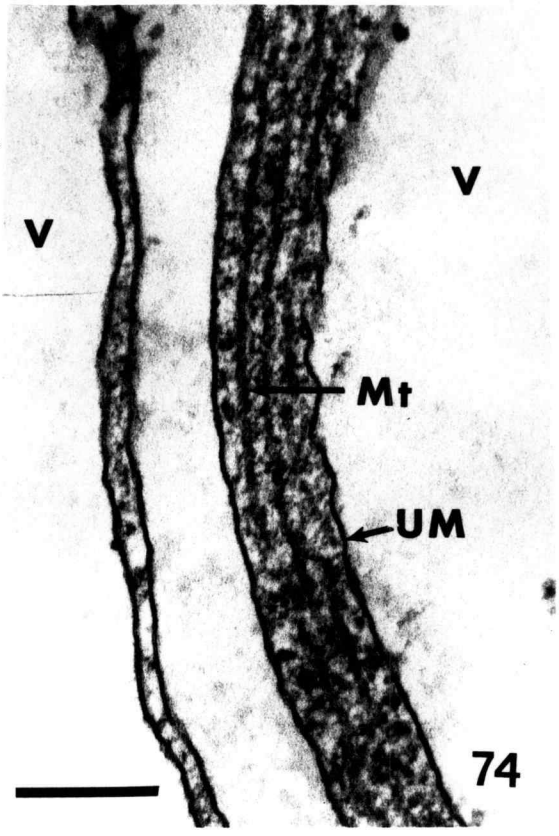

74

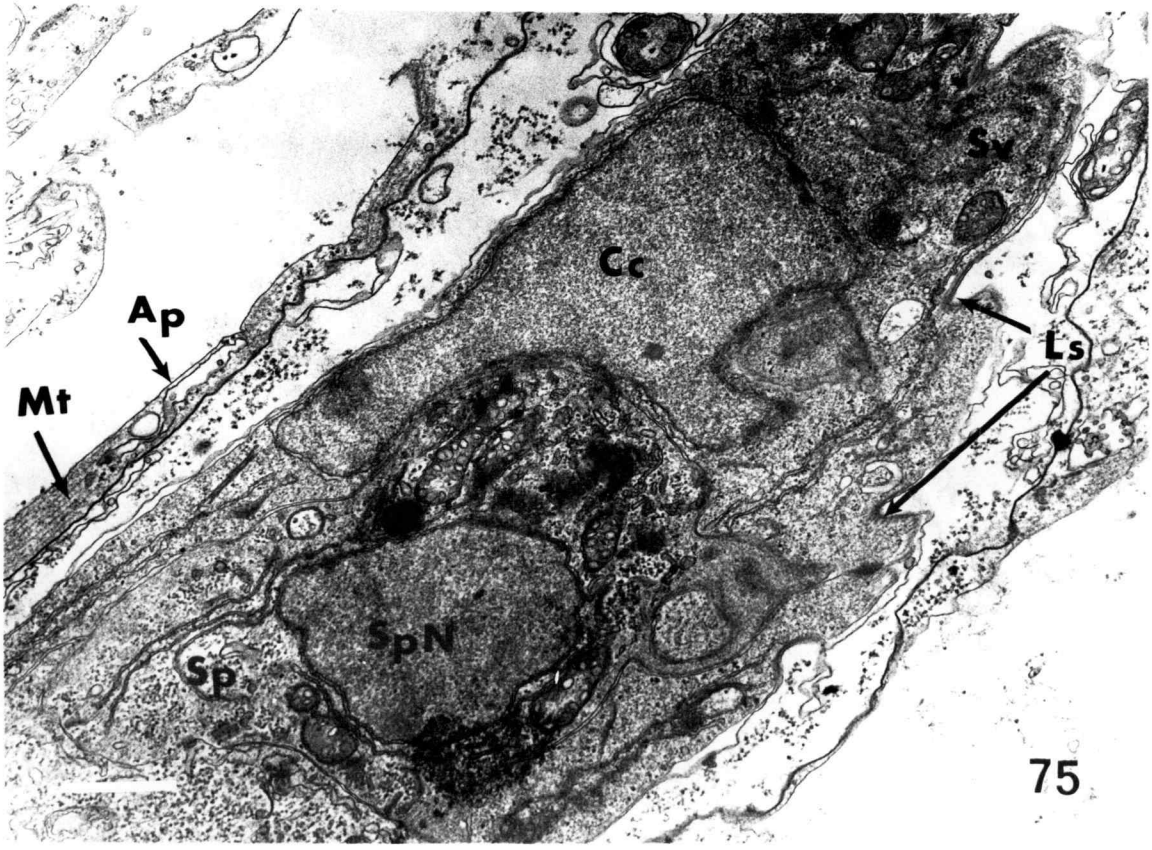

75

Figure 76. Cross section of the outer endoplasmic region. Autophagic vacuoles, Av; Ectoplasm, Ec; Ectoplasmic endoplasmic junction, EE; Mitochondria, M; and developing sporoblast, St. (Scale = 0.5 μm; 30,000x)

Figure 77. Low power electron micrograph showing several sporoblasts in different developmental stages. Enveloping cell, EvC; Enveloped cell, EnC; Myeloid figure, Mf; Pseudopodial extensions of the enveloping cell, Ps; Golgi complex, Gc; Nucleus of enveloped cell, N; Polar capsule, Pc. (Scale = 1.0 μm; 11,500x)

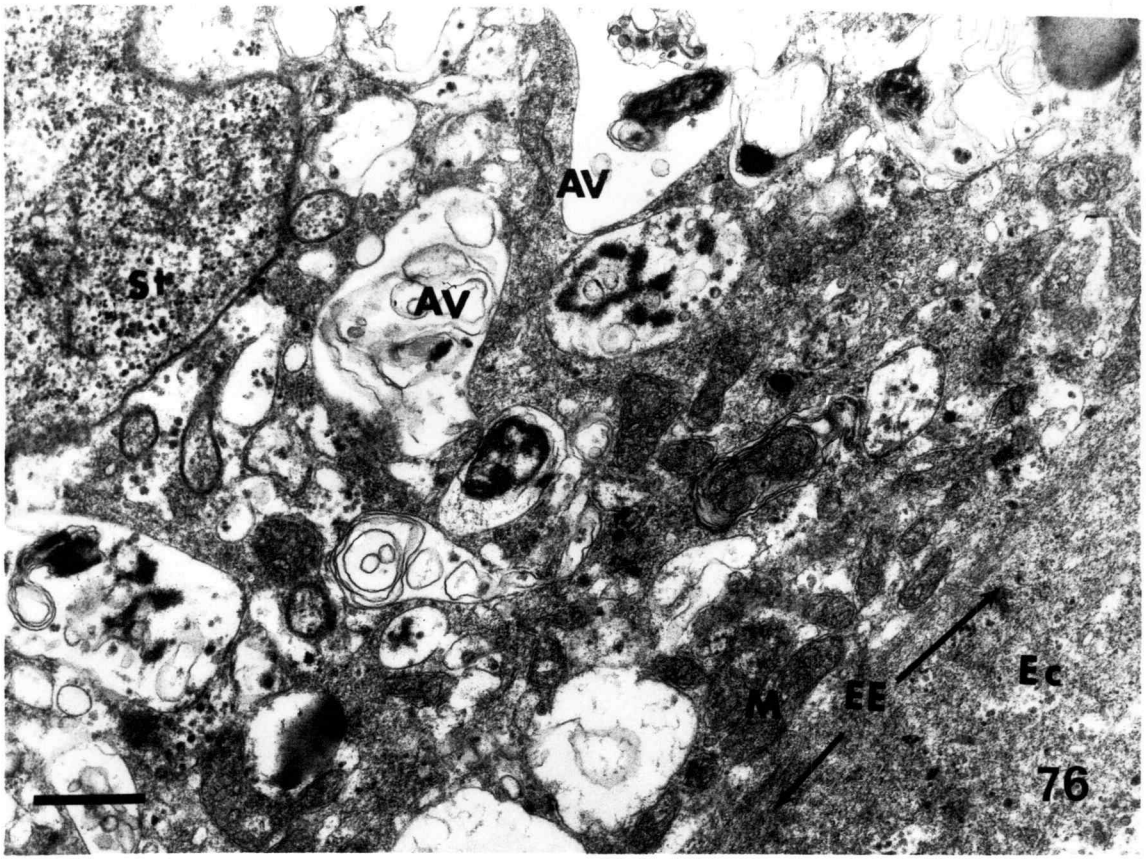
AV
St
AV
M
EE
Ec
76

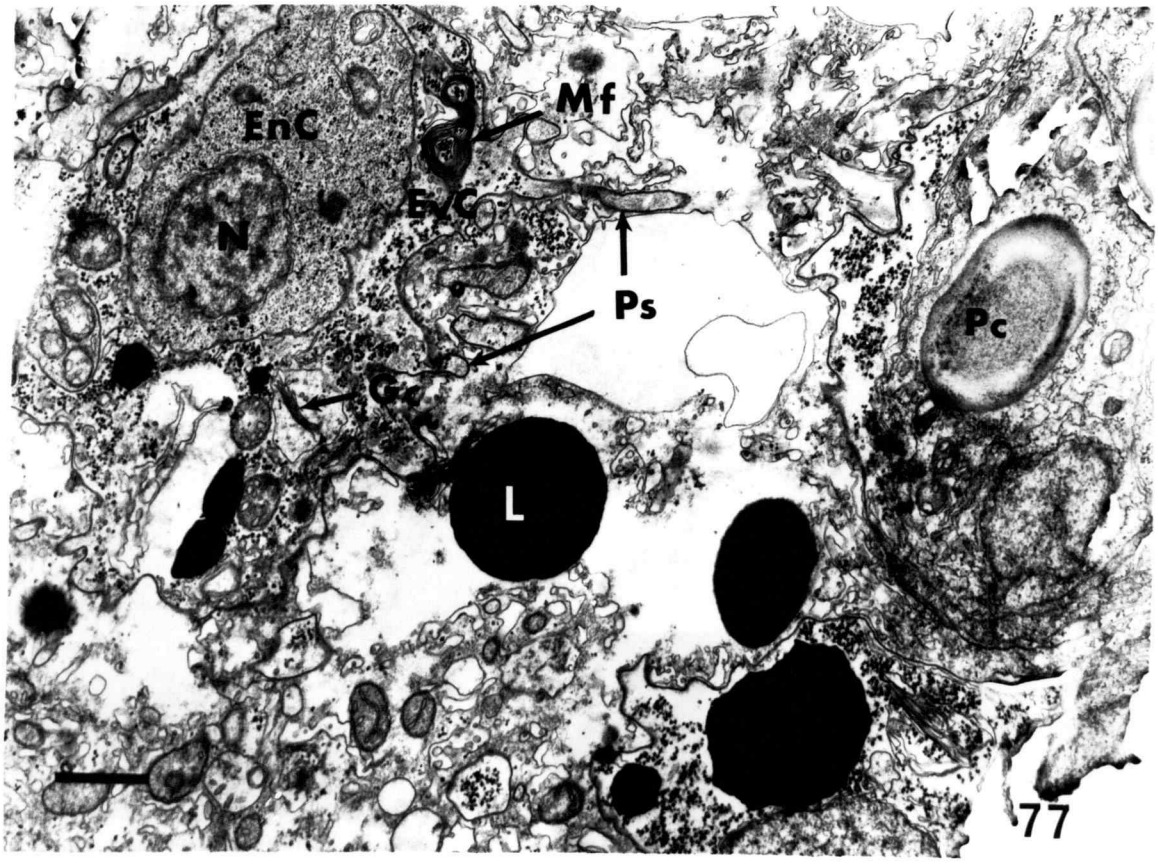
EnC
Mf
N
E/C
Ps
Pc
L
77

Figure 78. Cross section of the polar capsule region of a nearly mature spore. Microtubules, Mt; Shell valve cells, Sv; Suture line, SL; Residual membrane around exterior of spore, RM; Nucleus of capsulogenous cell, Cn; Vacuole surrounding spore, V; Mitochondria of shell valve cell, M; Endoplasmic reticulum, ER; Polar filament folds, F1, F1A, F2, F2A, F3, F3A, F4 and F4A. (Scale = 1.0 μm; 32, 100x)

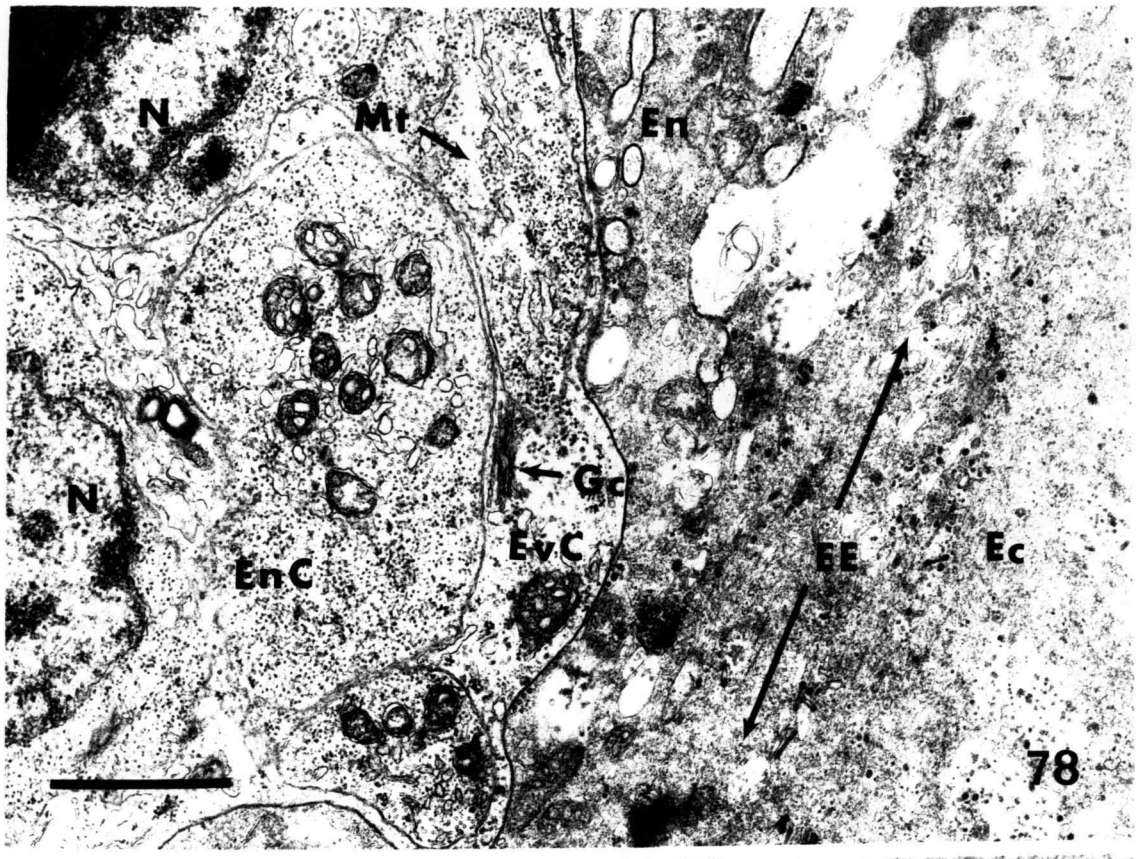
N
Mt
En
N
Gc
EvC
EnC
EE
Ec
78

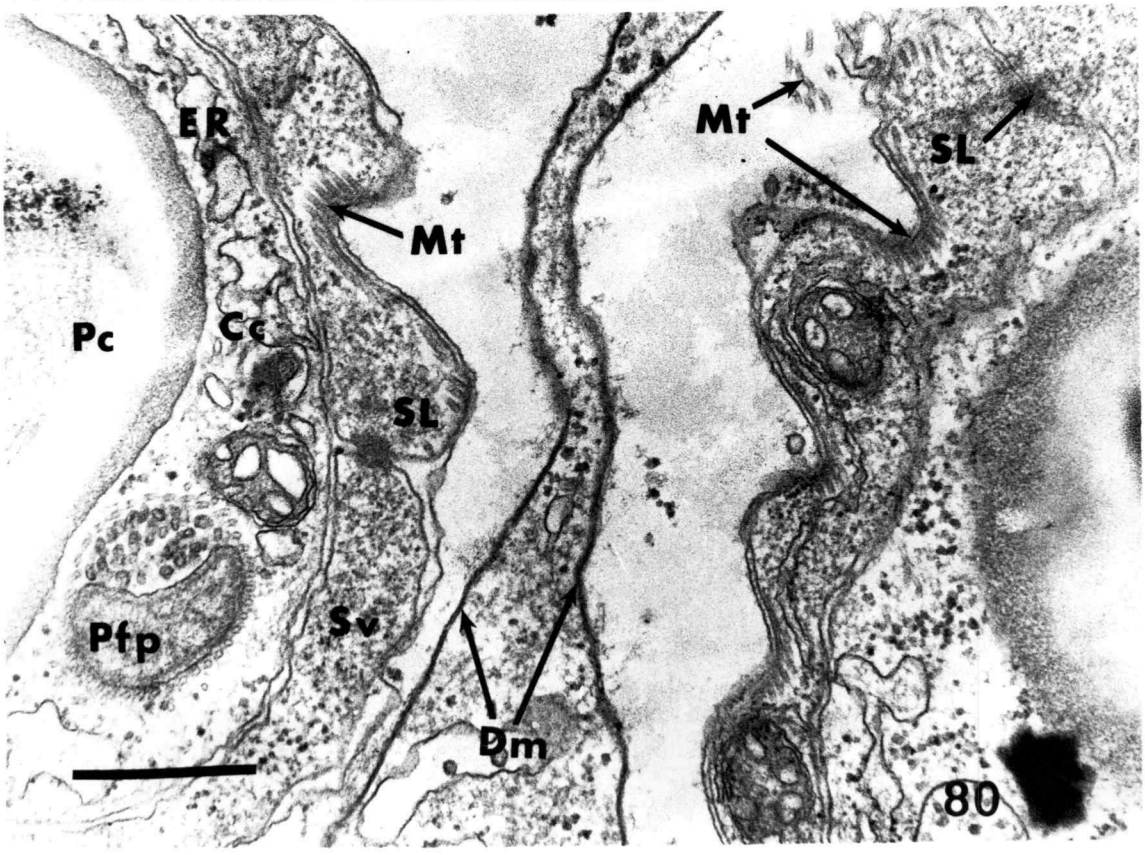
ER
Mt
Pc
Cc
SL
Pfp
Sv
Dm
Mt
SL
80

Figure 79. Slightly more advanced sporoblast than shown in Figure 77 containing several cells. Enveloping cell, EvC; Enveloped sporoblast cells, EnC; Nucleus, N; Golgi Complex, Gc; Microtubules, Mt. (Scale = 1.0 μm; 24,600x)

Figure 80. High power electron micrograph of two nearly mature spores showing the high concentrations of microtubules in the shell valve cells and in the capsulogenous cell. Polar filament primordium, Pfp; Polar capsule, Pc; Capsulogenous cell, Cc; Microtubuli, Mt; Shell valve cell, Sv; Sutural line, SL; Endoplasmic reticulum of shell valve cell, Er; Double membrane surrounding the sporoblastic vacuole, DM; Microtubules free within the sporoblastic vacuole, Mt. (Scale = 0.5 μm; 51,700x)

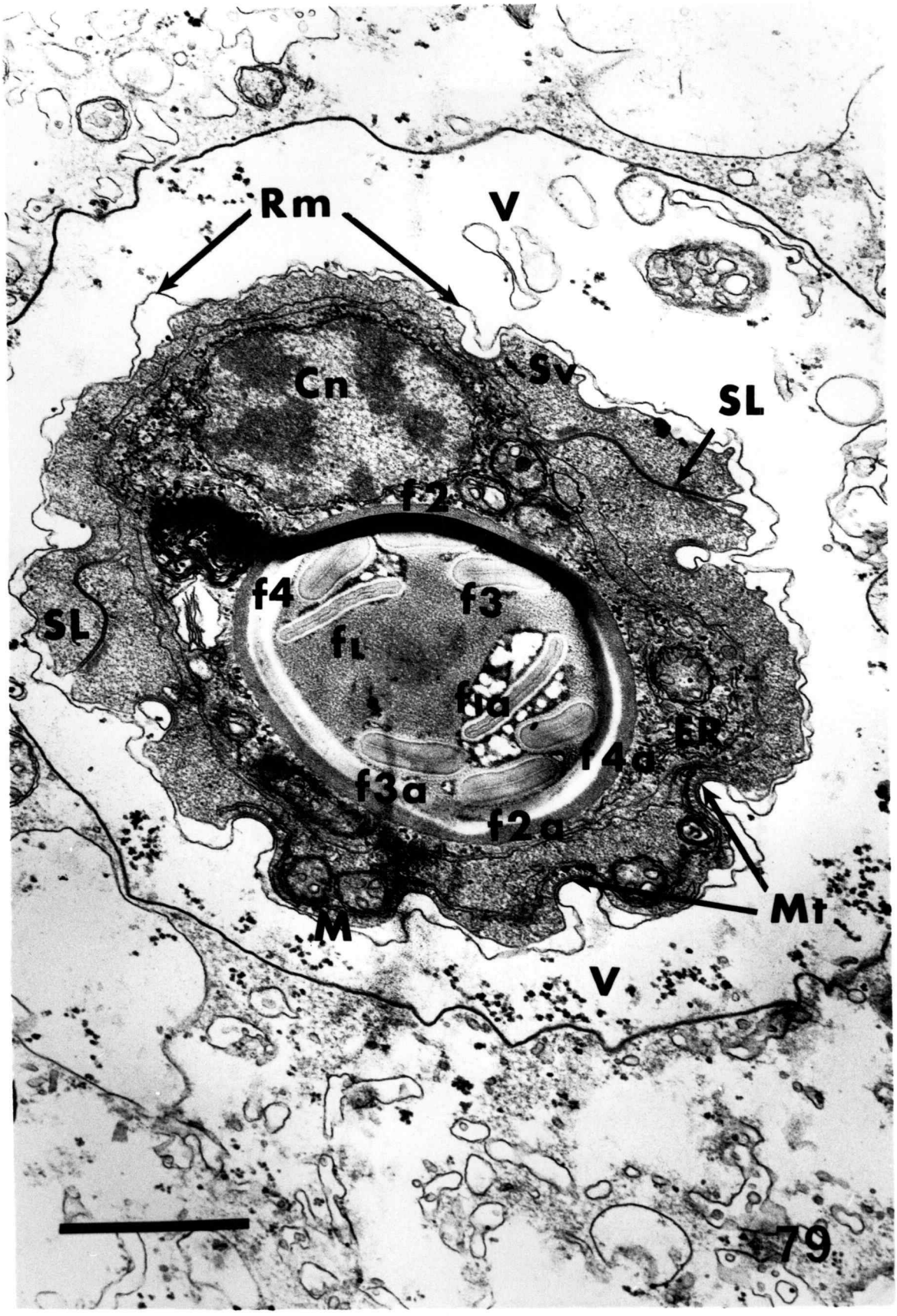
Rm
V
Cn
Sv
SL
f2
f4
f3
SL
fL
f1a
ER
f4a
f3a
f2a
Mt
M
V
79

Figure 81. Cross section of the medial capsular region of a spore during the process of shell valve cell contraction. The microtubules below the longitudinal furrows are no longer present. Sutural line and septate desmosomes, SL; Shell valve cells, Sv; Sporoplasm, Sp; Clasperlike extensions of sporoplasm cell partially surrounding the Capsulogenous cell (Cc), SpE; Residual membrane surrounding the spore, RM. (Scale = 1.0 μm; 15, 750x)

Figure 82. Cross section through the medial aspect of a polar capsule showing the capsular wall. Electron dense line, DL; Polar filament, Pf; Polar filament in the process of folding, Pf1; Separation between shell valve cell and the capsulogenous cell. Sep; Outer Electron dense layer of polar capsule, L1; Inner electron transparent layer of polar capsule, L2; Shell valve cell, Sv; Sutural line, SL; Microtubules along the sutural line, Mt; Longitudinal striations, Ls. (Scale = 0.25 μm; 63, 000x)

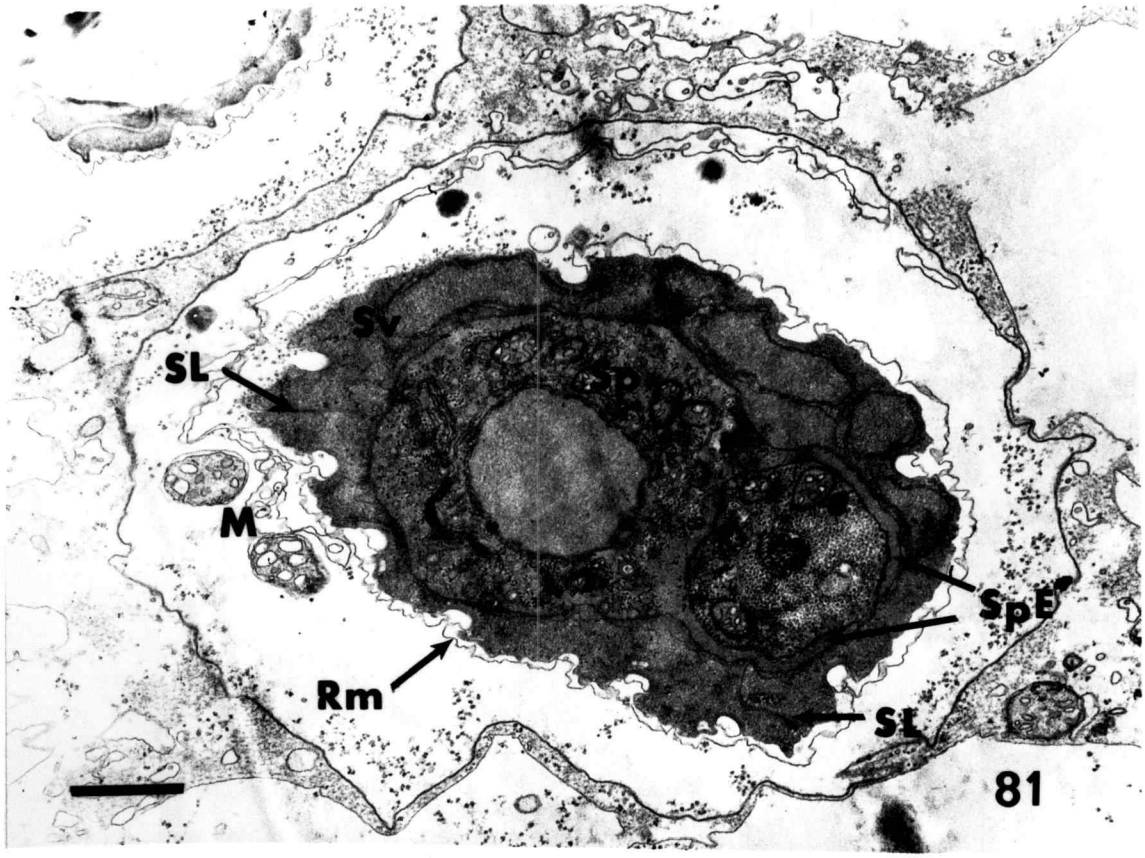
Sv
SL
M
SpE
Rm
SL
81

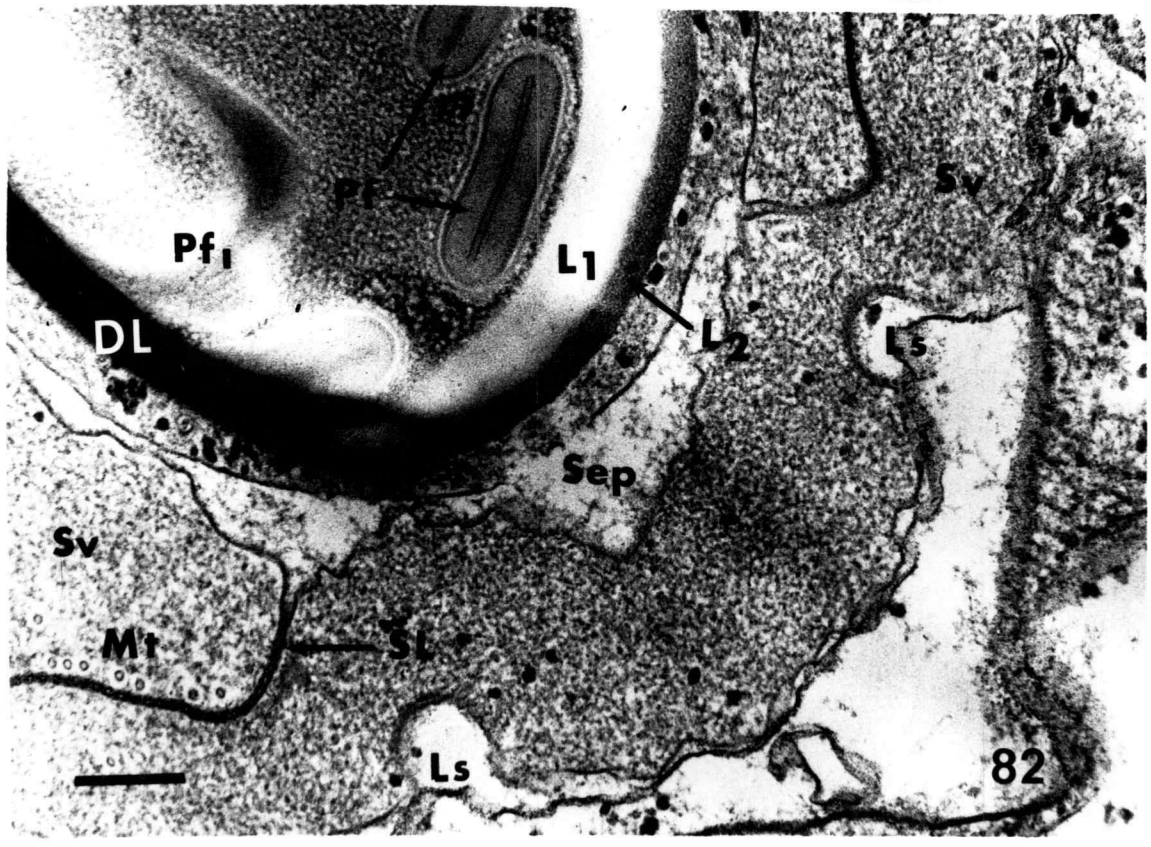
Pf
Pf1
L1
L2
Sv
DL
Ls
Sep
Sv
Mt
SL
Ls
82

Figure 83. Cross section of a polar capsule showing microtubules adjacent to the capsular wall within the capsulogenous cell. Capsulogenous cell, Cc; Electron dense line, DL; First polar filament coil, Fi; Remaining polar filament coils, F_2; Glycogen aggregates, G; Microtubules, Mt. (Scale = 0.25 μm; 63, 000x)

Figure 84. High magnification electron micrograph of the shell valve cell and the capsulogenous cell. Agranular endoplasmic reticulum, Aer; Capsulogenous cell, Cc; Inner electron transparent layer of the polar capsule, L_1, Outer electron dense layer of the polar capsule, L_2; Microtubules subtending the longitudinal furrows, Mt; Thin partition separating the microtubules from the shell valve cell membrane, Pt; Shell valve cell, Sv; Shell valve cell limiting membrane, Svm. (Scale = 0.2 μm; 131, 000x)

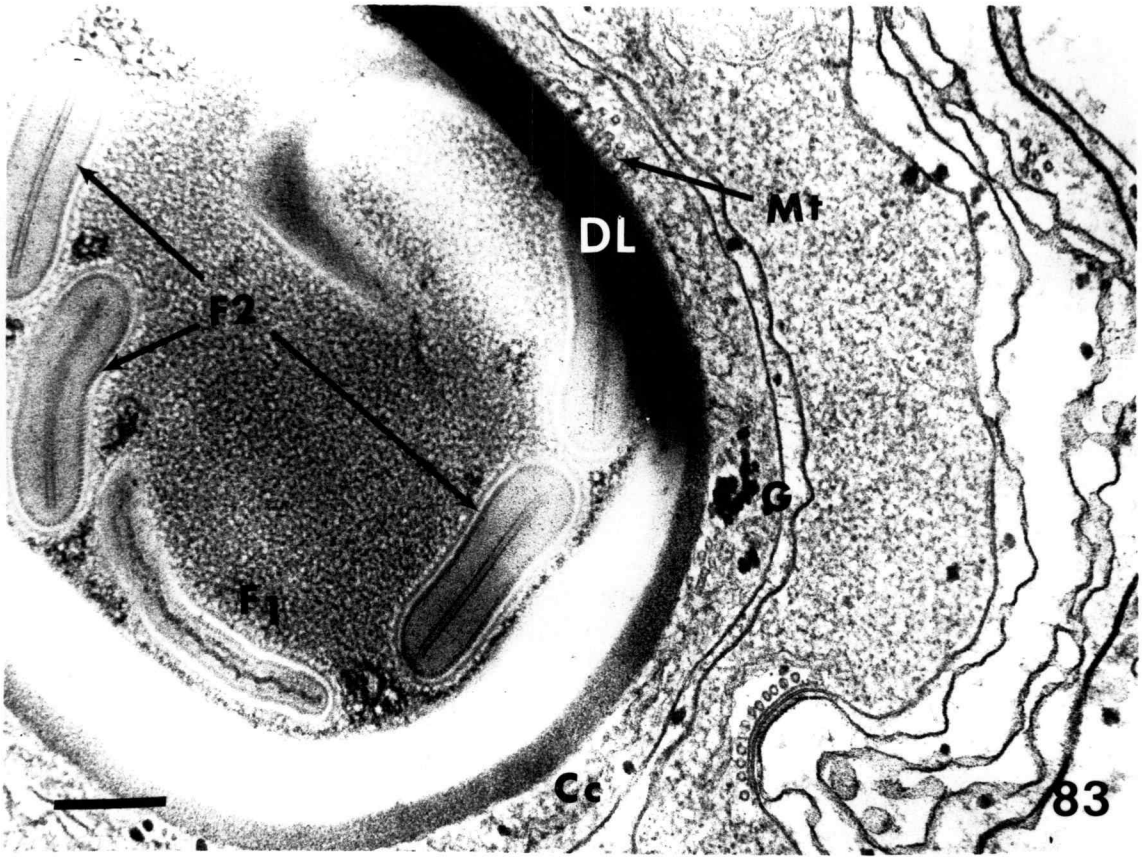
DL
Mt
F2
G
F1
Cc
83

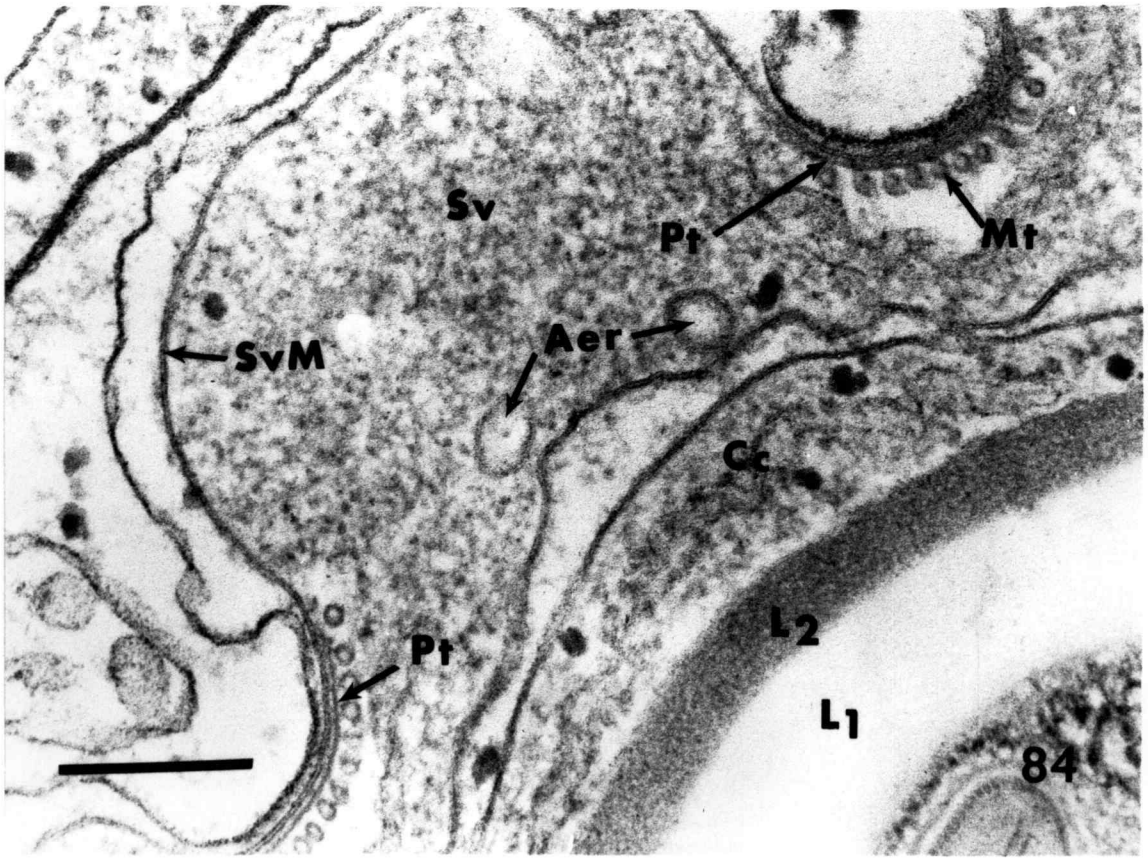
Sv
Pt
Mt
SvM
Aer
Cc
Pt
L2
L1
84

Figure 85. Longitudinal section of a developing polar capsule. Capsulogenous cell, Cc; A cross lattice material forming a plate between the polar filament and the shell valve cell, CL; Aperture in the polar capsule showing the connection of the polar filament to the margin of the polar capsule, O; Polar filament, Pf; Plug-like stopper situated within the shell valve cell, So; Shell valve cell, SV. (Scale = 0.5 μm; 37, 100x)

Figure 86. High magnification electron micrograph of the shell valve cell of a nearly mature spore. Inner and outer electron dense layer of shell valve cell, L_1; Central less electron dense layer of shell valve cell, L_2; Polar capsule, Pc; Shell valve cell limiting membrane, SVM. (Scale = 0.2 μm; 112, 000x)

Figure 87. High magnification electron micrograph of the sutural line of a nearly mature spore showing the degenerating shell valve cells. Inner and outer electron dense layers of the shell valve cells, L_1; Central less electron dense layer of the shell valve cell, L_2; Sutural line, SL. (Scale = 0.2 μm; 97, 000x)

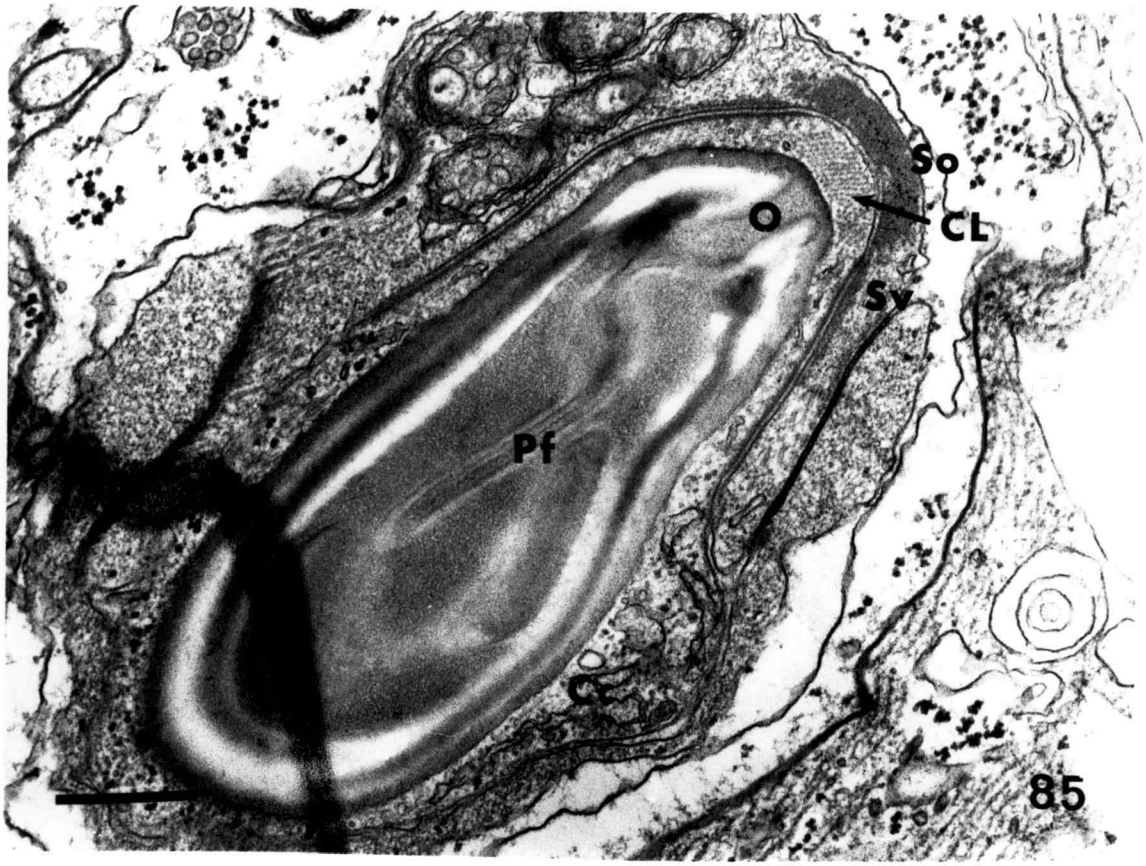
So
CL
O
Sy
Pf
Ce
85

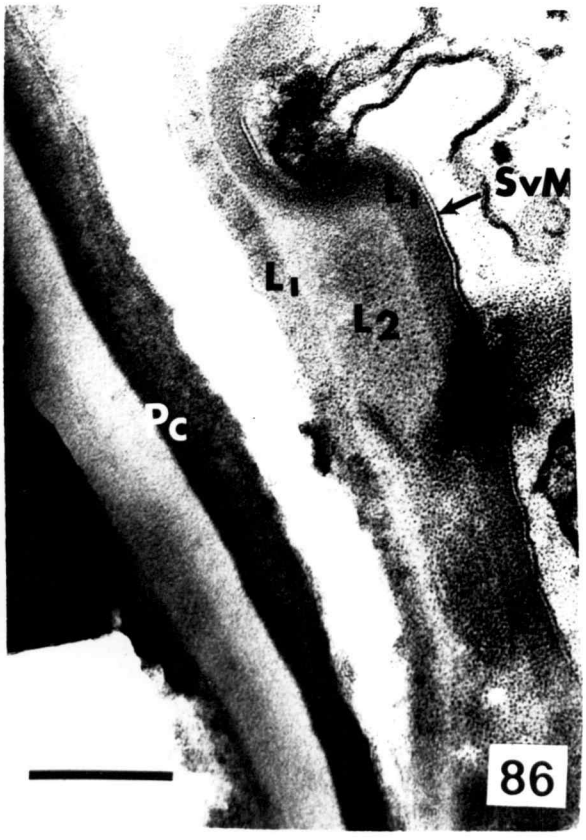
SvM
L1
L2
Pc
86

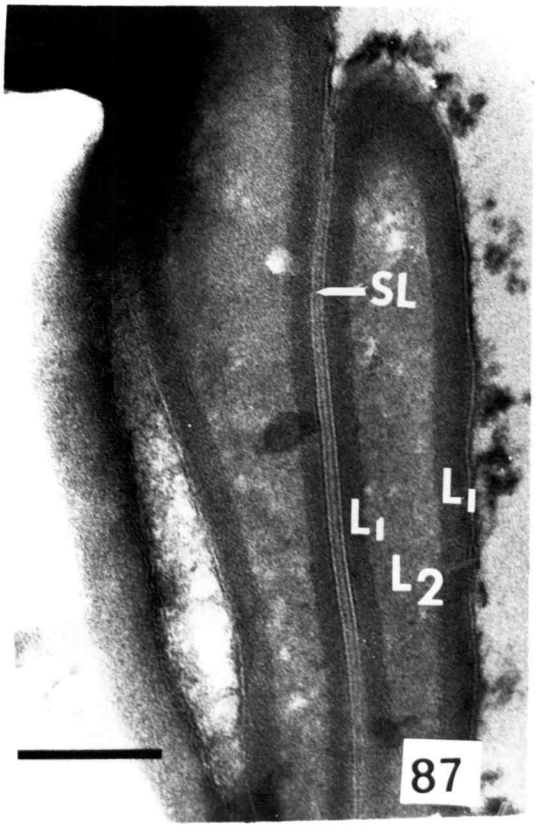
SL
L1
L1
L2
87

Figure 88. Cross section of a developing spore showing the polar capsule region and the sutural line between adjacent shell valve cells. Microtubules, Mt; Septate desmosomes, Sd; Sutural line, SL. (Scale = 0.2 μm; 156, 000x)

Figure 89. Low magnification electron micrograph of a longitudinal section of a developing spore showing the centrally situated sporoplasm, extensions from the sporoplasm partially surrounding the capsulogenous cell, and the dense material within the polar capsule wall. Capsulogenous cell, Cc; Capsulogenous cell nucleus, Ccn; Dense line in polar capsule, DL; Degenerating enveloping cell, EVC; Sporoplasm nucleus, Sn; Sporoplasm, Sp; Extensions from the sporoplasm surrounding the capsulogenous cell, SpE; Shell valve cells, SV. (Scale = 2.0 μm; 9700x)

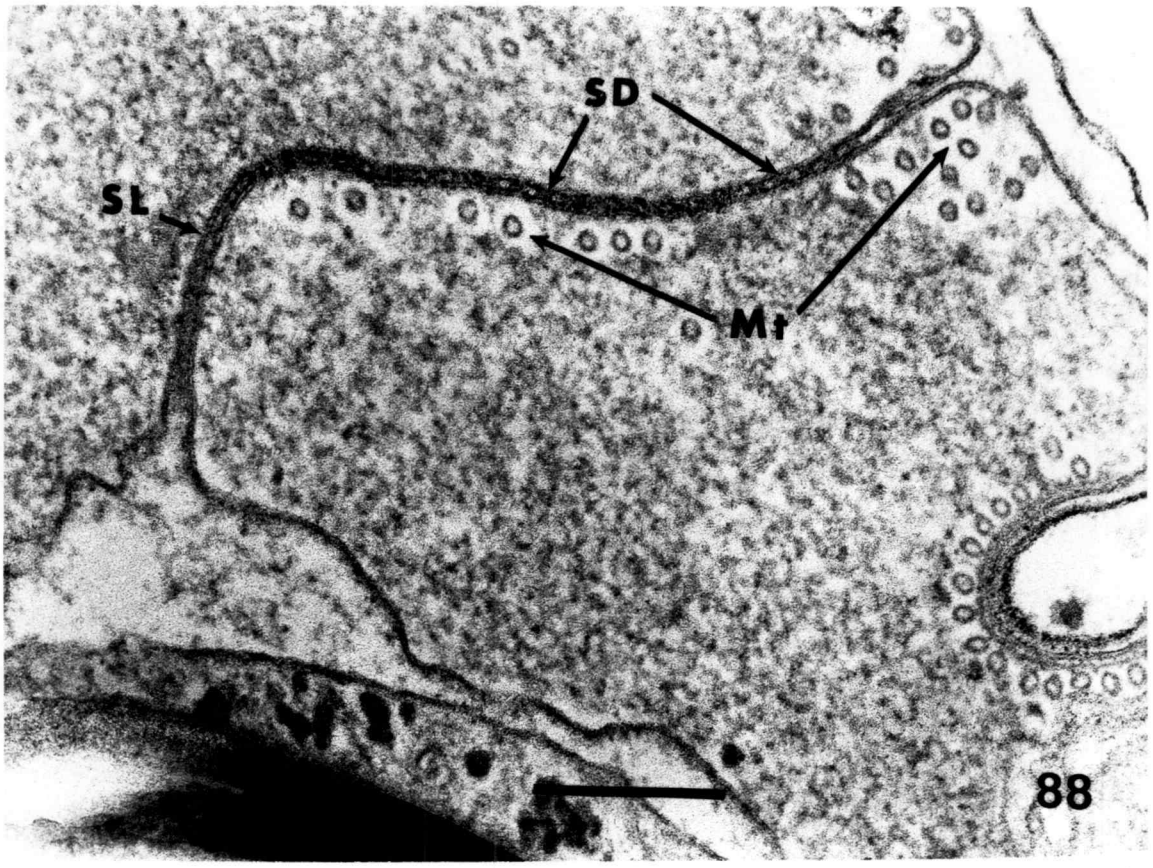
SD
SL
Mt
88

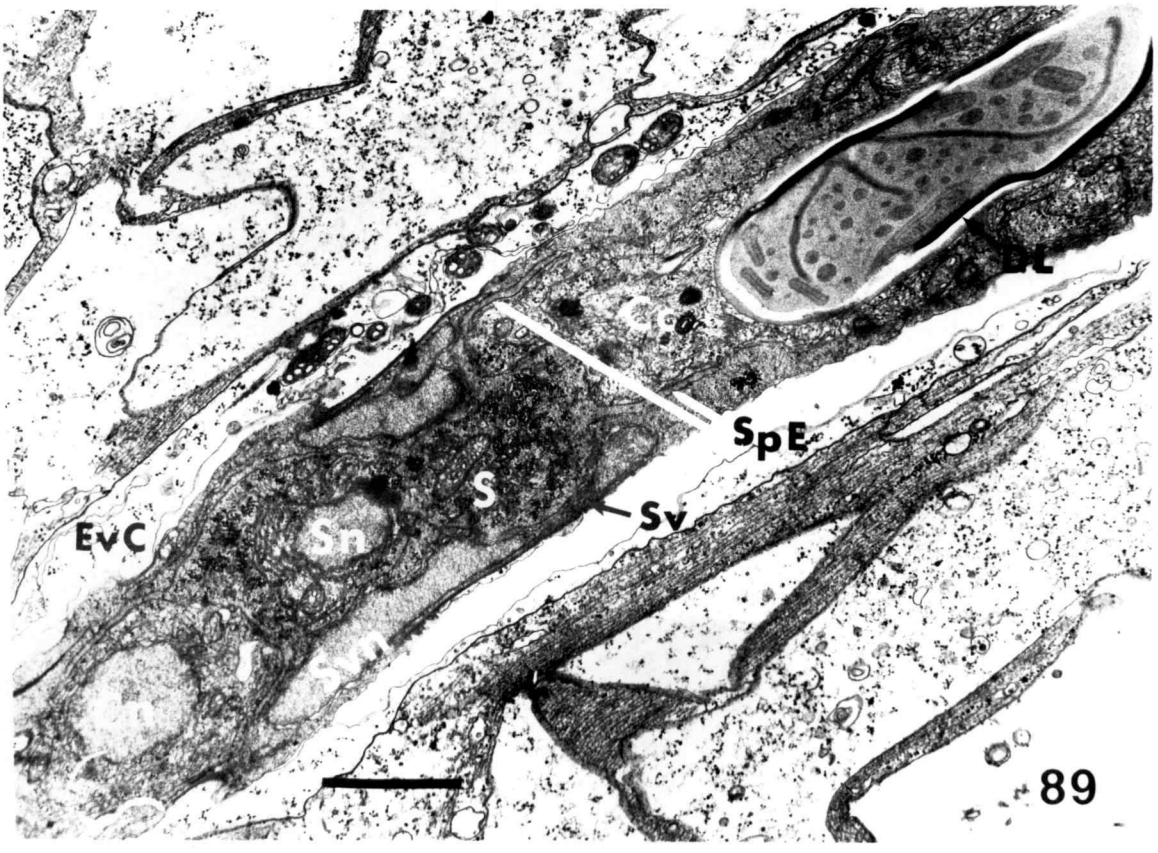
SpE
S
Sv
EvC
Sn
89

Figure 90. Longitudinal section of a spore showing the sporoplasm, capsulogenous and shell valve cells. Note the extension, SpE; of the sporoplasm cell between the capsulogenous cell and the shell valve cell. Capsulogenous cell, Cc; Golgi complex of capsulogenous cell, Gc; Polar capsule, Pc; Sporoplasm, Sp; Extension of the sporoplasm cell, SpE; Shell valve cell, Sv. (Scale = 0.5 μm; 37,200x)

Figure 91. Longitudinal section of the tip of a maturing spore showing degenerating mitochondria within the shell valve cell. Capsulogenous cell, Cc; Cross lattice, CL; Mitochondria of the shell valve cell, M; Opening of the polar capsule, O; Polar filament, Pf; Plug-like stopper in the shell valve cell, SO; Shell valve cell, SV. (Scale = 0.2 μm; 100,900x)

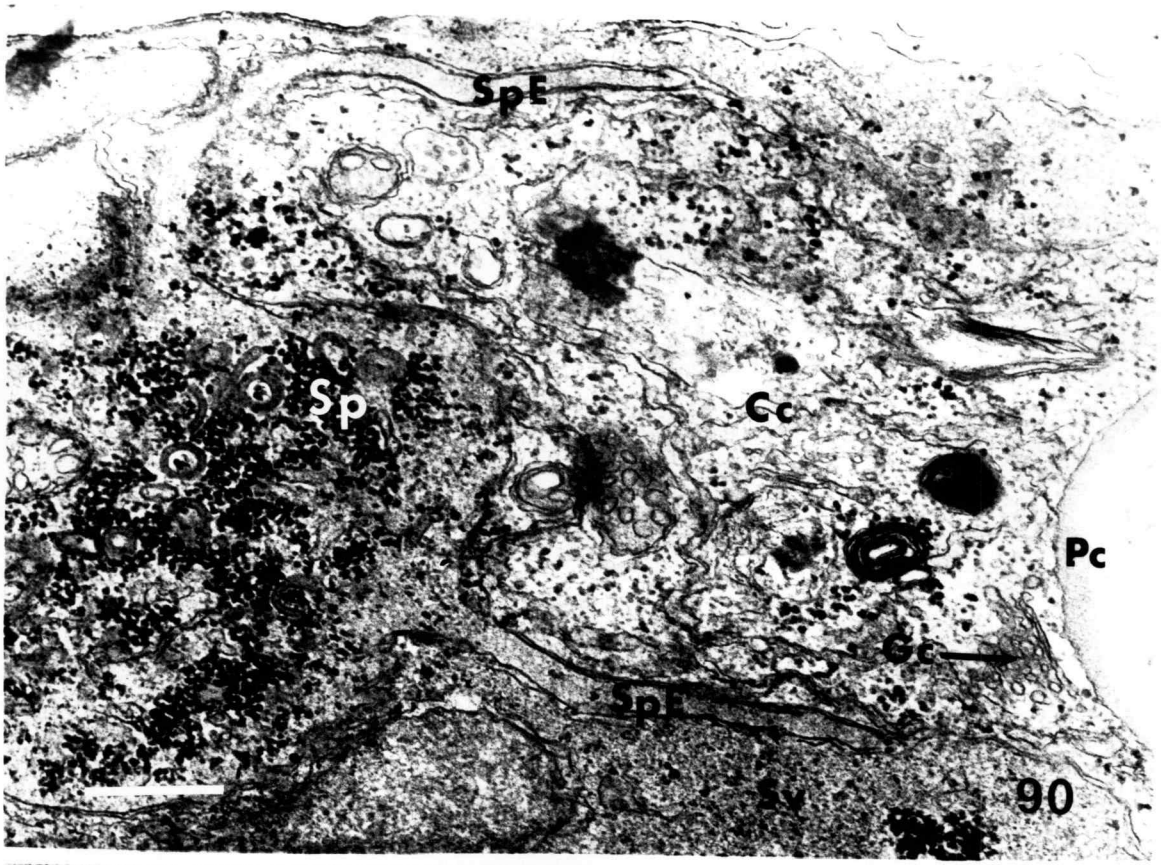
SpE
Sp
Cc
Pc
Cc
SpE
Sv
90

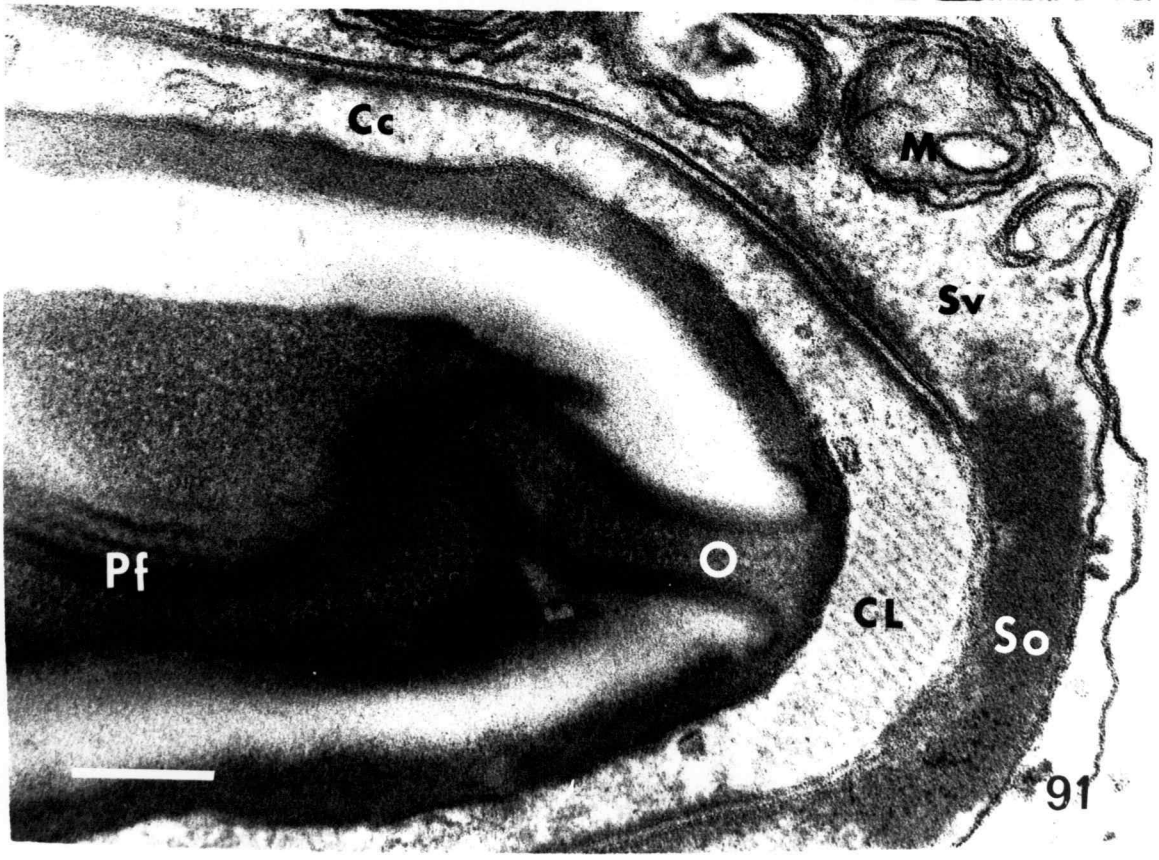
Cc
M
Sv
Pf
CL
So
91

Figure 92. Longitudinal section of a developing spore in the early stages of polar filament formation. Capsulogenous cell, Cc; Endoplasmic reticulum, Er; First loop of the polar filament, F_1; Opening of the polar capsule, O; Developing stopper in the shell valve cell, SO. (Scale = 1.0 μm; 20,200x)

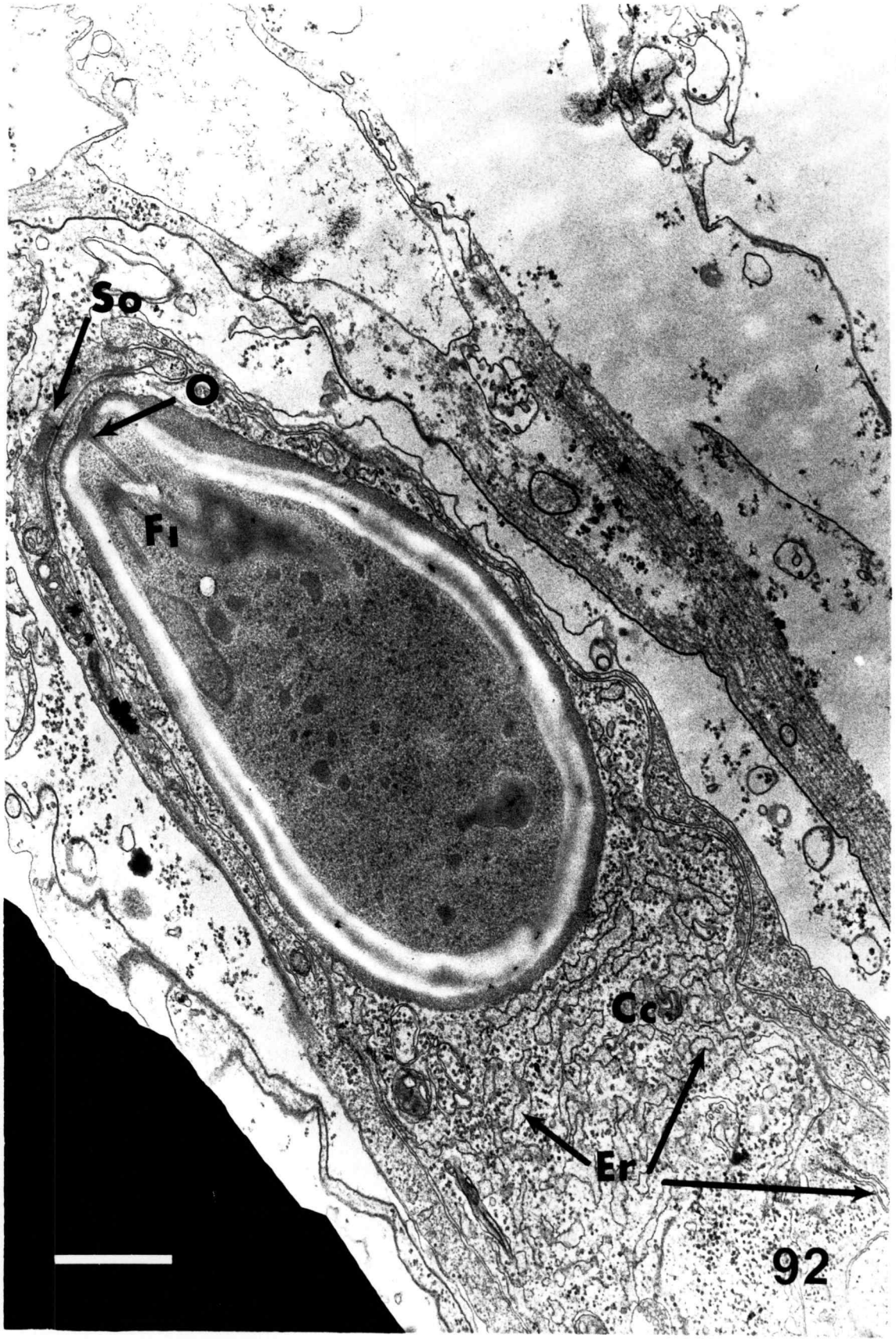
So
O
F1
Cc
Er
92

Figure 93. Developing polar capsule showing the highly electron dense layer, DL; in the polar capsule wall. (Scale = 0.5 μm; 30, 100x)

Figure 94. High magnification electron micrograph of a cross section of a polar capsule showing two polar filament coils. Capsulogenous cell, Cc; Polar capsule matrix, Cm; Electron lucent layer, Lt; Inner luminal space of the undischarged filament, Lu; Polar capsule wall, Pc; Inner surface limiting sheath of the undischarged filament, Sh; Shell valve cell, SV; Serrated zone forming the external boundary of the undischarged filament, Sz. (Scale = 0.2 μm; 156, 000x)

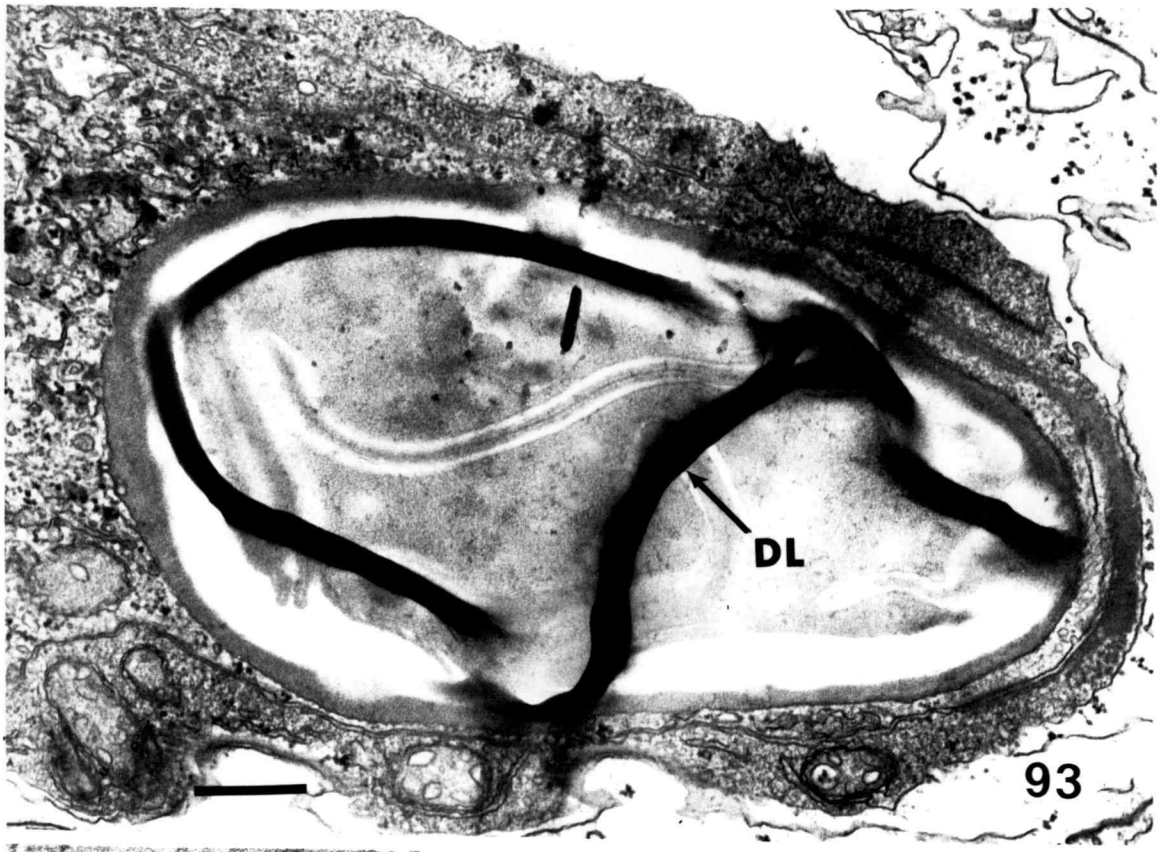
DL
93

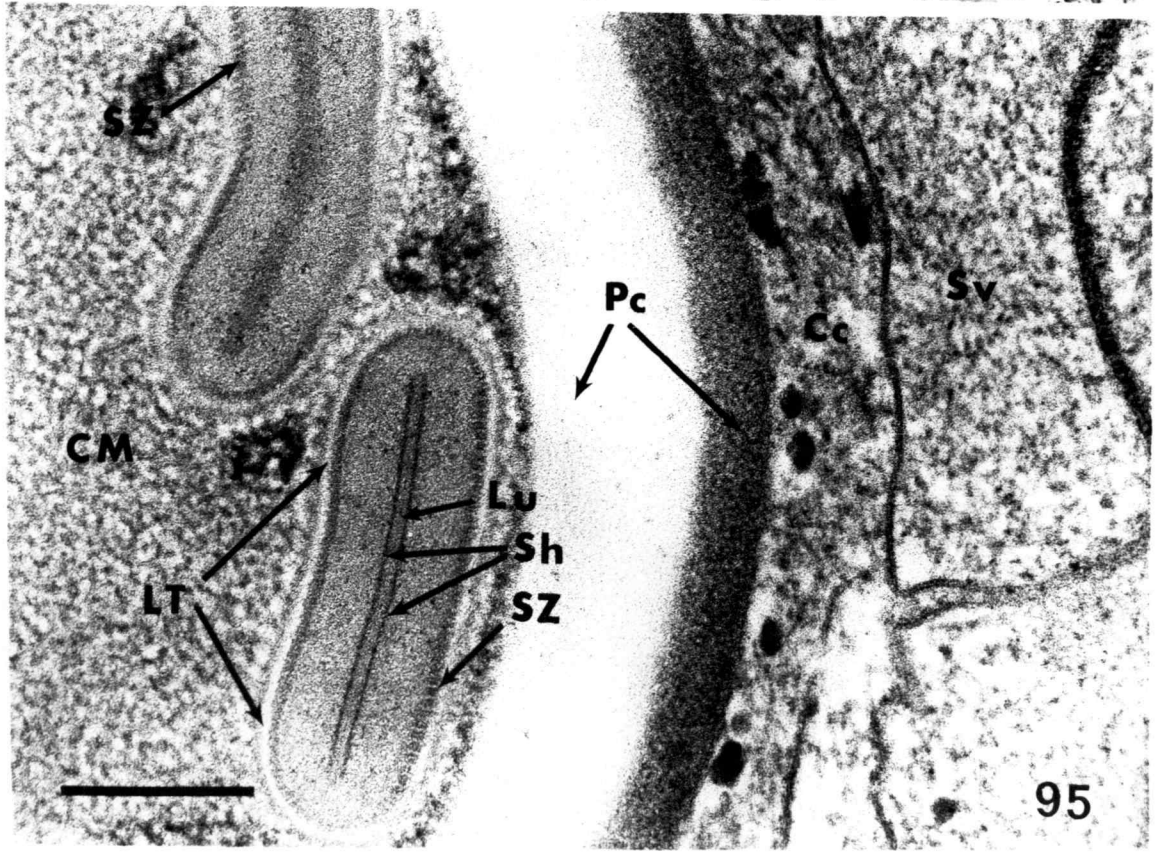
SZ
CM
LT
Lu
Sh
SZ
Pc
Cc
Sv
95

Figure 95. Tangential section of a polar capsule showing the folding of the polar filament within the polar capsule. Folds of the polar filament, F_1-F_4. (Scale = 1.0 μm; 32, 100x)

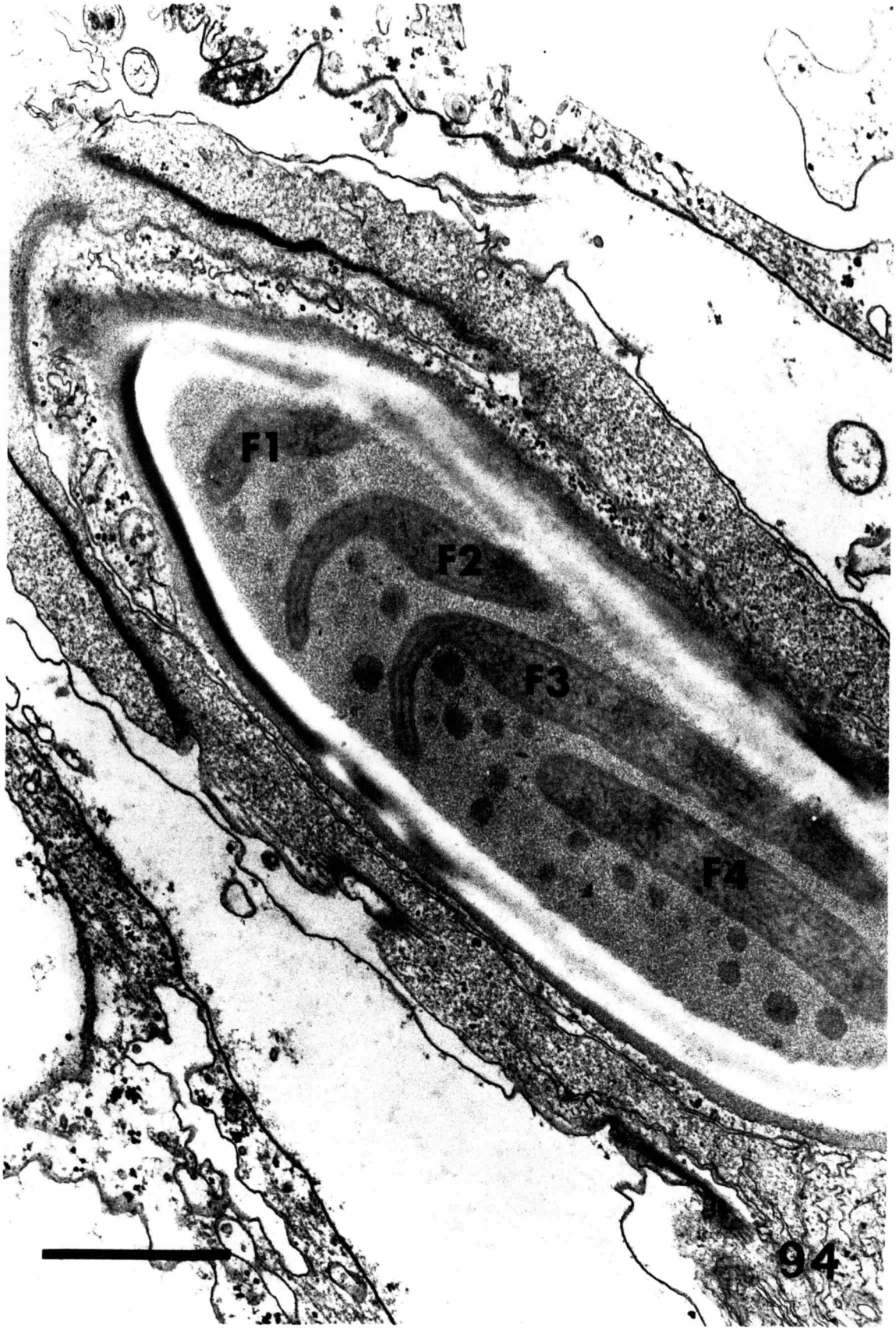
F1
F2
F3
F4
94

Figure 96. Cross section of a developing spore showing the sporoplasm centrally located within the shell valve cells. Golgi complex in sporoplasm, Gc; Sporoplasm, Sp; Sporoplasm nucleus, SpN; Shell valve cell, SV. (Scale = 1.0 μm; 18,840x)

Figure 97. Low magnification electron micrograph of an immature spore during early capsulogenesis showing the eccentrically located sporoplasm. Capsulogenous cell, Cc; Capsulogenous cell nucleus, Cn; Endoplasmic reticulum, ER; Golgi complex of sporoplasm, Gc; Sporoplasm, Sp; Extensions of the sporoplasm, SpE. (Scale = 1.0 μm; 11,500x)

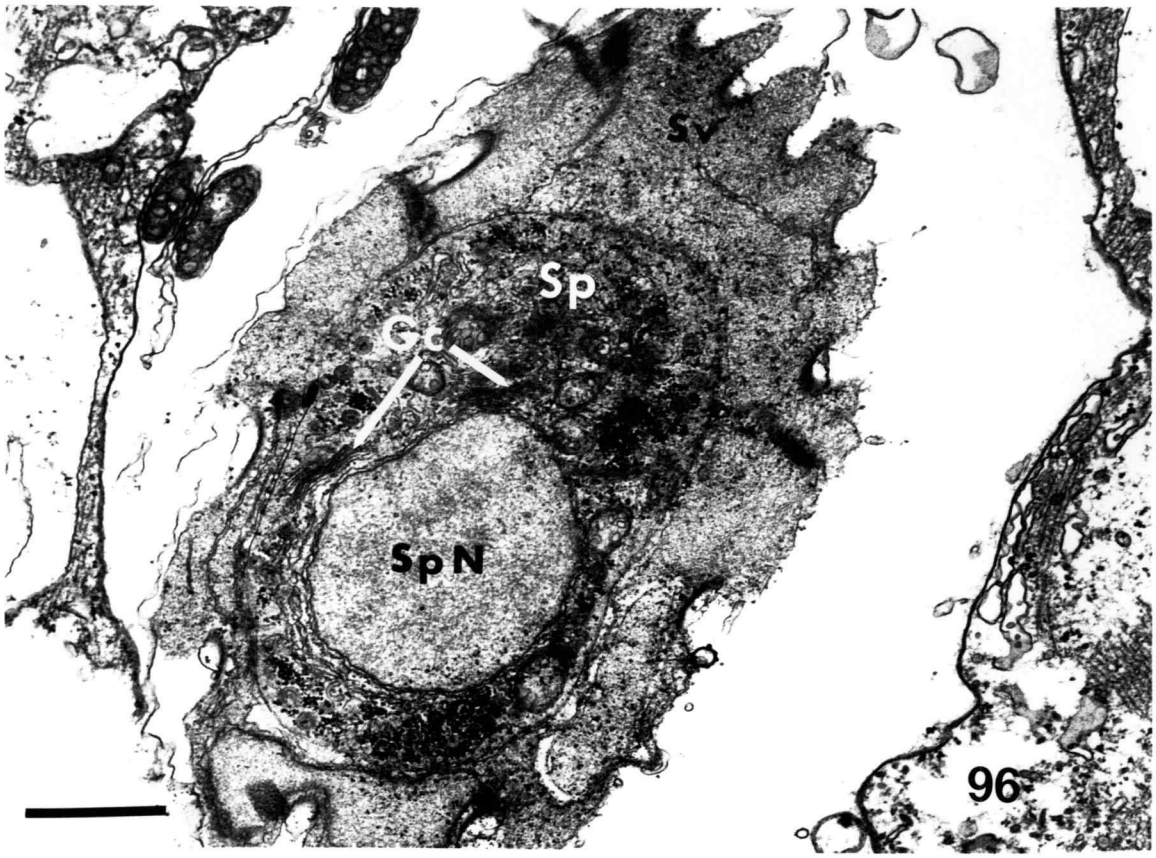
Sv
Sp
Gc
SpN
96

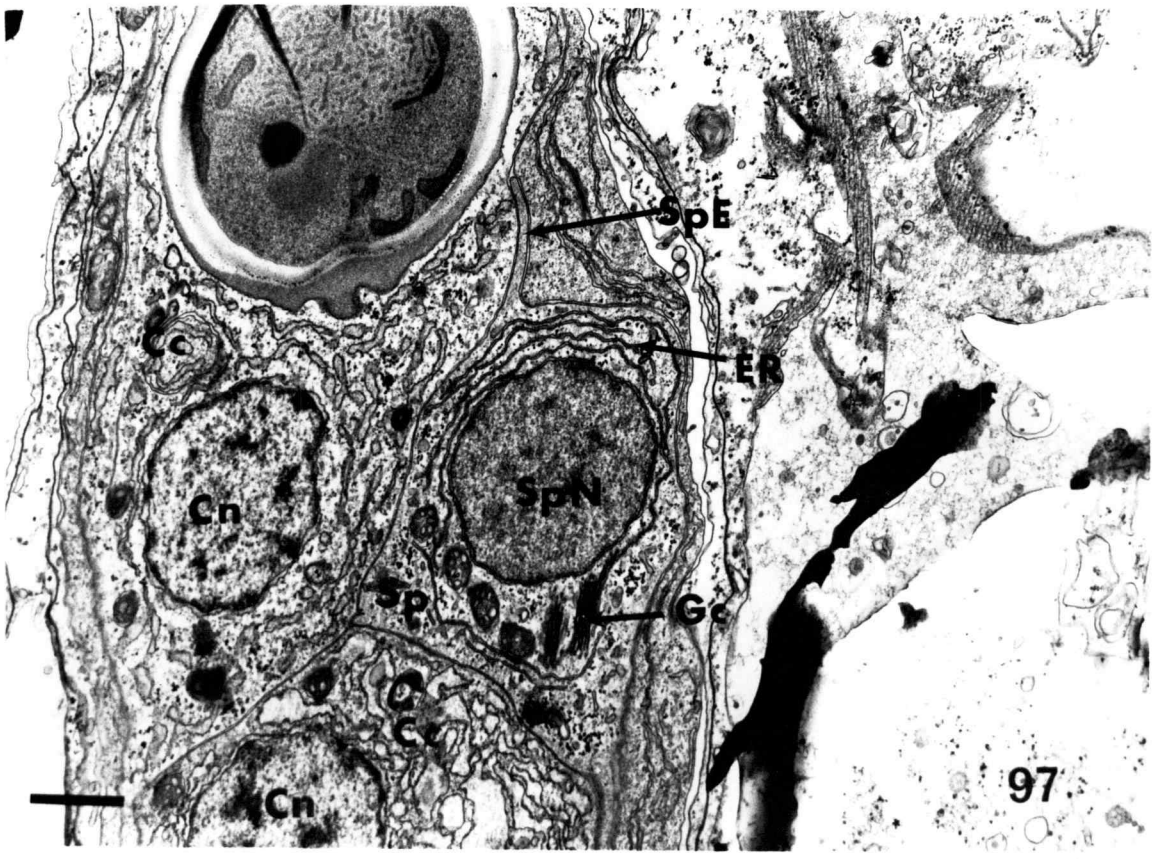
SpE
ER
Cc
Cn
SpN
Sp
Gc
Cc
Cn
97

Figure 98. Longitudinal section of a developing spore showing both polar capsules. Capsulogenous cell, Cc; Capsulogenous cell nucleus, Cn; Polar capsule, Pc; Polar filament primordium, Pfp; Sporoplasm, Sp; Extensions of the sporoplasm, SpE; Sporoplasm nucleus, SpN. (Scale = 2.0 μm; 7550x)

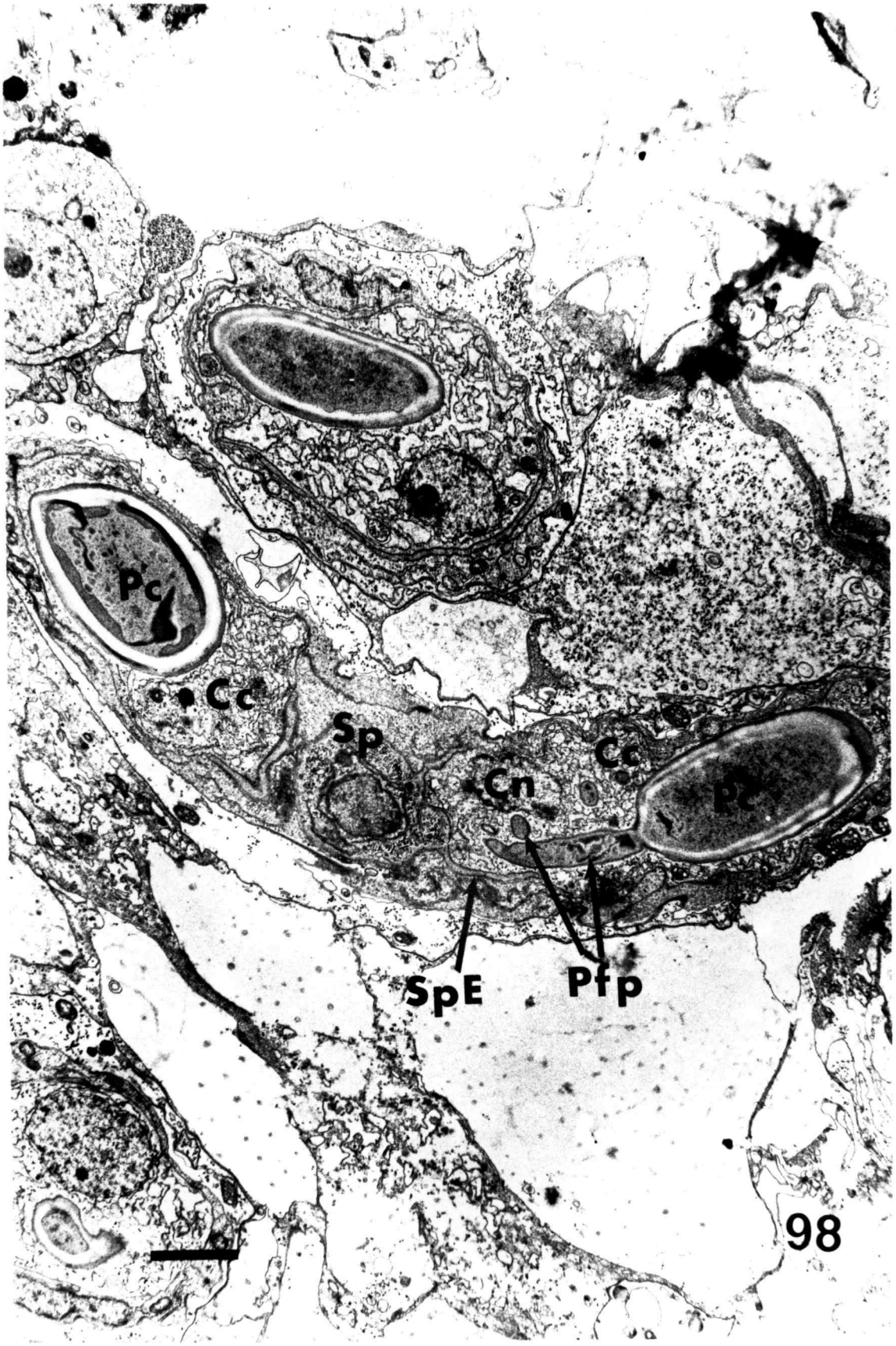
Pc
Cc
Sp
Cn
Cc
Pc
SpE
Pfp
98

Figure 99. Longitudinal section of the sporoplasm. Capsulogenous cell, Cc; Endoplasmic reticulum, ER; Glycogen aggregates, G; Mitochondria, M; Sporoplasm, Sp; Extensions of the sporoplasm, SpE; Sporoplasm nucleus, SpN; Shell valve cells, Sv. (Scale = 0.5 μm; 50,000x)

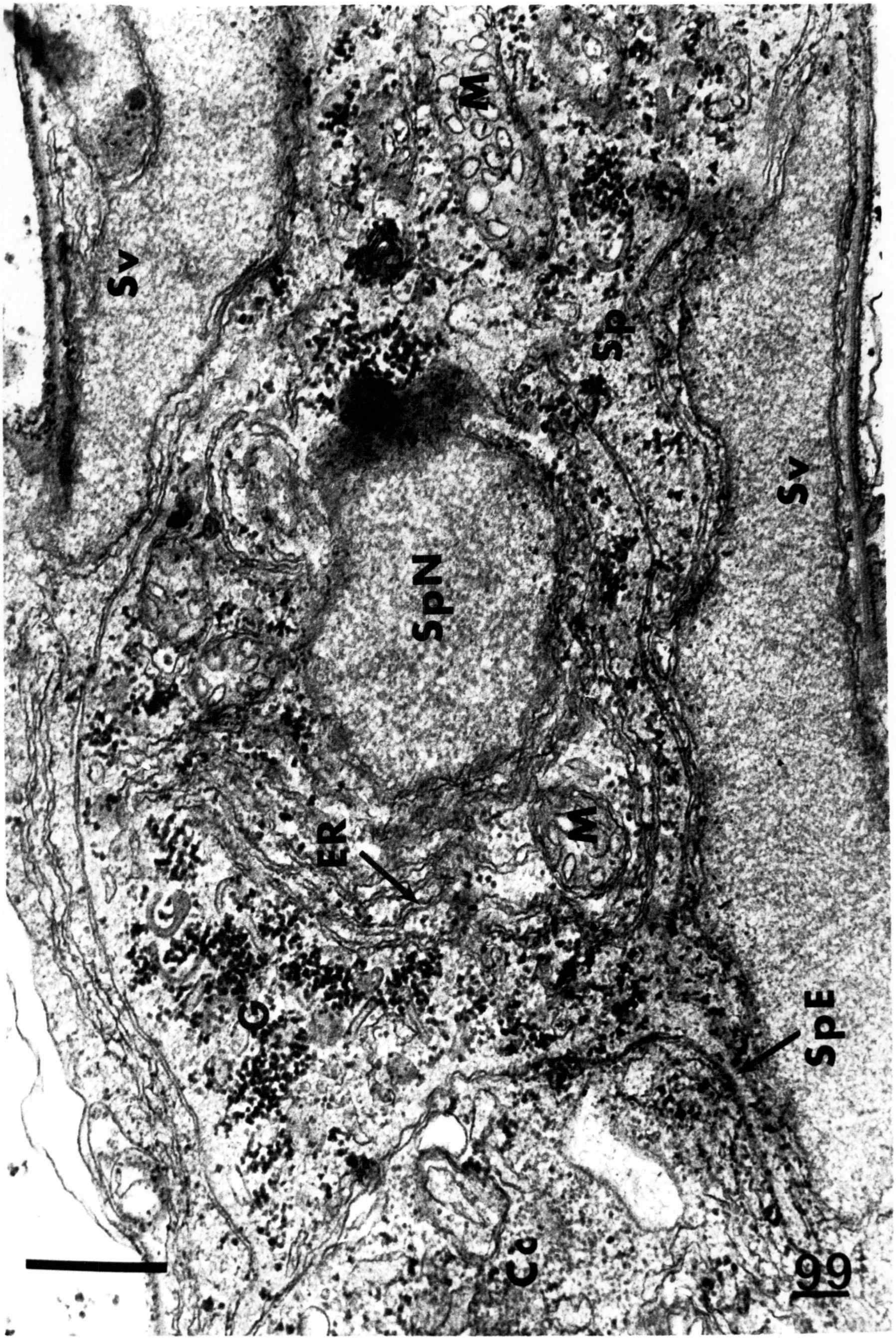
Sv
M
Sp
SpN
Sv
ER
M
G
SpE
Cc
66